Introduction to Geophysics – Lecture Notes

Jan Valenta

March 23, 2015

CZECH REPUBLIC
DEVELOPMENT COOPERATION

Contents

1

Introduction

1.1 What is geophysics?

Essentially, as the word suggests, geophysics is the application of method of physics to the study of the Earth. The rocks does not differ only by their macroscopic or microscopic properties studied field geologists or petrologists. They also differ by their chemical and physical properties. Hence as the rocks differ according to their origin, structure, texture, etc. they also differ by their density, magnetisation, resistivity, etc. The bad news is that the physical properties do not always clearly correlates with geological classifications and do not necessarily easily translates into the geological terms. What does this mean?

Lets take the density as an example. We have a rock sample and we have measured the value of density to be 2.60 g/cm3. According to this value we could assume that the rock sample could be, e. g. a limestone, some shale, compact sandstone, rhyolite, phonolite, andesite, granite, possibly some kindof schist and many others. The wide range of possible rock types suggests that the physical properties does not directly refer to the geological classification. This is a principal problem of geophysics, however, as we will see later, there are ways to overcome this.

So, what we can conclude from this example? The geophysics is a kind of proxy in our attempts to study the geological structures. It does not "talk" to us in geological terms and we have to interpret obtained physical parameters in a ge olog-ical sense. Moreover, the icentrifugal forcenter-pretation is not unique as we have seen in our example. The successful interpretation is based on experiences of an interpreter and on the a priori knowledge of the geological environment studied. In the terms of our example – if we know that we are working in the crystalline complex we can mostly likely leave sedimentary rocks out of our interpretation and we are left with rhyolite, phonolite, andesite, granite or schist. And if we study the geological sources a little bit more we could also discriminate between the rock types left.
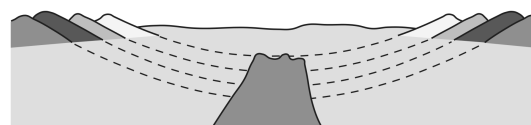
(a) symmetrical syncline
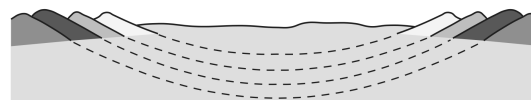
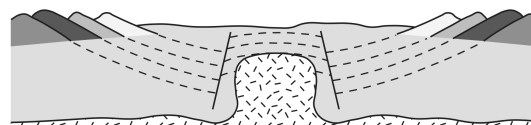(b) faulted syncline
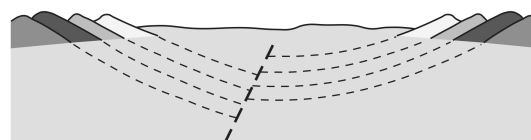
(c) intrusion

(d) salt dome

Figure 1.1: *Possible inferences of structure at depth (Musset and Khan 2000).*

When we have discussed the essential and unavoidable drawback of geophysics it is time to look on the bright side. Why do people bother with geophysics, what problems can it solve and how it can help me in my particular problem? The advantage of geophysics is that it is able to image hidden structures and features inaccessible to direct observation and inspection. That from measurements on the surface we can deduce what is in the depth. Moreover, we can measure on traverses or even make a grid and hence obtain a profile view, map or even a 3d image of a subsurface. Compare this with a geological mapping where we study the outcrops and, if we are lucky, have also a few trenches or boreholes. There we have just a surface situation and we can only guess how the surface structures continues to the depth.

Imagine the situation illustrated in the Figure 1.1. From the surface geological mapping we would see a sediment filled valley with inclined strata on both sides. However, we have no clue how it looks like in the depth. Four possibilities are sketched in the figure. The surface geological mapping cannot give us any hint which of these is correct unless we would make a line of boreholes. This, of course, would be both – time consuming and extremely expensive. How the geophysics can help us here?

Lets assume that we have collected geophysical data on a traverse across the structure. The methods used were gravimetry, magnetometry and a DC resistivity profiling. The gravimetry distinguish rocks according to their densities, hence if we see an increase in gravity we can assume rocks with increased densities – e.g. a mafic intrusion (Fig. 1.1c). Decreased densities of rocks would also decrease the gravity readings we can assume presence of rocks with low densities – e.g. a salt dome (Fig. 1.1d). The magnetometry indicates rocks with increased magnetisation – in case of mafic intrusion (Fig. 1.1c) we would see an increase in magnetometry data. The fault zones are usually connected with low resistivities. Hence if Fig. 1.1b or Fig. 1.1d would be the case we would see a low resistivity zone over the fault. In such a manner the geophysics can add to the surface geological prospection. In this particular case the geophysics provided us with the third (desperately needed) dimension. The only necessary condition is that the target structure must differ in some of the physical properties from its surroundings (Tab. 1.1).

Material	Density Mg m^{-3}	Susceptibility SI $\times 10^6$	Resistivity Ohm-m	Conductivity mS m^{-1}
Air	0	0	8	0
Ice	0.9	−9	100 000–8	0–0.01
Fresh water	1	0	1 000 000	0.001
Seawater	1.03	0	0.2	5000
Topsoil	1.2–1.8	0.1–10	50–100	10–20
Coal	1.2–1.5	0–1000	500–2000	2–0.5
Dry sand	1.4–1.65	30–1000	1000–5000	1–0.02
Wet sand	1.95–2.05	30–1000	500–5000	0.2–2
Gravel	1.5–1.8	20–5000	100–1000	1–10
Clay	1.5–2.2	10–500	1–100	10–1000
Weathered bedrock	1.8–2.2	10–10 000	100–1000	1–10
Salt	2.1–2.4	−10	10–10 000 000	0.01–1
Shale	2.1–2.7	0–500	10–1000	1–100
Siltstone	2.1–2.6	10–1000	10–10 000	0.1–100
Sandstone	2.15–2.65	20–3000	200–8000	0.125–5
Chalk	1.9–2.1	0–1000	50–200	5–20
Limestone	2.6–2.7	10–1000	500–10 000	0.1–2
Slate	2.6–2.8	0–2000	500–500 000	0.002–2
Graphitic schist	2.5–2.7	10–1000	10–500	2–100
Quartzite	2.6–2.7	−15	500–800 000	0.00125–2
Gneiss	2.6–2.9	0–3000	100–1 000 000	0.001–10
Greenstone	2.7–3.1	500–10 000	500–200 000	0.005–2
Serpentinite	2.5–2.6	2000–100 000	10–10 000	0.1–100
Granulite	2.7–2.9	100–5000	500–1 000 000	0.001–2
Granite	2.5–2.7	20–5000	200–1 000 000	0.001–5
Rhyolite	2.5–2.7	100–5000	1000–1 000 000	0.001–1
Basalt	2.7–3.1	500–100 000	200–100 000	0.01–5
Dolerite	2.8–3.1	500–100 000	100–100 000	0.01–10
Gabbro	2.7–3.3	100–10 000	1000–1 000 000	0.001–1
Peridotite	3.1–3.4	10–10 000	100–100 000	0.01–10
Pyrite	4.9–5.0	100–5000	0.01–100	10–1 000 000
Pyrrhotite	4.4–4.7	1000–50 000	0.001–0.01	1 000 000– 10 000 000
Sphalerite	3.8–4.2	10–100	1000–1 000 000	0.001–1
Galena	7.3–7.7	10–500	0.001–100	10–10 000 000
Chalcopyrite	4.1–4.3	100–5000	0.005–0.1	10 000–200 000
Chromite	4.5–4.7	750–50 000	0.1–1000	1–10 000
Hematite	5.0–5.1	100–1000	0.01–1 000 000	0.001–100 000
Magnetite	5.1–5.3	10 000– 10 000 000	0.01–1000	0.001–1
Cassiterite	7.0–7.2	10–500	0.001–10 000	0.1–10 000 000

Table 1.1: *Physical properties of common rocks and ore minerals (Milsom 2011).*

Gravimetry

The gravimetry detects tiny differences in the gravitational force. Since, according to the Newton's law, the gravitational force depends on masses of the bodies, it allows us to differentiate underground bodies and structures if their densities differ.

2.1 Newton's Law of Gravitation

Everyone is familiar with the Earth pull or attractive force. It causes thing s to fall and is also responsible for a pretty hard work if we need to carry stones to build a house. The man who discovered that every mass attracts another one was Sir Isaac Newton. In 1687 he formulated his discovery into the equation (2.1) called the Newton's Law of Gravitation:

$$F = \gamma \frac{m_1 m_2}{r^2}, \tag{2.1}$$

where F denotes the gravitational force, γ is the universal gravitational constant ($6.673 \times 10^{-11} \, \text{N(m/kg)}^2$), m are weights of attracting bodies and r is the distance between them. This equation (2.1) enables us to calculate a gravitational force the Earth is pulling e.g. a rock on the Earth surface:

$$F = \gamma \frac{M_E m_r}{R_E^2}, \tag{2.2}$$

where M_E is the weight of the Earth, m_r is the weight of the rock and R_E is the diameter of the Earth. We can see that it is inconvenient to use and measure the gravitational force, since it depends on weights (masses) of both bodies M_E and m_r. Dividing both sides of equation (2.2) by m_r we get:

$$\frac{F}{m_r} = \gamma \frac{M_E}{R_E^2}. \tag{2.3}$$

Since the force is computed as *weight* × *acceleration* we can transform the equation (2.3) into:

$$g = \gamma \frac{M_E}{R_E^2}, \tag{2.4}$$

defining the acceleration caused by the Earth. The acceleration g is called the "acceleration due to gravity" or "acceleration of gravity". The value of g on the Earth surface is $9.80665 \, \text{m/s}^2$ which is often simplified to $10 \, \text{m/s}^2$. The unit of acceleration of gravity – $1 \, \text{cm/s}^2$ – is also referred to as galileo or Gal, in honour of Galileo Galilei, who was the first who measured its value. The modern gravimeters are capable of readings with the precision of $0.001 \, \text{mGal}$ ($0.01 \, \text{µm/s}^2$).
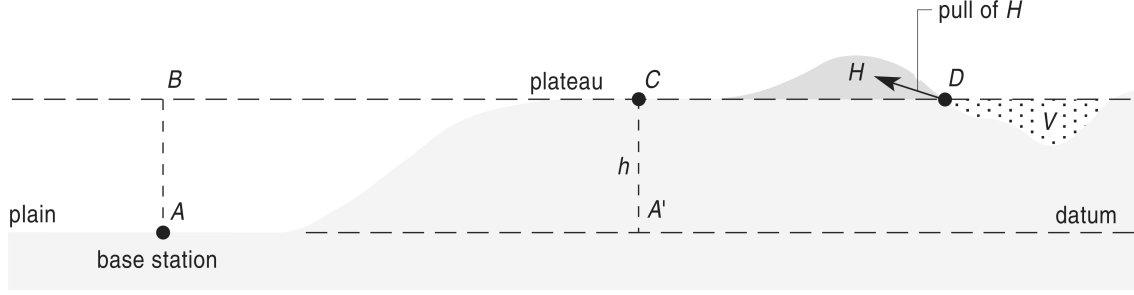
Figure 2.1: *Topographic corrections (Musset and Khan 2000)*

2.2   Gravity field of the Earth and data reduction

Because the Earth is not a perfect homogeneous sphere, the gravitational acceleration is not constant over the whole Earth's surface. Its magnitude depends on five following factors: latitude, elevation, topography of the surrounding terrain, earth tides and density variations in the subsurface. Within the geophysical prospection, we are interested in the last one, which is usually much smaller then the latitude and altitude changes. The removal of unwanted components is often referred to as *reduction*.

Latitude correction. The reason for the latitude correction is two-fold. First of all, it is caused by the Earth's centrifugal force being added to the gravitational force (vector sum). This decreases the gravitational force with an increase of a radius of rotation. Hence the smallest gravitational force is on the equator (maximal centrifugal force) and the largest is on the pole. Second, the gravitational force is further affected by the fact that the Earth is not spherical but ellipsoidal. This further decreases the gravitational force on the equator. Both of these effects could be removed by the International Gravity Formula:

$$g_\lambda = 978031.8(1 + 0.0053024 \sin^2 \lambda - 0.0000059 \sin^2 2\lambda) \,\mathrm{mGal} \tag{2.5}$$

It is clear that the centrifugal force changes only in the N–S direction, not in the W–E.

As we have seen from the Newton's Law of Gravity – equation (2.1) – the gravity decreases with the square of distance. Hence, if we lift the gravimeter from the surface (or any other datum), the gravity will change. To be able to compare data measured in different elevations we have to reduce them to a common datum. This correction for the topographic effects has several steps. Their description follows.

Free-air correction. This is the first step of reducing topography effects. It simply corrects for the change in the elevation of the gravity meter, considering only air (hence a free-air) being between the meter and selected datum (leftmost part of the Figure 2.1). To get the change in gravity acceleration with height we can differentiate the equation (2.4):

$$\frac{\Delta g_{FA}}{\Delta R} = -2\gamma \frac{M_E}{R^3} = -\frac{2g}{R} \,\mathrm{mGal/m}. \tag{2.6}$$

Raising the gravity meter (e.g. extending its tripod) decreases the measured gravity values by $0.3086\,\mathrm{mGal/m}$. Hence to measure with an accuracy of $0.01\,\mathrm{mGal}$ we have to measure the elevation of the gravity meter with an accuracy of $3\,\mathrm{cm}$. The free-air correction varies slightly with latitude:

Clearly, the $\sin^2 \lambda$ and h^2 parts are very small and could be neglected and we end up with the above mentioned ratio.

Bouguer correction. The Bouguer correction removes from the data an effect of rocks laying between the measured point and reference datum (Fig. 2.1 in the centre). This effect was
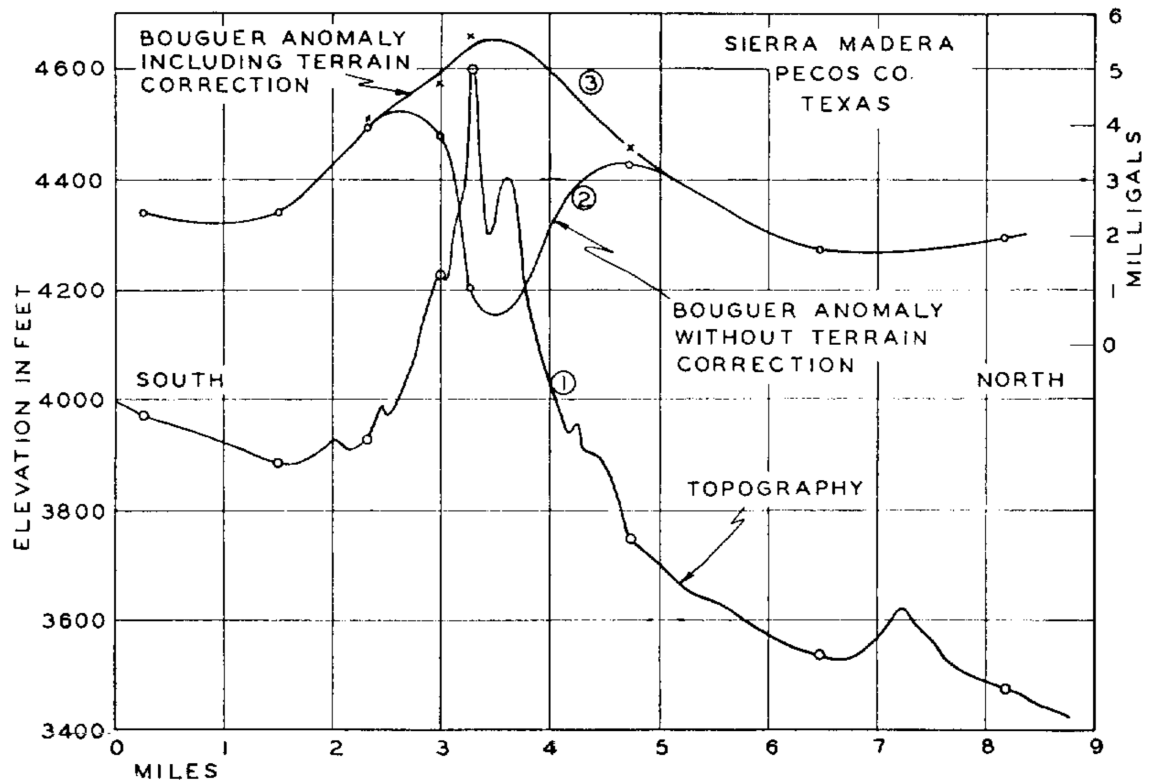
Figure 2.2: *Gravimeter profile across Sierra Madera, Pews County, Texas, illustrating the importance of terrain corrections (Hammer 1939).*

ignored during the free-air corrections. Hence we add a slab with an average density of surrounding rocks – the Bouger correction:

$$\frac{\Delta g_B}{\Delta R} = 2\pi\gamma\rho = 0.04192\rho \,\text{mGal/m}, \tag{2.7}$$

where ρ is the density of the Bouguer slab.

The free-air and Bouguer correction is often combined into an elevation correction:

$$\frac{\Delta g_E}{\Delta R} = \frac{\Delta g_{FA}}{\Delta R} - \frac{\Delta g_B}{\Delta R} = (0.3086 - 0.04192\rho) \,\text{mGal/m}. \tag{2.8}$$

Terrain correction. The Bouguer correction assumed the slab to be infinite in the horizontal direction. This is not true, due to a topography and Earth curvature. The correcton for the Earth curvature is used in a large scale surveys and we will leave it out now. The topography correction, however, might be important (Fig. 2.1, right). The hill above the Bouguer slab with its own gravity force pulls in the opposite direction than the Earth, therefore decreasing the measured acceleration (Fig. 2.2). In a similar way, the valley also decreases the value, because when computing the Bouguer correction we have already subtracted the Bouguer slab (with a flat surface) and did not account for the missing masses of the valley. Hence the terrain correction is always added.

There are several methods of calculating terrain corrections. In any of these we need to know the relief to certain distance from the station in detail. The common method is to divide the surroundings of the gravity stations into zones, estimate average altitude in every zone and compute the gravity effect of the zones. Several versions of these zones were already published (e.g. Hammer 1939). The easiest way is to print the zoning chart (Fig. 2.3) into the transparent sheet and overlay it over the topographic map. Then the average altitude in each zone and compartment is estimated and the difference between estimated value and
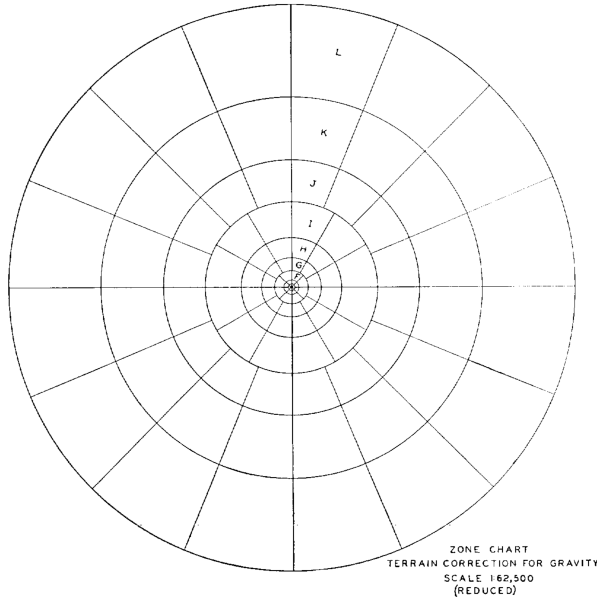
Figure 2.3: *Zone chart for use in evaluating terrain corrections at gravity stations (Hammer 1939).*

station elevation is computed and a gravity effect of this compartment is found in the table (Figs. 2.4 and 2.5). Finally, sum of effects in all compartments and zones forms the terrain correction for the current station.

It is clear that this method of computing terrain corrections is very tedious. Hence now usually the computer programs compute the corrections based from the DEM (digital elevation model of the terrain).

Note that the effect of the innermost zone – A – is not computed in the table. The reason is that in such small surroundings the terrain should be flat if possible. The gravity effects of irregularities in such close vicinity is very large, precise topography maps in scales large enough are not common and dense precise measurements of relief would be inadequately expensive.

Tidal correction. The tidal correction accounts for the gravity effect of Sun, Moon and large planets. Modern gravity meters compute the tide effects automatically. For the older instruments, one must compute the corrections by himself, e.g. according to the Longman (1959), or consider the tides as a part of the drift of the instrument and remove it via a drift correction.

Drift correction. This correction is intended to remove the changes caused by the instrument itself. If the gravimeter would be at one place and take periodical readings, the readings would not be the same. These are partly due to the creep of the measuring system of the gravimeter, but partly also from the real variations – tidal distortion of the solid Earth, changes of the ground water level, etc.

The drift is usually estimated from repeated readings on the base station. The measured data are then interpolated, e.g. by a third order polynomial, and a corrections for profile readings are found.

2.3   Gravity meters

Basically, there are two main gravity types – the absolute and relative gravity meters. In geophysical prospection solely the former are used. They measure relative gravity – the gravity changes, not the value of gravity itself. If we want to measure the absolute value of gravity we must use some point with already known gravity value and start our measurements there. Then, by adding the measured differences, we know the absolute values of gravity on all our points. However, this is needed only in large scale mapping, where we want to add our data to already existing grid.

Each zone is a circular ring of given radii (in feet) divided into 4, 6, 8, 12, or 16 compartments of arbitrary azimuth. "h" is the mean topographic elevation in feet (without regard to sign) in each compartment with respect to the elevation of the station. The tables give the correction "T" for each compartment due to undulations of the terrain in units of 1/100 mg. for density $(\sigma) = 2.0$. This correction, when applied to Bouguer anomaly values which have been calculated with the simple Bouguer correction, is always positive.

Zone B 4 compartments 6.56 to 54.6*		Zone C 6 compartments 54.6 to 175		Zone D 6 compartments 175 to 558		Zone E 8 compartments 558 to 1280		Zone F 8 compartments 1280 to 2936		Zone G 12 compartments 2936 to 5018	
±h (ft.)	T	±h (ft.)	T	±h (ft.)	T	±h (ft.)	T	±h (ft.)	T	±h (ft.)	T
0 to 1.1	0	0 to 4.3	0	0 to 7.7	0	0 to 18	0	0 to 27	0	0 to 58	0
1.1– 1.9	0.1	4.3– 7.5	0.1	7.7–13.4	0.1	18– 30	0.1	27– 46	0.1	58– 100	0.1
1.9– 2.5	0.2	7.5– 9.7	0.2	13.4–17.3	0.2	30– 39	0.2	46– 60	0.2	100– 129	0.2
2.5– 2.9	0.3	9.7–11.5	0.3	17.3–20.5	0.3	39– 47	0.3	60– 71	0.3	129– 153	0.3
2.9– 3.4	0.4	11.5–13.1	0.4	20.5–23.2	0.4	47– 53	0.4	71– 80	0.4	153– 173	0.4
3.4– 3.7	0.5	13.1–14.5	0.5	23.2–25.7	0.5	53– 58	0.5	80– 88	0.5	173– 191	0.5
3.7– 7	1	14.5– 24	1	25.7– 43	1	58– 97	1	88–146	1	191– 317	1
7 – 9	2	24 – 32	2	43 – 56	2	97–126	2	146–189	2	317– 410	2
9 –12	3	32 – 39	3	56 – 66	3	126–148	3	189–224	3	410– 486	3
12 –14	4	39 – 45	4	66 – 76	4	148–170	4	224–255	4	486– 552	4
14 –16	5	45 – 51	5	76 – 84	5	170–189	5	255–282	5	552– 611	5
16 –19	6	51 – 57	6	84 – 92	6	189–206	6	282–308	6	611– 666	6
19 –21	7	57 – 63	7	92 –100	7	206–222	7	308–331	7	666– 716	7
21 –24	8	63 – 68	8	100 –107	8	222–238	8	331–353	8	716– 764	8
24 –27	9	68 – 74	9	107 –114	9	238–252	9	353–374	9	764– 809	9
27 –30	10	74 – 80	10	114 –120	10	252–266	10	374–394	10	809– 852	10
		80 – 86	11	120 –127	11	266–280	11	394–413	11	852– 894	11
		86 – 91	12	127 –133	12	280–293	12	413–431	12	894– 933	12
		91 – 97	13	133 –140	13	293–306	13	431–449	13	933– 972	13
		97 –104	14	140 –146	14	306–318	14	449–466	14	972–1009	14
		104 –110	15	146 –152	15	318–331	15	466–483	15	1009–1046	15

* Radii of the zone in feet.

Figure 2.4: *Original Hammer's table for the terrain corrections (Hammer 1939).*

Zone H 12 compartments 5018 to 8578		Zone I 12 compartments 8578 to 14,662		Zone J 16 compartments 14,662 to 21,826		Zone K 16 compartments 21,826 to 32,490		Zone L 16 compartments 32,490 to 48,365		Zone M 16 compartments 48,365 to 71,996	
±h (ft.)	T	±h (ft.)	T	±h (ft.)	T	±h (ft.)	T	±h (ft.)	T	±h (ft.)	T
0 to 75	0	0 to 99	0	0 to 167	0	0 to 204	0	0 to 249	0	0 to 304	0
75– 131	0.1	99– 171	0.1	167– 290	0.1	204– 354	0.1	249– 431	0.1	304– 526	0.1
131– 169	0.2	171– 220	0.2	290– 374	0.2	354– 457	0.2	431– 557	0.2	526– 680	0.2
169– 200	0.3	220– 261	0.3	374– 443	0.3	457– 540	0.3	557– 659	0.3	680– 804	0.3
200– 226	0.4	261– 296	0.4	443– 502	0.4	540– 613	0.4	659– 747	0.4	804– 912	0.4
226– 250	0.5	296– 327	0.5	502– 555	0.5	613– 677	0.5	747– 826	0.5	912–1008	0.5
250– 414	1	327– 540	1	555– 918	1	677–1119	1	826–1365	1	1008–1665	1
414– 535	2	540– 698	2	918–1185	2	1119–1445	2	1365–1763	2	1665–2150	2
535– 633	3	698– 827	3	1185–1403	3	1445–1711	3	1763–2086	3	2150–2545	3
633– 719	4	827– 938	4	1403–1592	4	1711–1941	4	2086–2366	4	2545–2886	4
719– 796	5	938–1038	5	1592–1762	5	1941–2146	5	2366–2617	5	2886–3191	5
796– 866	6	1038–1129	6	1762–1917	6	2146–2335	6	2617–2846	6	3191–3470	6
866– 931	7	1129–1213	7	1917–2060	7	2335–2509	7	2846–3058	7	3470–3728	7
931– 992	8	1213–1292	8	2060–2195	8	2509–2672	8	3058–3257	8	3728–3970	8
992–1050	9	1292–1367	9	2195–2322	9	2672–2826	9	3257–3444	9	3970–4198	9
1050–1105	10	1367–1438	10	2322–2443	10	2826–2973	10	3444–3622	10	4198–4414	10
1105–1158	11	1438–1506	11	2443–2558	11						
1158–1209	12	1506–1571	12	2558–2669	12						
1209–1257	13	1571–1634	13	2669–2776	13						
1257–1305	14	1634–1694	14	2776–2879	14						
1305–1350	15	1694–1753	15	2879–2978	15						

Figure 2.5: *Original Hammer's table for the terrain corrections – continue (Hammer 1939).*

Figure 2.6: *Schematic sketch of the astatic gravity meter. The zero-length spring supports the mass M and keeps it in balance in a selected gravity field g. Measurements are done by rotating the dial, which raises or lowers the measuring spring and provides additional force $M \cdot \delta g$ to return the mass to the standard position (Milsom 2011).*
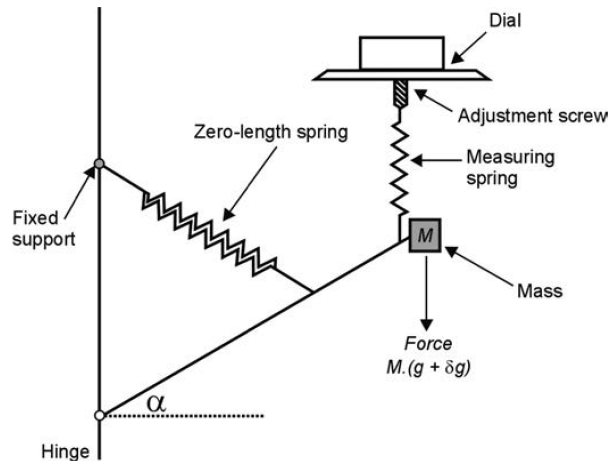
The gravity meters used for the geophysical prospection are the *astatic gravity meters* (Fig. 2.6), where the mass is hold by the measuring spring. Elongation of this spring is proportional to the gravity force pulling the mass. The older models of gravity meters used a dial to raise or lower the measuring spring to place the mass to a standard position. In modern gravimeters this is done automatically.

From the sketch it is clear that the springs used in the meters must be extremely thin and sensitive. There are two main types of the springs – steel springs in the LaCoste-Romberg gravity meters and quartz springs in the others. Currently, there are two manufacturers of the prospection gravity meters – the Scintrex with quartz springs and Burris, resembling the old LaCoste-Romberg and using the steel springs.

To minimise effects of thermal changes, the spring is in thermally insulated chamber (vacuum chamber), the new models are also equiooed with an additional heater to keep the internal temperature as stable as possible. Hence, removing batteries from the gravity meter leads to change in the inner temperature resulting in unstable and unreliable readings due to changes of mechanical properties of the measuring spring. When the gravimeter is without the power supply for a long time (several hours) it could take as long as 48 hours before realiable readings could be done again.

2.4 Rock densities

The densities of rocks (Tab. 1.1), naturally, depends on the mineral composition of particular rock. However, not only mineral composition, but also other factors influences densities. The next main factor, mainly when dealing with sedimentary rocks, is the porosity and kind of media filling the pores. Increasing porosity decreases the density, since air (or any other media filling the pores (water, gas, oil, etc.) has lower density than any of minerals. The other factors are weathering of rocks, fractures and joints, etc. Combining all these factors clearly explains the high variance of measured values reported in a literature.

Densities needed for a data and interpretation interpretation (e.g. for the Bouguer anomalies) could be either measured in laboratory (keeping in mind the laboratory values could differ from the reality mainly due to change of the media filling the pores in the nature and in laboratory) or could be estimated from the gravity measurements.

One of widely used methods for density estimation is the *Nettleton's method* (Nettleton 1939). This method is based on the fact that the Bouguer anomaly depends on the density of rocks as well as on the topography. If the topography along the profile is changing but the density is constant then, according to the equation (2.7), the Bouguer anomaly should be constant as well. If it is not constant then the density estimate is wrong and the topography changes are not compensated well. Therefore, if we compute a set of Bouguer anomaly curves with different densities and compare them with the topography the Bouguer curve which correlates the least with a topography is the curve with a correct density estimate.
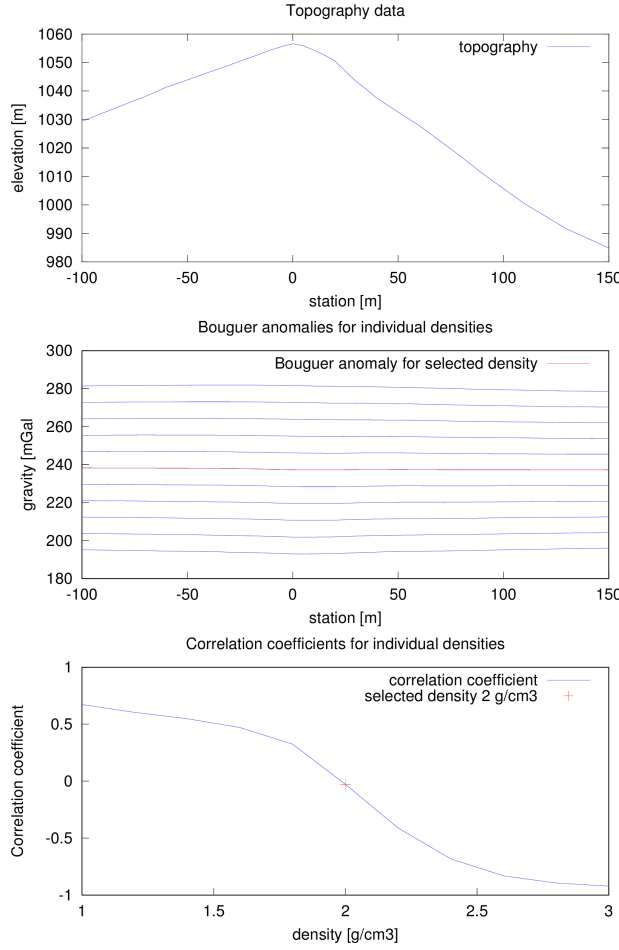
Figure 2.7: *Illustration of the Nettleton's method for density estimate. The Bouguer curve which correlates least with the topography is calculated with a correct density estimate. The top graph shows the topography along the profile. In the middle graph Bouguer curves for different densities are plotted, the curve for the selected density estimate is plotted in red. The bottom graph depicts correlation (Spearman's correlation coefficient) of topography and Bouguer curves for different densitites.*

This method could be applied if a) the profile crosses some distinct topographical feature, b) the density of the subsurface is not expected to change substantially.

2.5   Gravity effect of selected bodies

The simple geometrical bodies are often used for the modelling before the survey is carried out. The aim is to get a rough estimate of the anomaly effect of the target structure. If we, for example, find that the amplitude of a modelled anomaly is lower than sensitivity of our instrument then there is no need to do any measurements at all…Estimating the amplitude and width of the anomaly also enables us to plan a density of profiles and station spacing. For an interpretation at least three stations within the anomaly are necessary.

There is a small number of simple basic bodies, however, combining them together can build up even a complex model.

Gravity effect of a sphere A sphere is the most basic body and usually is used as a part of other models or could approximate symmetrical bodies. The gravity effect of a sphere at point P (Fig. 2.8) is:

$$g = g_r \cos\Theta = \frac{\gamma M}{r^2} = \frac{\frac{4\pi\gamma}{3}\rho a^3 z}{(x^2 + z^2)^{\frac{3}{2}}}, \tag{2.9}$$

where ρ is a density of the sphere, a is a radius of the sphere and z is the depth of the center of the sphere.
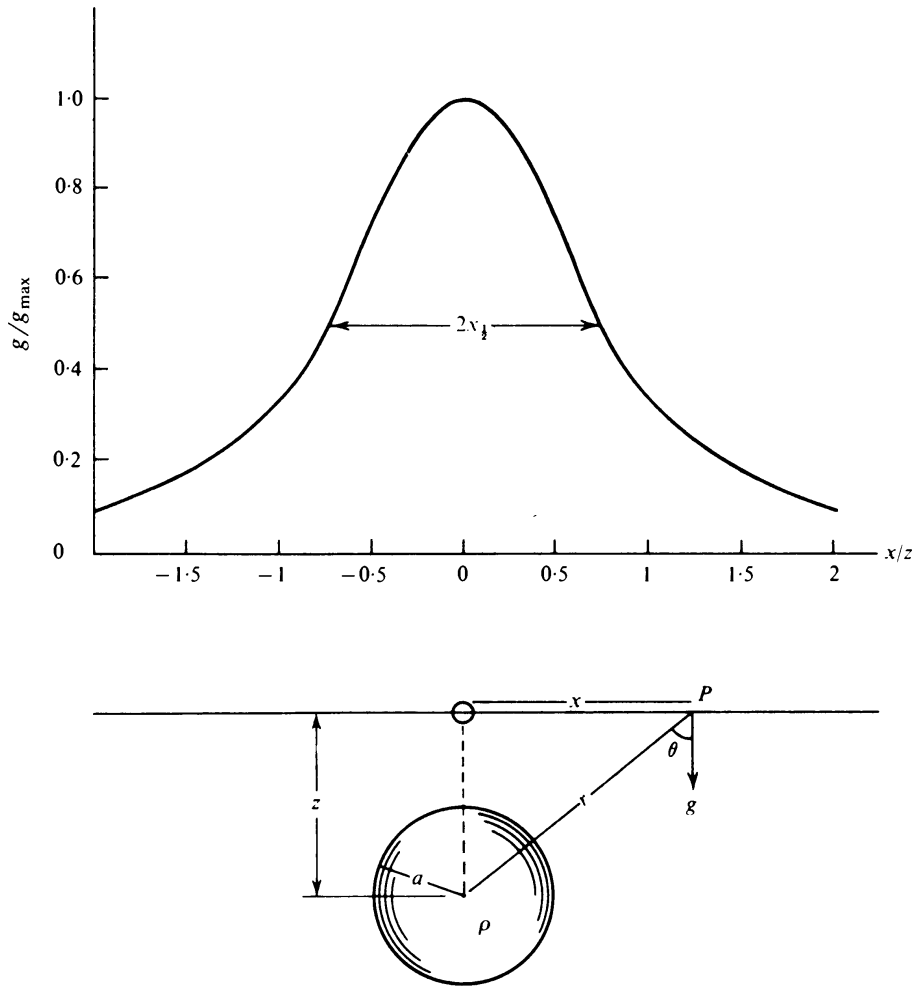
Figure 2.8: *Gravity effect of a sphere (Telford et al. 1990)*

The depth z of the sphere could be estimated from the measured anomaly. When $g = \frac{g_{max}}{2}$ then $z = 1.3x_{\frac{1}{2}}$. In other words, the depth of the sphere center could be estimated from the half-width of the anomaly at half of its value (see Fig. 2.8).

Gravity effect of a vertical cylinder The gravity effect on the axis aces of a vertical cylinder is:

$$g = 2\pi\gamma\rho\left\{L + (z^2 + R^2)^{\frac{1}{2}} - \left[(z+L)^2 + R^2\right]^{\frac{1}{2}}\right\}, \tag{2.10}$$

where L is the vertical size (length) of the cylinder z is the depth of its top and R is its diameter. If $R \to \infty$, we have an *infinite horizontal slab*, which we used also for the Bouguer correction (2.7):

$$g = 2\pi\gamma\rho L. \tag{2.11}$$

Gravity effect of a horizontal rod Assuming a horizontal rod perpendicular to the x axis at a depth z, the gravity effect is:

$$g = \frac{\gamma m}{z\left(1 + \frac{x^2}{z^2}\right)}\left\{\frac{1}{\left[1 + \frac{x^2+z^2}{(y+L)^2}\right]^{\frac{1}{2}}} - \frac{1}{\left[1 + \frac{x^2+z^2}{(y-L)^2}\right]^{\frac{1}{2}}}\right\}, \tag{2.12}$$

(a)

(b)

(c)

(d)
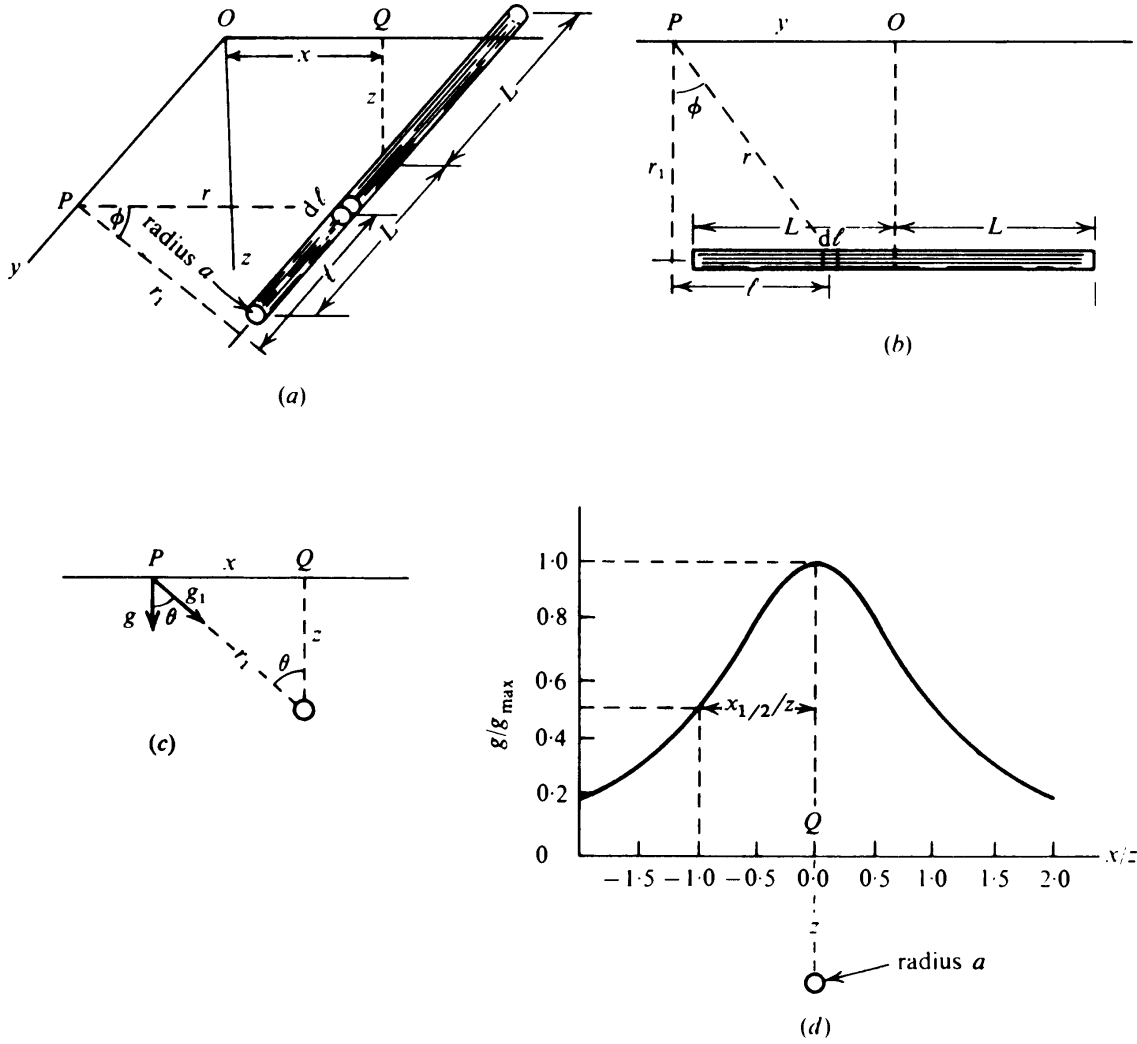
Figure 2.9: *Gravity effect of a horizontal rod. a) Three dimensional view. b) Projection of the plane containing the rod and the y axis. c) Projection on the xz plane. d) Gravity profile along the x axis. (Telford et al. 1990)*

where m is the mass of the rod. If the rod is expanded into the cylinder with a dimension a then $m = \pi a^2 \rho$. When the length L of the rod is infinite (usually a good approximation when the $L > 10z$ then the (2.12) simplifies into the:

$$g = \frac{2\gamma m}{z\left(1 + \frac{x^2}{z^2}\right)}. \tag{2.13}$$

The depth z of the rod could be estimated from the half-width of the anomaly: $z = x_{\frac{1}{2}}$.

A lot of other geometric bodies could be found in the literature, enabling us to build a complex models. Examples of changes in gravity effect of dofferent bpdies with depth could be found in Figs. 2.10 and 2.11. Two examples of models using the spheres and cylinders are plotted in the Figs. 2.12 and 2.13.

More complex modelling could be done using the computer modelling and irregular bodies. Check, e.g. the Gordon Cooper's web page at the University of Witwatersrand (Cooper 2012).
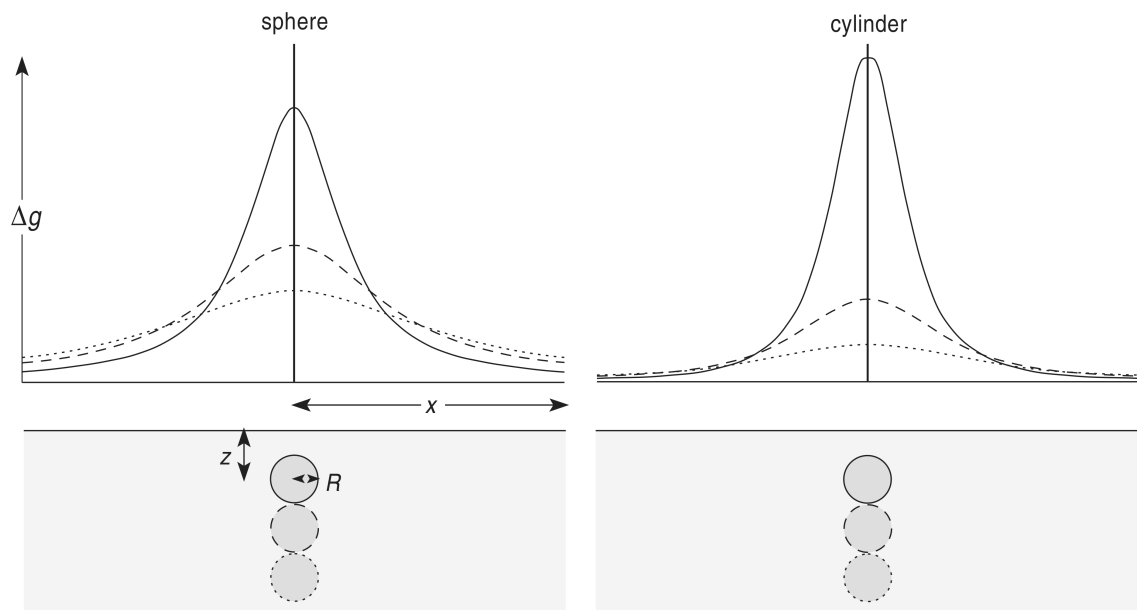
Figure 2.10: *Anomalies of a sphere and a horizontal cylinder at different depths. (Musset and Khan 2000)*
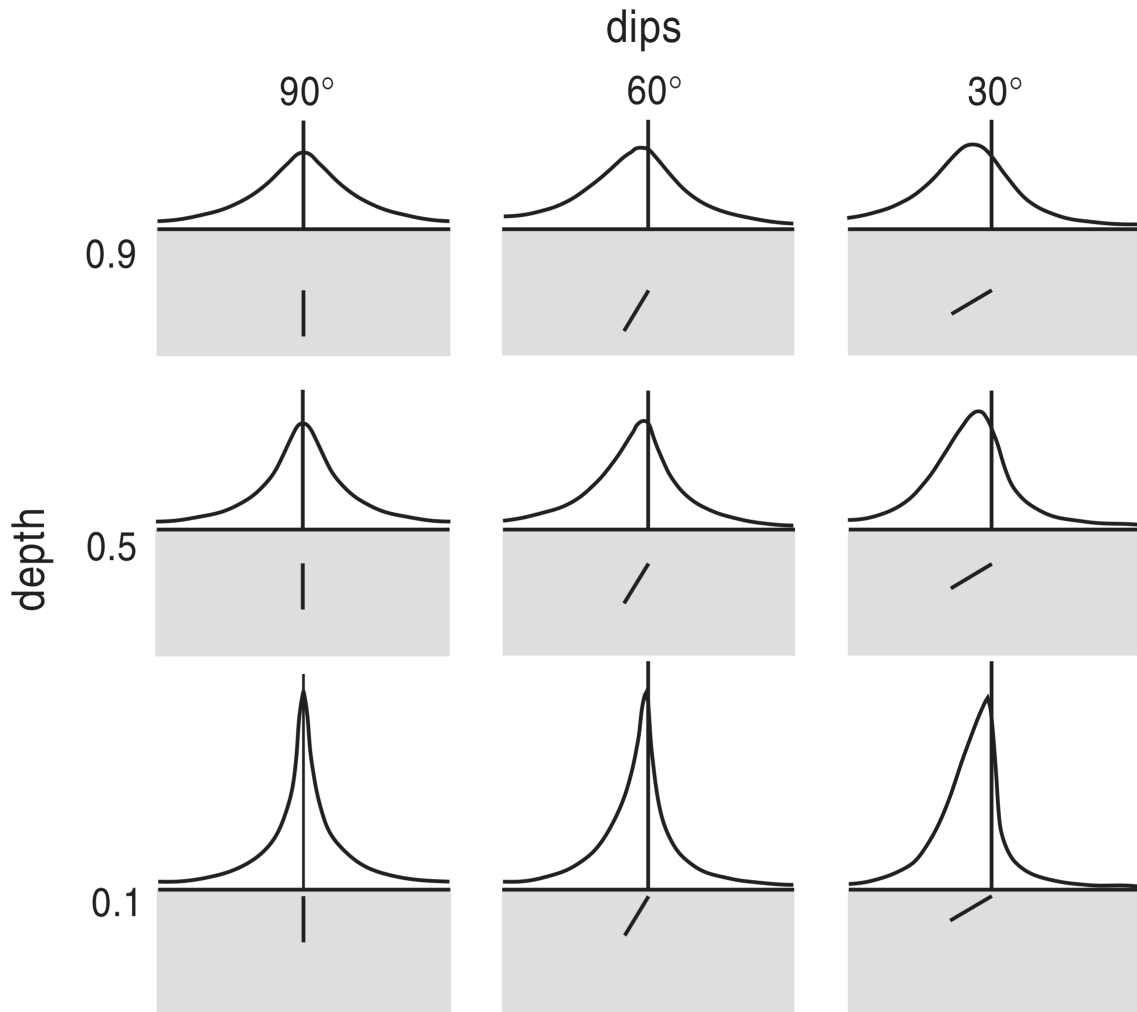
Figure 2.11: *Anomalies of narrow sheets at different depths and dips. (Musset and Khan 2000)*

2.6   Gravity data processing

Once the gravity data are measured the more demanding task is to be carried out – the data processing and interpretation. Some procedures of data processing has been already mentioned in the section 2.2.
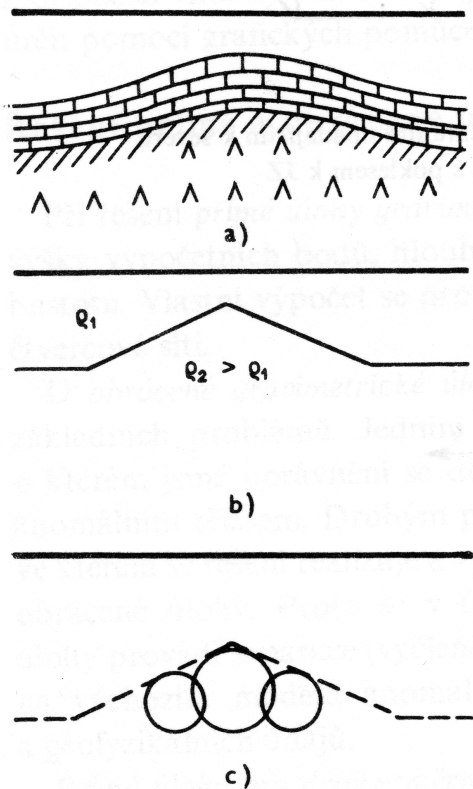
Figure 2.12: *Approximation of an anticline (Mareš and Tvrdý 1984). a) A geological section of an anticline. b) A schematic representation with density distribution. c) An approximation of the anticline by three infinite horizontal cylinders.*
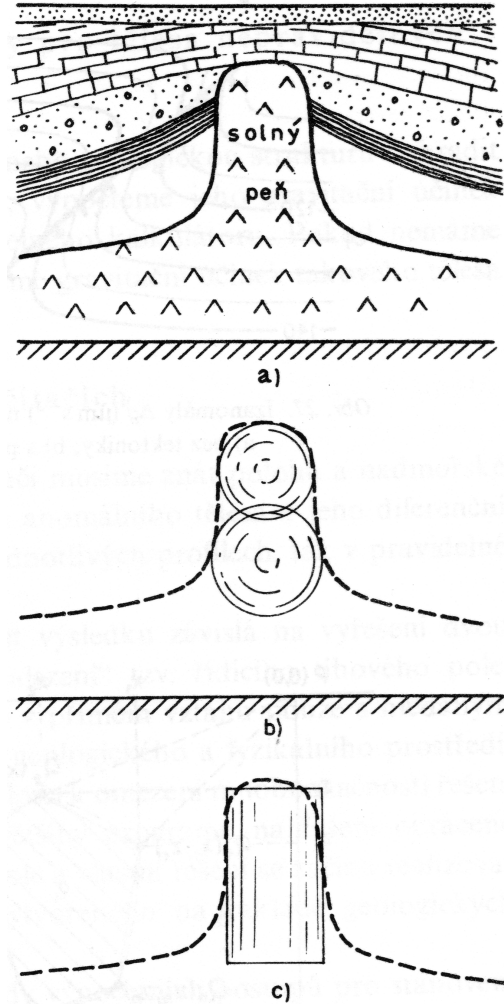
Figure 2.13: *Approximation of a salt diapir (Mareš and Tvrdý 1984). a) A geological section of a diapir. b) An approximation of the diapir by two spheres. c) An approximation of the diapir by a vertical cylinder.*

The first step in the data processing is deleting of wrong gravity readings. During the the field measurements there is usually several gravity readings taken at every station. Now, the *outliers* are removed and the rest of gravity readings from every station are averaged.

Next, the readings from the base station are taken to determine the *drift* of the instrument. First, these data need to be corrected for the different heights of the tripod, the free-air correction – equation (2.6). Second, the drift should be estimated – usually the data are interpolated using the second or third-order polynomial (Fig. 2.14).

Third, the readings at individual stations are corrected from the drift. The drift is estimated from the fitted polynomial according to the time of the gravity reading.
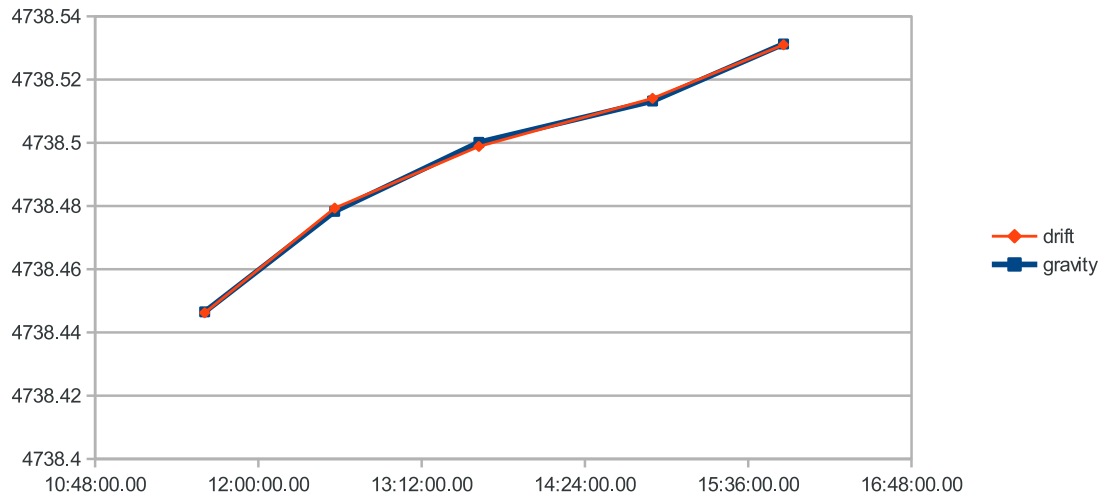
Figure 2.14: *Drift correction. The blue line shows the gravity readings at the base station corrected for the free-air. The red line depicts the third-order polynomial fitted into the gravity readings. This polynomial will be used to estimate the drift values for the readings at individual stations.*

Fourth, the drift corrected data are reduced again, now using the latitude, free-air and Bouguer reductions – see equation 2.8). If necessary, the density for the Bouguer slab is estimated (e.g. Nettleton's method).

There are also additional steps, which depends on the type of the survey and target structures. However, usually we want to suppress regional anomalies and enhance the local ones or vice versa.

The *regional anomalies* is a general term depending on the size of target structures. These anomalies are caused by large and deep structures, often larger than our survey area. In the data they usually represent the long-wavelength high-amplitude anomalies (Fig 2.15c, d). Sometimes they are also referred to as a *trend* (Fig. 2.15d). There are numerous techniques to remove the trend, the easiest are based on approximation by a polynomial. In this case we take the part of the data without our target anomaly and fit a polynomial through them. This polynomial approximates the effect of large-scale regional structures and we can subtract it from our data leaving us with *residual* anomalies. The residual anomalies are, in an ideal world, anomalies caused only by our target structures.

2.7 Gravity data interpretation

The interpretation of gravity data could be only a simple qualitative analysis in a way: "Look, there is a sharp local decrease of gravity, this could be a cave!" Or a more complex quantitative analysis, where, based on the qualitative assignment, we try to somehow model the subsurface. In this respect we have to bear in mind that the interpretation (inversion) of geophysical data is non-unique. In gravity prospection not only that different bodies could have similar anomalies (cf. figures 2.8 and 2.9) they can also produce exactly the same anomaly (Fig. 2.16). The non-uniqueness is inherent to gravity data and could not be overcome e.g. by adding more gravity data. The only way how to get sound and reliable interpretation is to include an a priori geological knowledge and, if possible, also data from another geophysical methods.

Another aspect is that the measured anomaly depends solely on the density contrast (difference) between the bodies. Hence a sphere with the density of $2.3\,\mathrm{g/cm^3}$ surrounded by the rocks with a density $2.5\,\mathrm{g/cm^3}$ will produce exactly the same anomaly as a sphere with the density of $2.5\,\mathrm{g/cm^3}$ surrounded by the rocks with a density $2.7\,\mathrm{g/cm^3}$. In a similar manner a half slab on one side of a fault with a positive density contrast could produce the same anomaly as a half slab on the other side with a negative density contrast (Fig. 2.17).
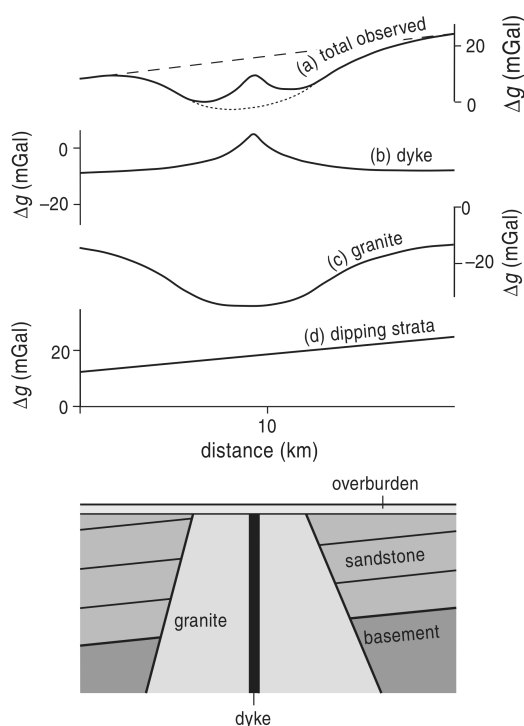
Figure 2.15: *Illustration of regional and residual anomalies (Musset and Khan 2000). The observed gravity curve contains information about all geological structures (topmost curve). If we are looking for the dyke, then the anomalies due to the dipping strata and granitic pluton are not relevant to our research and we would like to remove them from the data to ease the interpretation.*
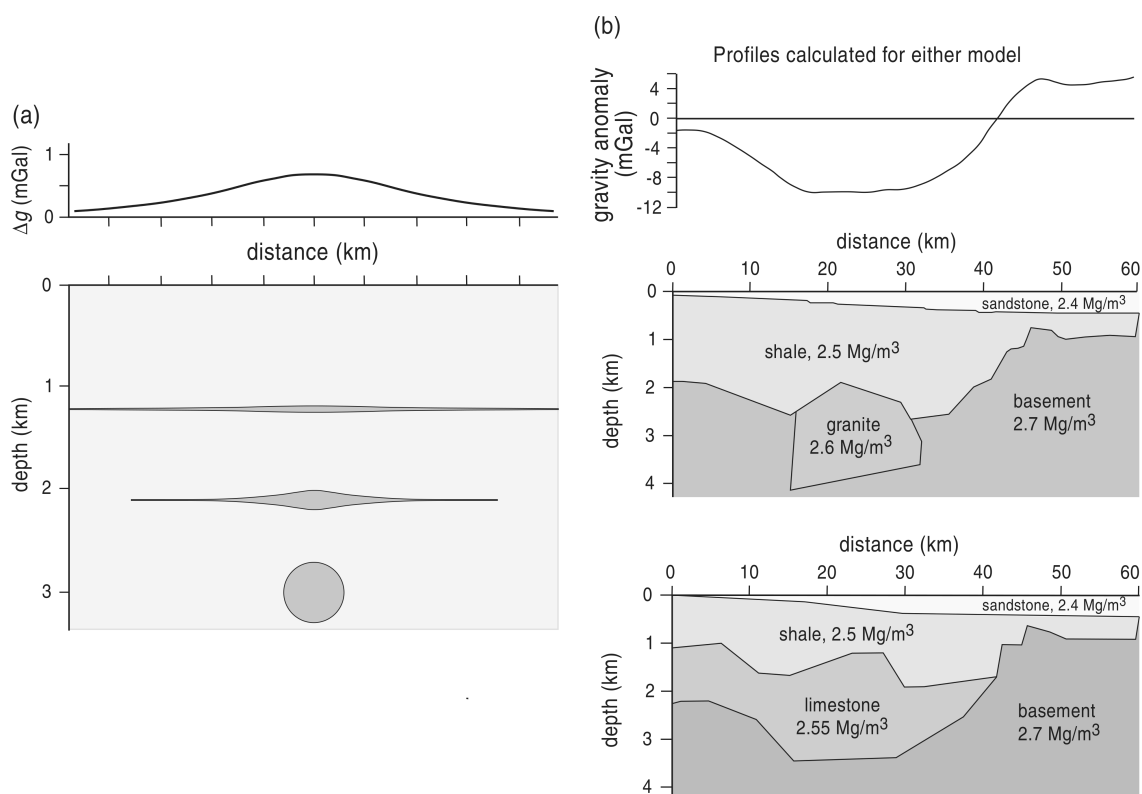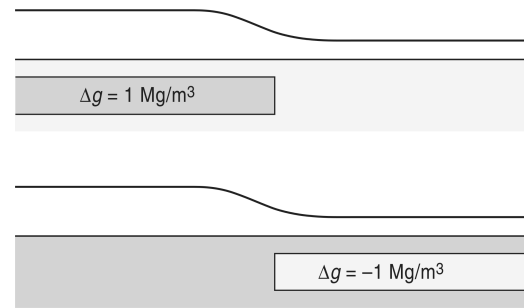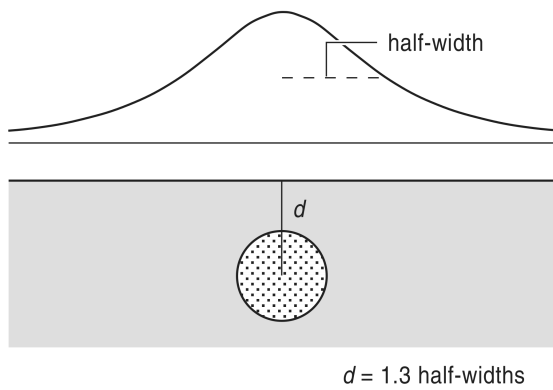

Figure 2.16: *Non-uniqueness of the gravity interpretation. The plotted models produce exactly the same gravity anomalies (Musset and Khan 200).*

Figure 2.17: *Two half slabs with the same anomaly (Musset and Khan 2000).*
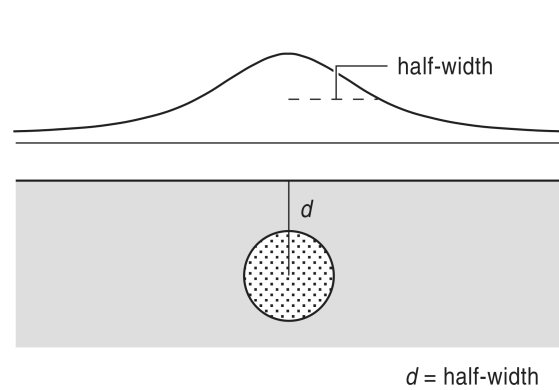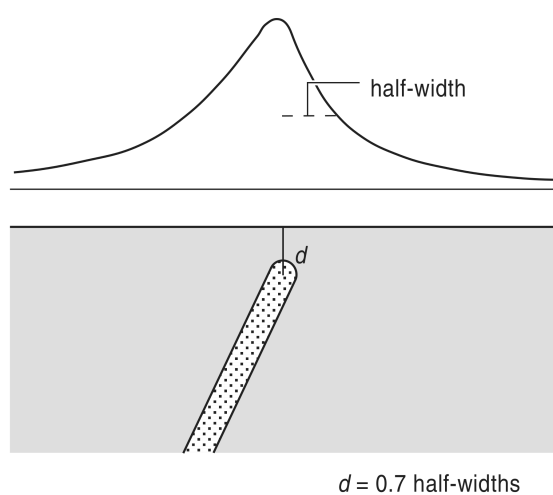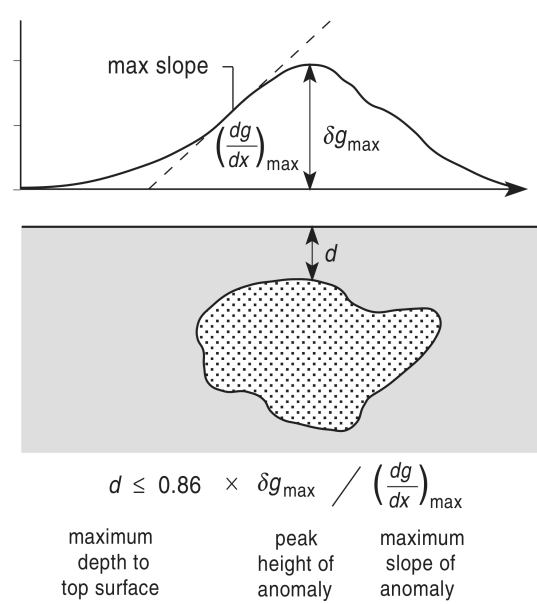

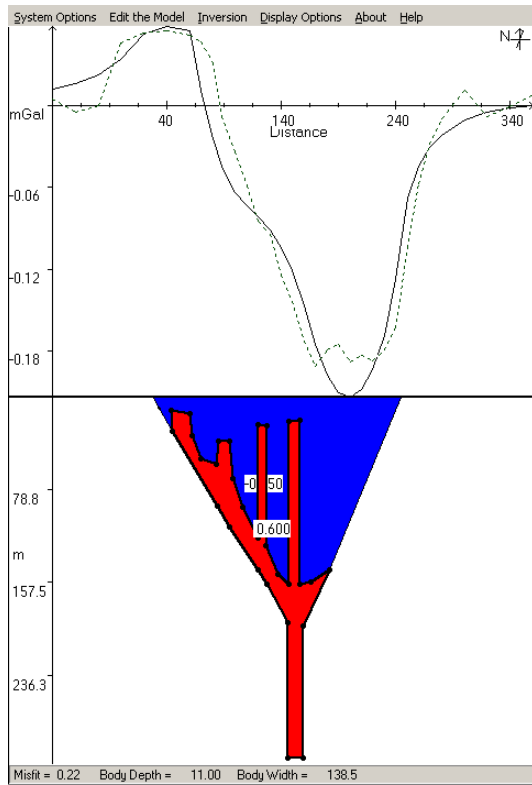**Figure 2.18:** *Depth rules for various bodies (Musset and Khan 2000).*

Figure 2.19: *Modelling a maar-diatreme volcano as a set of 2.5D bodies. In the top graph the measured gravity curve (broken line) and computed curve for the current model (solid line) can be seen.*

As we have already seen in the section 2.5, simple rules for estimation of depth of some simple bodies could be derived. There are some more in the figure 2.18. These rules are useful for estimating initial parameters for further modelling.

Building models from simple geometrical bodies is easy, however, one can easily see that not all the geological bodies could be easily approximated by them. Therefore, another modelling techniques were developed.

One of these is building the models from polygonal bodies with arbitrary number of corners (Figs. 2.16b, 2.19). There are formulas for computing gravity effects of such bodies, often based on the original Talwani's algorithm developed in late fifties (Talwani 1959). The modelled bodies are usually 2D (infinite in the y direction) or 2.5D (bodies have limited length in the y direction). However, equations for 3D modelling are also available. The advantage of this (polygonal) approach is in fact that the computations are fast and memory cheap and can be easily run on any of current computers. There are number of such computer programs available here and there (e.g. Cooper 2012, Fig. 2.19). The usual approach is to build an initial model estimated according to the measured gravity data and geological evidence and then using either a trial and error technique and to some extent also with automated inversion procedures we try to match the measured and modelled gravity curves. Due to the non-uniqueness of the gravity data, there are, unlike to some other geophysical methods, no "black-box" automated inversions. Currently, it is not possible to put data into some computer program, press a button and get the result. Although there are some attempts to achieve this.

Another approach is to divide the model into regular cells and assign each cell some density value (e.g. Snopek and Casten 2006). The cells are usually cubes, but any geometrical representation is possible. This kind of discretisation is common to many geophysical methods. The advantage is that arbitrarily complex models could be achieved. The drawback – the number of cells (and hence also the parameters) very quickly arises, mainly for the 3D case, and the computing gravity effect of such model is (computationally) very expensive.

2.8   Applications of the gravity method

The gravity measurements could, obviously, be applied anywhere where sufficient density contrast is expected. Nevertheless, there are situations and field conditions suitable and unsuitable. Lets start with the former.

One of the scenes where gravity excels is a regional geological mapping. It is due to the fact that the gravity meter is easily portable, does not need any wires and cables and one or two people are enough to operate it. Therefore, there is no logistic problem in measuring long (several kilometres or even more) traverses. Another advantage is the high depth reach – it is common to model structures in the depth of several kilometres (Fig. 2.20, 2.21).

Another field where the gravity measurements are indispensable is the mapping of voids (cavities). There are not many geophysical methods that could directly detect voids (ground penetration radar being the second). Therefore, the gravity method is often used to search caves (Fig. 2.22), old mines and galleries, or different voids and cavities beneath the roads.

Figure 2.20: *Bouguer anomaly map of the NW Czech Republic (Blecha 2009).*

Very common application of the gravity method is mapping of the sedimentary basins for the oil prospection. If the densitites of sediments are known (e.g. from boreholes) then not only the lateral extent but also the depth of the basins could be mapped. Another example from the oil prospection is the mapping of salt domes, since they often form oil and gas deposits.

This set of examples could be finished by a volcanological example – maar-diatreme volcanoes are often mapped using the gravity data. The eruption of the maar volcano is very forceful, the explosion creates a large crater and shatters the country rock. After the explosion, part of the material falls back to the crater, however, is "fluffed up" by the explosion and hence its density is lower then used to be. Therefore a gravity profile crossing the diatreme shows a distinct gravity low (Fig. 2.21). However, the best results are always obtained by combination of several geophysical methods. An example combining gravity and resistivity data is plotted in the figure 2.24.
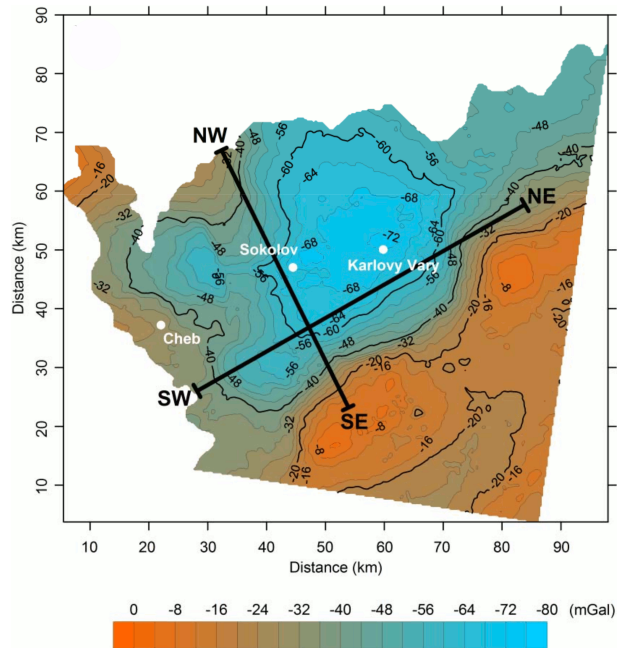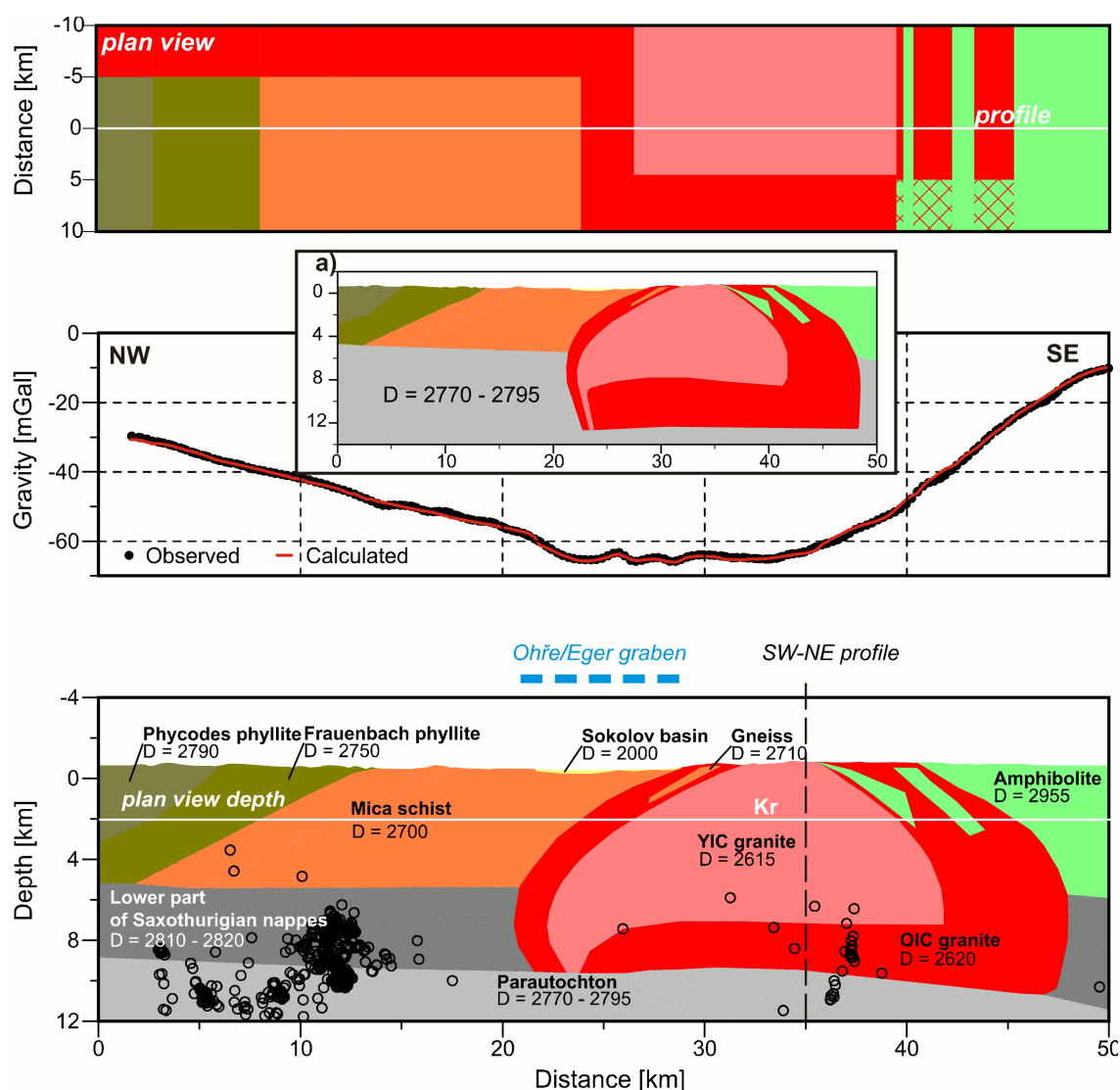
Figure 2.21: *Geological model along NW-SE gravity profile. Rock densities D are in kg/m 3. Kr - Krudum massif, intrusion of YIC granites. Inlet a): the depth of pluton floor would increase by about 2 km in case that the high density lower part of Saxothuringian nappes is omitted. Earthquake hypocenters less than 8 km from the profile are indicated by black circles. The upper panel shows the plan view of the model at a depth of 2 km b.s.l.; crossed areas in amphibolites (green color) indicate two different types of rocks in the area of plan view. (Blecha 2009).*
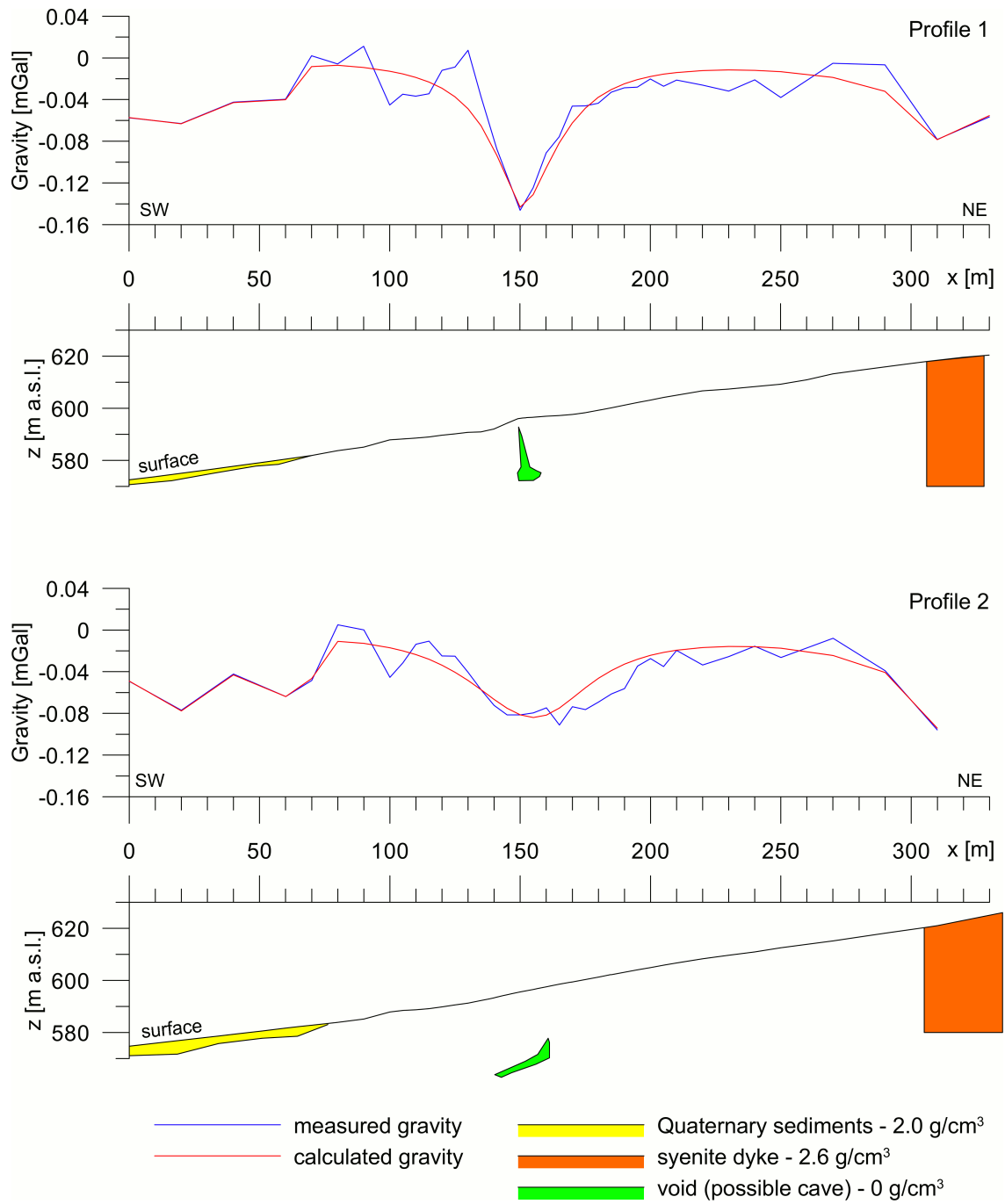
Figure 2.22: *Gravimetry profiles showing possible occurrence of an underground cavity.*
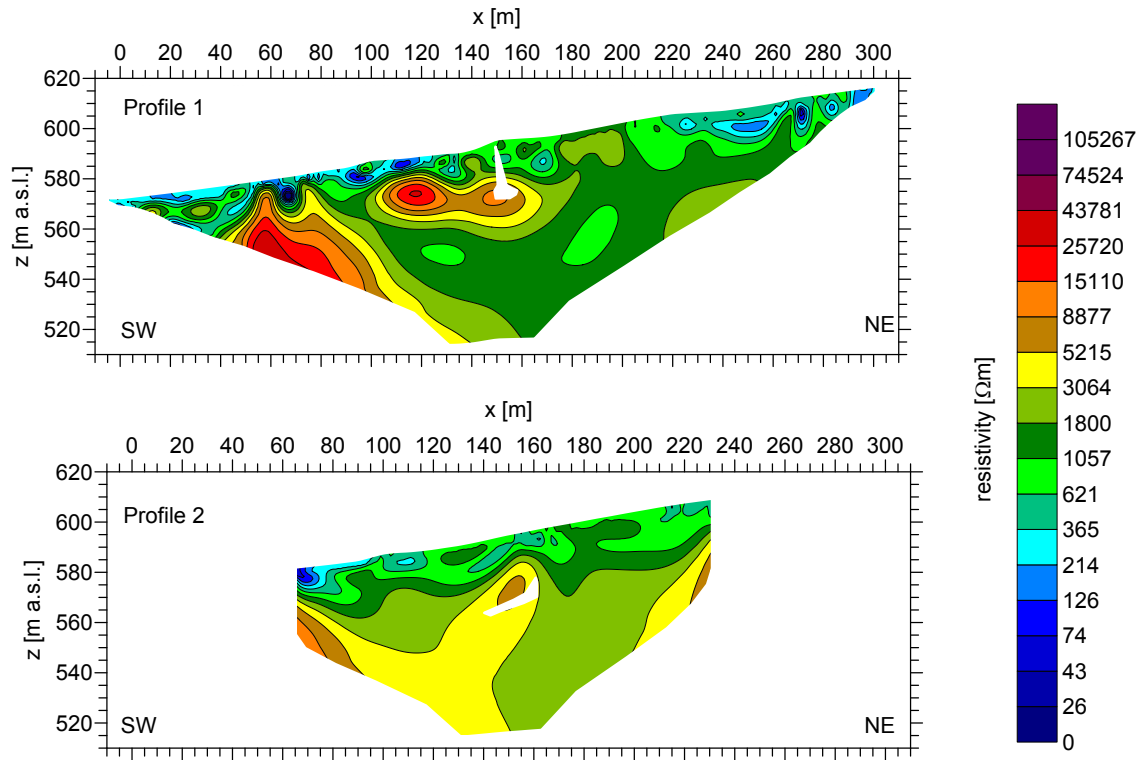
Figure 2.23: *Resistivity cross-sections along the gravimetric profiles from the figure 2.22. Areas with high resistivities (yellow, brown and red colors) represents blocks of marble where the caves could evolve. White areas represent caves modeled according to the gravity data.*
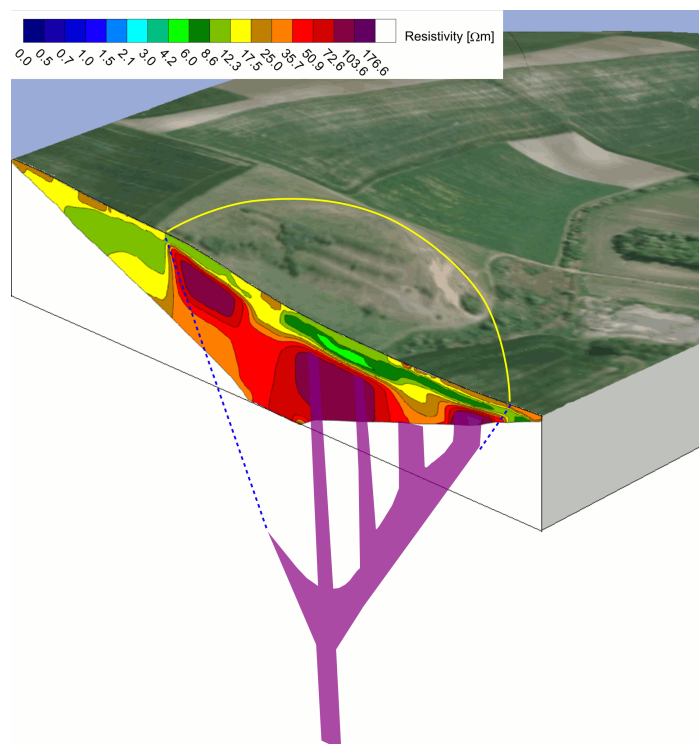

Figure 2.24: *A resistivity cross-section on the Tertiary maar-diatreme volcano from the Fig.2.19. High resistivities (in red) depicts area of volcanoclastic sediments and basaltic dikes. The yellow line highlights the extent of the diatreme on the surface, the blue dashed line depicts an interpreted shape of the diatreme. The interpreted basaltic dikes from are plotted in violet. The depth of the resistivity cross-section is 60 metres, the diameter of the diatreme is 220 metres.*

3

Magnetometry

The basic task of magnetic methods in prospection geophysics is to differentiate subsurface according to its magnetic properties. The original use of magnetometry was in the field of iron-ore prospection. The very iron rich ores in Sweden contained a considerable proportion of magnetite deviating the direction of Earth's magentic field. The expoloration was carried out with a regular compass – places, where it pointed to the Earth's magnetic north were places with increased amount of magnetite and hence the position of ore veins. Later on, where more sensitive measuring devices were constructed, the magnetometry started to be used also in other fields like geological mapping or archaeological prospection.

Magnetometry, being a potential method, has a lot of common with gravimetry and hence they are often measured and interpreted together. However, there are also significant differences. There are no magnetics monopoles (in contrast to gravity) and hence dipoles (and higher orders – quadrupoles and more) are the principal units. The magnetic field of the Earth is also less stable then the gravity field and could change quickly. In contrast to gravity maps the magnetic maps are dominated mainly by local anomalies. On the bright side, the differences in magnetization of different rock types are often quite large (much larger differences then in the case of densities). Moreover, the magnetic measurements are very easy to carry out and the measurements are very quick, hence a large areas could be easily covered making this method ideal for a general-purpose geological mapping.

As any potential method the magnetometry suffers from the non-uniqueness, similarly to the gravity method.

3.1 Basic principles

According to the electromagnetic theory the magnetic field is a consequence of a flow of electrically charged particles (electric current). A curent $\mathbf{I}$ in a conductor of length Δl creates at a point P a magnetizing field $\Delta \mathbf{H}$ (the Ampère's law - Fig. 3.1):

$$\Delta \mathbf{H} = (\mathbf{I} \Delta l) \times \frac{\mathbf{r}_1}{4 \pi r^2}, \tag{3.1}$$

where the $\mathbf{H}$ is the magnetizing field in amperes per meter, r and l are in metres, $\mathbf{I}$ is in amperes and the directions are as shown in Fig. 3.1. A current flowing in a circular loop acts as a magnetic dipole located in the canter of the loop (Fig. 3.2). The orbital motions of electrons around an atomic nucleus constitute circular currents and cause atoms to have magnetic moments. Molecules also have spin, which gives them magnetic moments.

A magnetizable body placed into the magnetic field becomes magnetized by induction. The magnetization is caused by reorientation of atoms and molecules so that their spins line up. The magnetization is measured by the *magnetic polarization* $\mathbf{M}$ (also called *magnetization intensity* or *dipole moment per unit volume*). The lineup of internal dipoles produces a field $\mathbf{M}$, which is added to the magnetization field $\mathbf{H}$. The SI unit for magnetization is ampere per meter (A/m).
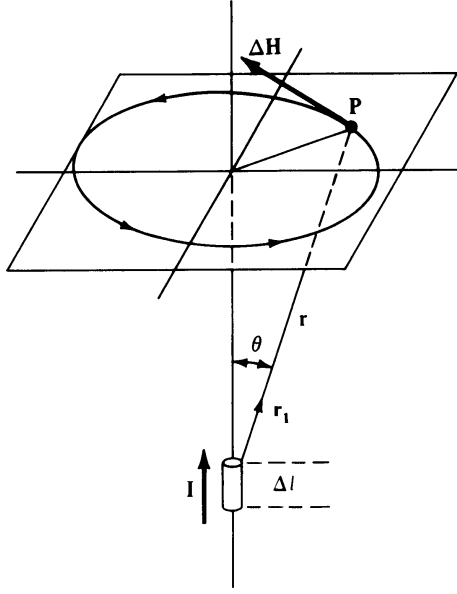
Figure 3.1: *Ampère's law. A current* **I** *through a length of conductor* Δl *creates a magnetizing field* $\Delta\mathbf{H}$ *at a point P. (Telford et al. 1990).*

For low magnetic fields, **M** is proportional to **H** and is in the direction of **H**. The degree to which a body is magnetized is determined by its *magnetic susceptibility k*, which is defined by

$$\mathbf{M} = k\mathbf{H}. \qquad (3.2)$$

The magnetic susceptibility is the basic rock physical parameter determining the applicability of a magnetic survey. The overall magnetic response of rocks is determined by amounts and susceptibilities of magnetic minerals in them. The susceptibilities of selected rocks can be found in Tab. 1.1.

The *magnetic induction* **B** is the total field including the effect of magnetization:

$$\mathbf{B} = \mu_0(\mathbf{H} + \mathbf{M}) = \mu_0(1 + k)\mathbf{H} = \mu\mu_0\mathbf{H}, \qquad (3.3)$$

where μ_0 is the permeability of free space which has the value of $4\pi \times 10^{-7}$ Wb/Am (Weber per ampermeter). In vacuum the $\mu = 1$ and in air $\mu \approx 1$. The SI unit for **B** is the tesla (1 T = 1 newton/ampere-meter = 1 weber/meter^2).

In magnetic prospection, the quantity measured is **B** although we are interested in Earth's field **H**. However, since usually the $\mu \approx 1$ we can treat a maps of **B** as if they were **H**.

3.2 Magnetic field of the Earth

From the point of view of the magnetic exploration we can divide the Earth's magentic field onto three componenets:

1. The main field originating within the Earth's interior and changing relatively slowly.

2. A small field (compared to the main field) which varies relatively rapidly and originates outside of the Earth.

3. Spatial variations of the main field, usually smaller than the main field and usually invariant in the time and place, caused by the inhomogeneities of the Earth's crust. These are the target of the magnetic exploration.

3.2.1 The main field

According to the electromagnetic theory the magnetic field is a consequence of a flow of electrically charged particles (electric current). A current flowing in a circular loop acts as a magnetic dipole located in the canter of the loop (Fig. 3.2).

The magnetic field of the Earth (the geomagnetic field) is supposed to be formed like this – by the electric currents flowing in the outer core, the geodynamo. The currents are generated by convection currents in the conductive liquid outer core, however, the process is complex and not fully understood so far. The principle component of the Earth's magnetic field is the dipole, but also higher orders are present. (These are predominating during the poles reversals, where the main (dipole) field is ceasing.)

Hence the geomagnetic field could be approximated by a dipole situated in the Earth's centre (Fig. 3.3). The dipole is not aligned with the rotation axis and hence the magnetic pole is deviated from the geographic pole. The deviation from the geographic direction is called the *magnetic declination* (Fig. 3.4). The angle at which the lines of the magnetic field intersects the Earth's
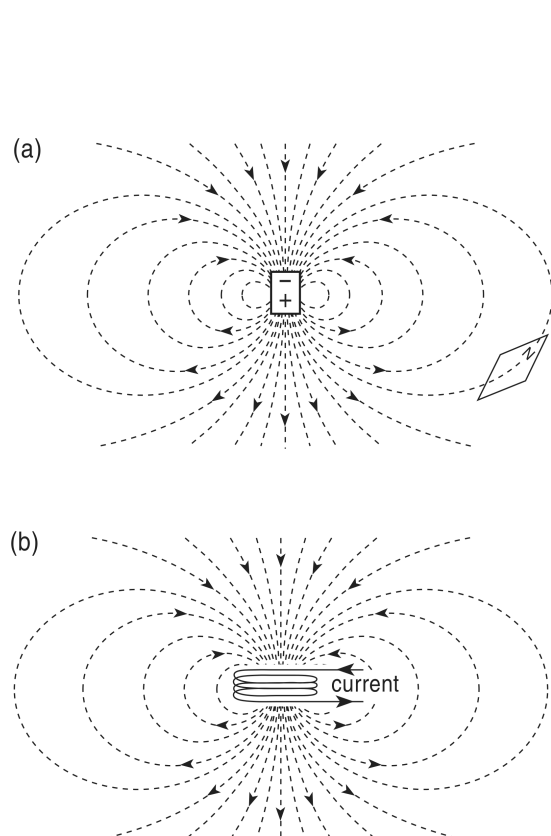
(a)

(b)

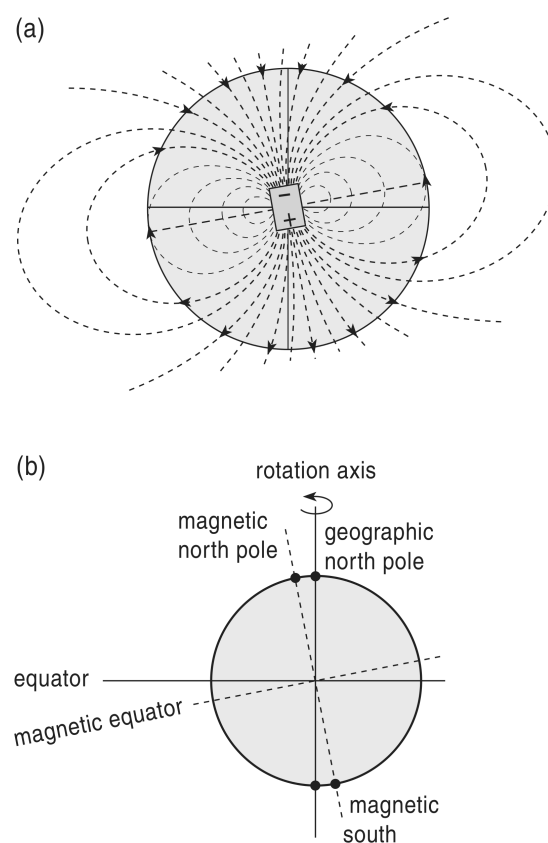**Figure 3.2:** *Magnetic field of a bar magnet and of a coil. (Musset and Khan 2000).*

(a)

(b)

Figure 3.3: *Magnetic field of the Earth. (Musset and Khan 2000).*
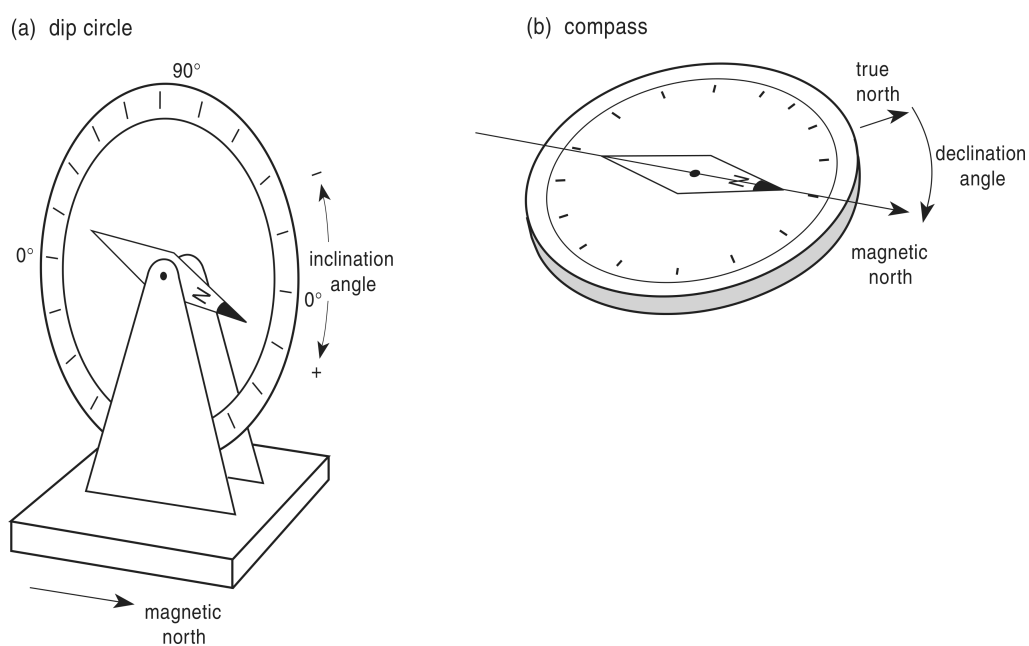
(a) dip circle

(b) compass

Figure 3.4: *Declination and inclination of the Earth's magnetic field. (Musset and Khan 2000).*
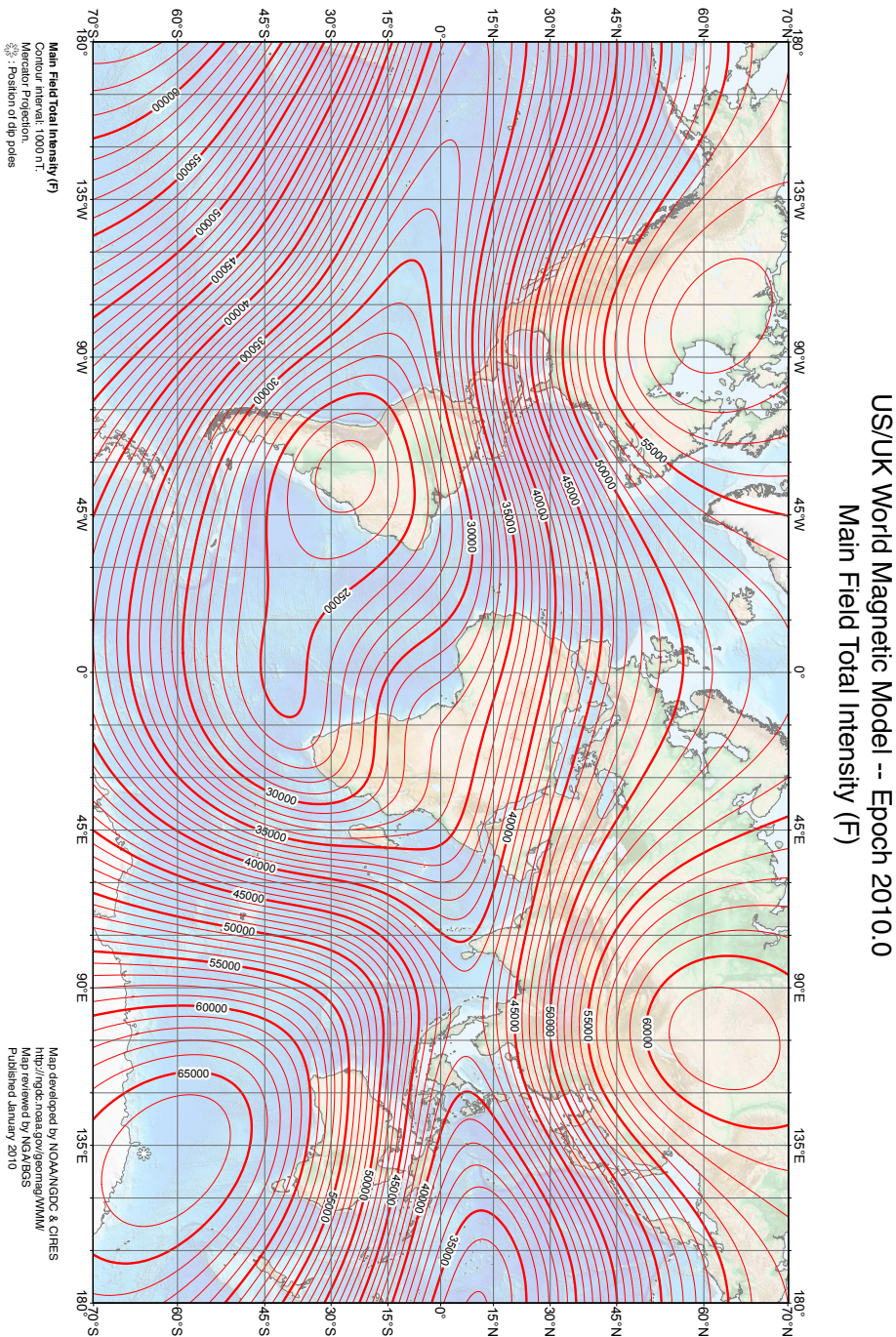
Figure 3.5: *The Earth's magnetic field in 2010 (source National Geophysical Data Center at NOAA). A world map of magnetic intensity.*
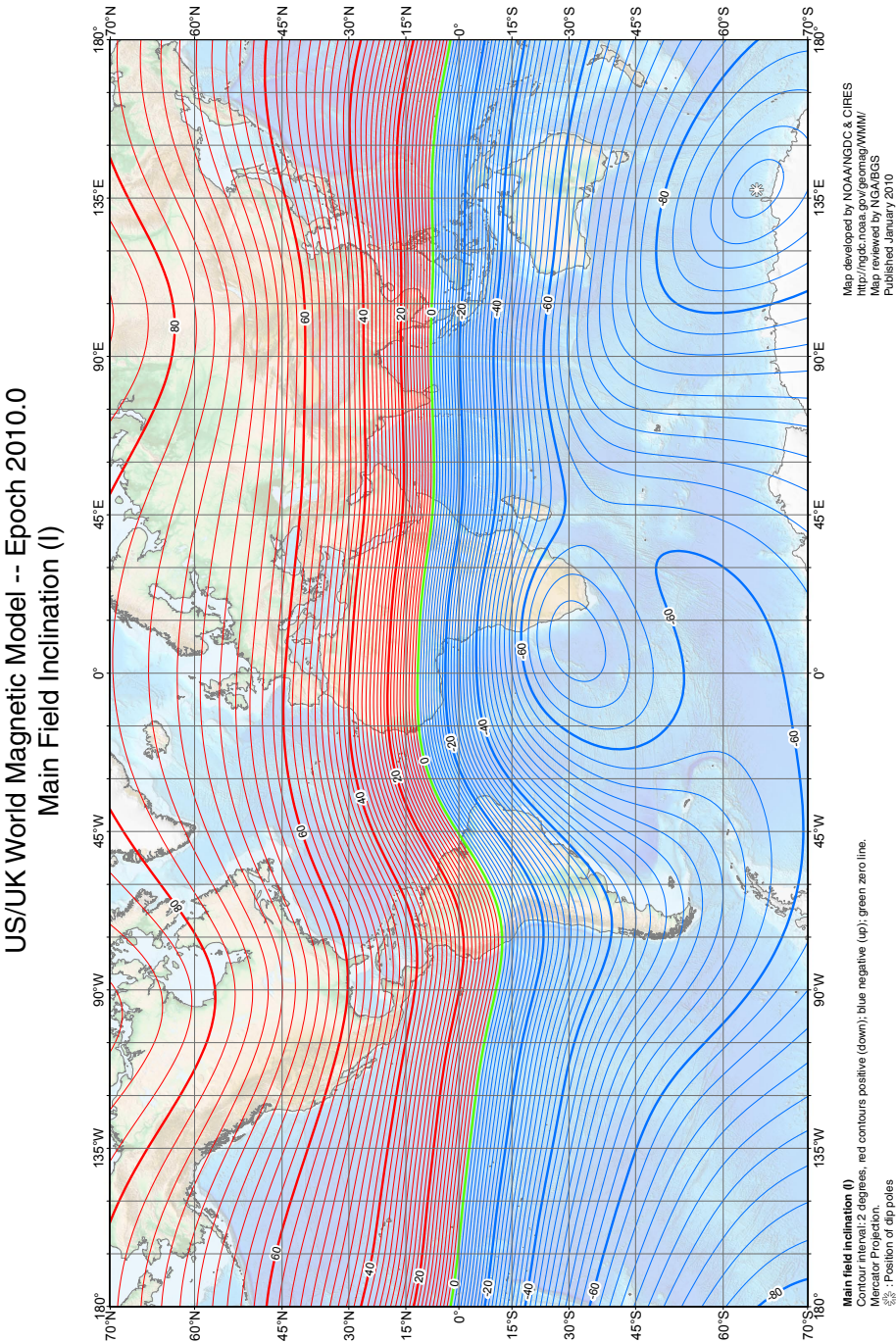
Figure 3.6: *The Earth's magnetic field in 2010 (source National Geophysical Data Center at NOAA). A world map of magnetic inclination.*
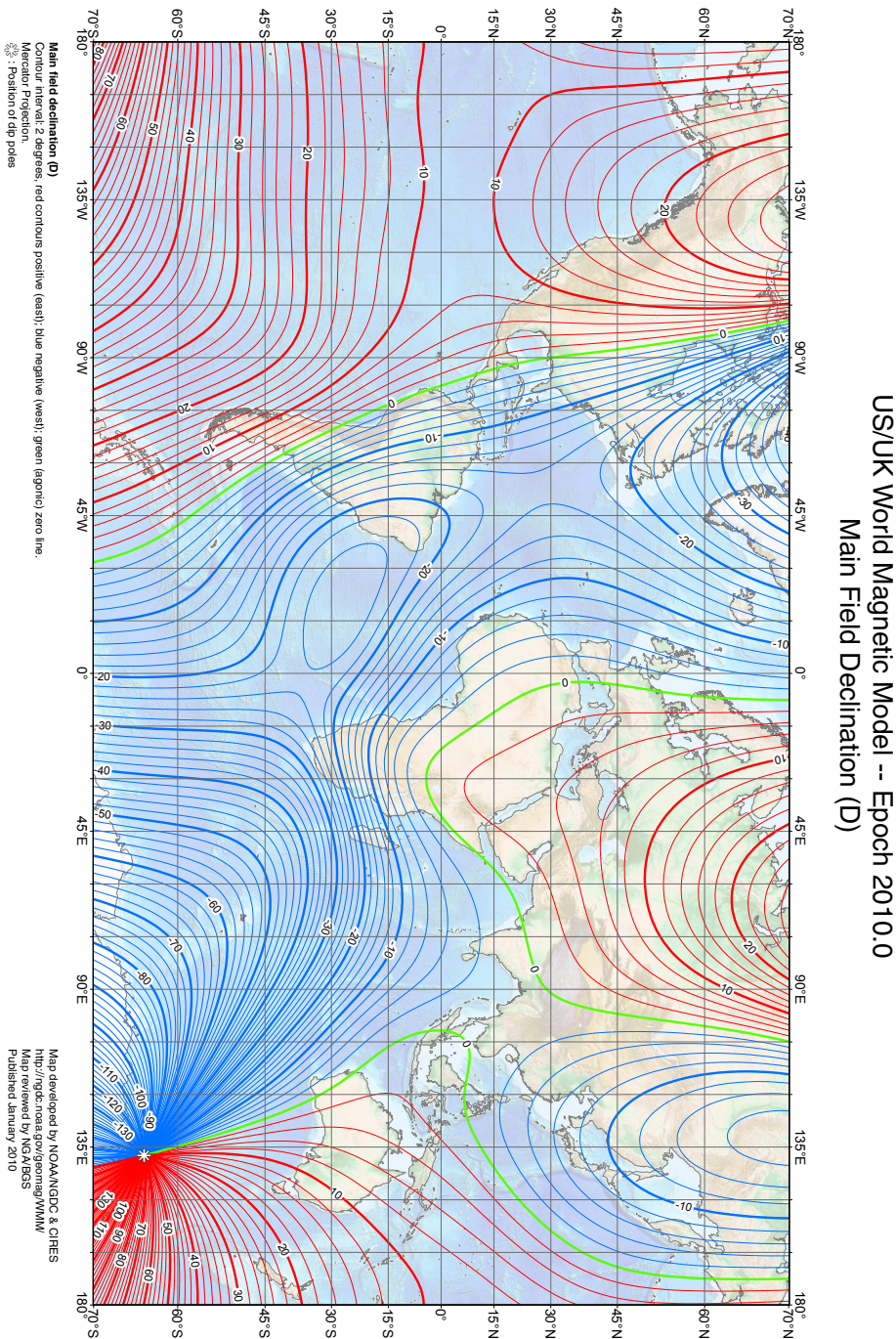
Figure 3.7: *The Earth's magnetic field in 2010 (source National Geophysical Data Center at NOAA). A world map of magnetic declination.*
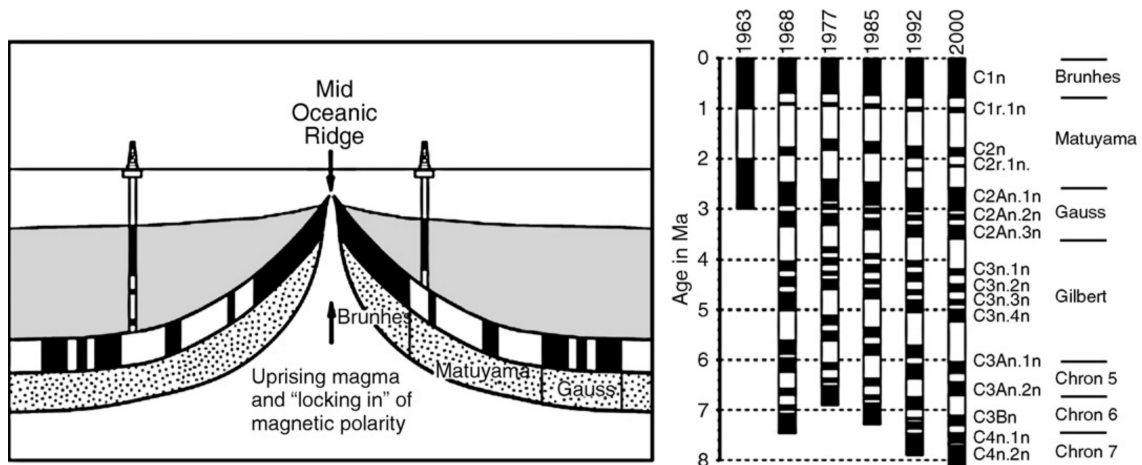
Figure 3.8: *Formation of marine magnetic anomalies during seafloor spreading (left). The oceanic crust is formed at the ridge crest, and while spreading away from the ridge it is covered by an increasing thickness of oceanic sediments. The black (white) blocks of oceanic crust represent the original normal (reversed) polarity thermoremanent magnetization (TRM) acquired upon cooling at the ridge. The black and white blocks in the drill holes represent normal and reversed polarity depositional remanent magnetization (DRM) acquired during deposition of the marine sediments. Development of the geomagnetic polarity time scale (GPTS) through time (right) shows that the initial assumption of periodic behavior (in 1963) was soon abandoned as new data became available. The first modern GPTS based on marine magnetic anomaly patterns was established in 1968. Subsequent revisions show improved age control and increased resolution (Krijgsman and Landereis 2008).*

surface is called the *magnetic inclination* (see Figs. 3.3 and 3.4). The inclination is called positive when the lines point down. Therefore, it ranges from 90°at the north magnetic pole through the 0°at the magnetic equator down to -90°at the south magnetic pole. See also Figures 3.5, 3.6 and 3.7. Since the overall geomagnetic field does not reflect any features of surface geology (mountain ranges, mid-ocean ridges, etc.) it implies that the source of the field is located deep within the Earth.

Paleomagnetic data show that the magnetic field has always been roughly oriented parallel to the Earth's rotation axis suggesting that the convective currents are connected to the Earth's spin.

The geomagnetic field slowly changes throughout the time – *secular variations* of the field. The position of the poles changes as well as its intensity. The period of these changes is long – e.g. there is a set of eight places with high changes of geomagnetic field (also called *foci*). These *foci* moves slowly westwards, it is estimated that they will travel around the globe in about 1800 years. Changes of the position of the poles (and consecutive changes of inclination and declination) are thought to be caused by changes in the convection currents within the Earth's core.

The orientation of the geomagnetic field is more or less stable for a long time (e.g. more than several tens or hundreds thousands of years). However, time to time the orientation swaps – the north pole moves suddenly to the south and vice versa. – *reversals of geomagnetic field*. The changes are sudden (in comparison with time of the stable field, the durations of reversals are modelled to last one or several thousands of years). During the reversals, the dipole field ceases and only the higher-pole fields are present, hence the overall geomagnetic field is much smaller and there is no magnetic north and south.

The sudden changes of geomagnetic field were documented on samples from boreholes and outcrops all around the globe and were assembled into a magnetostratigraphical chart (Fig. 3.8). The received "barcode" pattern could be used for dating geological samples (Fig. 3.9). First of all, one have to obtain some initial estimate of possible age of the sampled profile. Next, the reversal pattern could be correlated with the chart. The advantage of magnetostratigraphy (over e.g. the
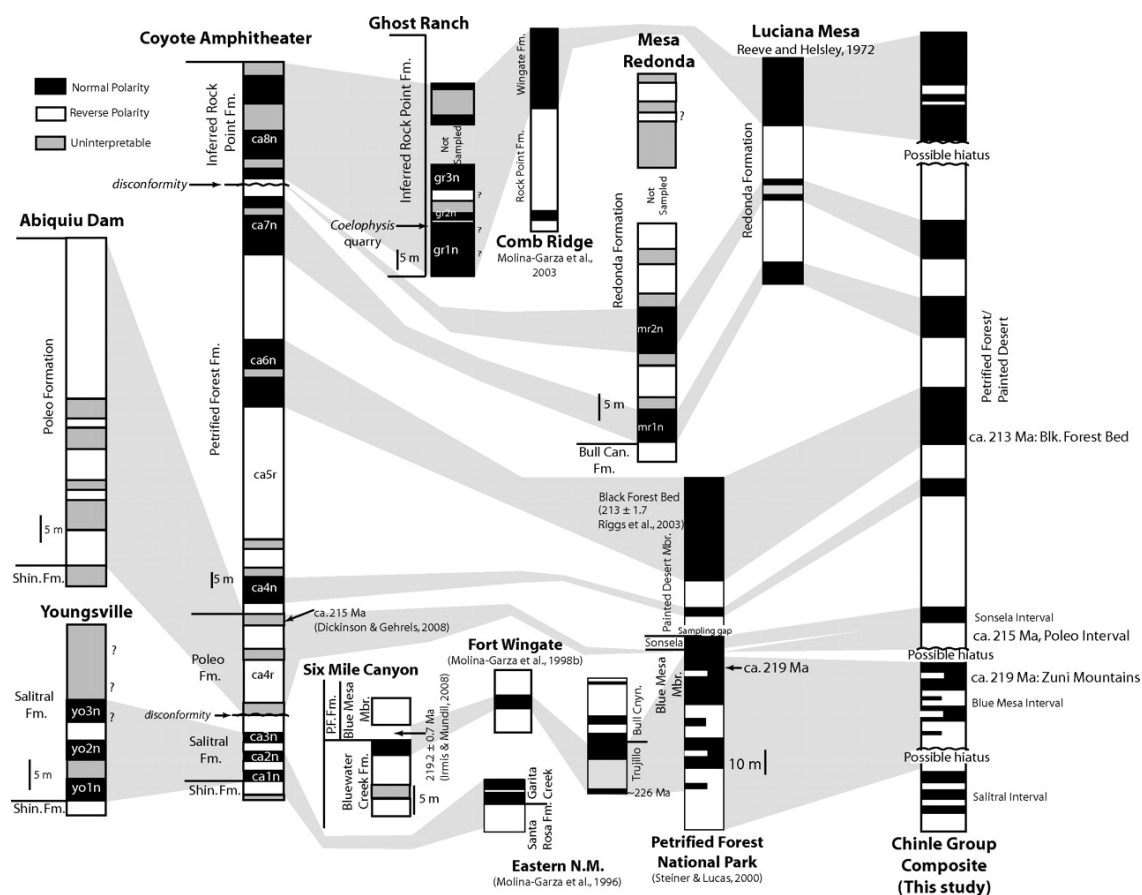
Figure 3.9: *Correlation of magnetostratigraphical profiles (Zigler and Geissman 2011).*

biostratigraphy) is in the fact that the polarity reversals are sudden, globally-synchronised, have the same effect on the shore and in the ocean and in all climatic zones.

3.2.2 The external magnetic field

The changes in geomagnetic field caused by external sources have lower amplitude than changes stemming from the internal changes, however, their period is much shorter and thus could seriously affect magnetic survey. The periodical variations are the *Solar diurnal variations* with period of 24 hours and amplitude of several tens of nT and *Lunar variations* with period of 25 hours and amplitude of 2 nT. Next, there are emphshort period variations with periods of tenth of seconds up to tu tens of minutes with amplitudes from tenth of nT up to tens of nT. These could be periodical or random and are mostly effects of the Solar activity. The most important are *magnetic storms*. They are effect of increased Solar activity, could appear several times per month and last even for several days. The amplitude of the storms could be several thousands of nT and have a random fluctuation.

Effects of these variations could be easily removed from the measured magnetic data in a similar way as in the gravity prospection – using a base station and subtracting the base-station data from the measured ones. However, the magnetic storm has such a high amplitudes and random course that it is best to avoid measurements during the storm.

3.2.3 Spatial variations of the main field

Local variations of the main field originates from the local change in concentration of magnetic minerals in the near surface rocks. The anomalies could have very different amplitudes, exceptionally they could even double the Earth's main field. They are usually localised and hence the
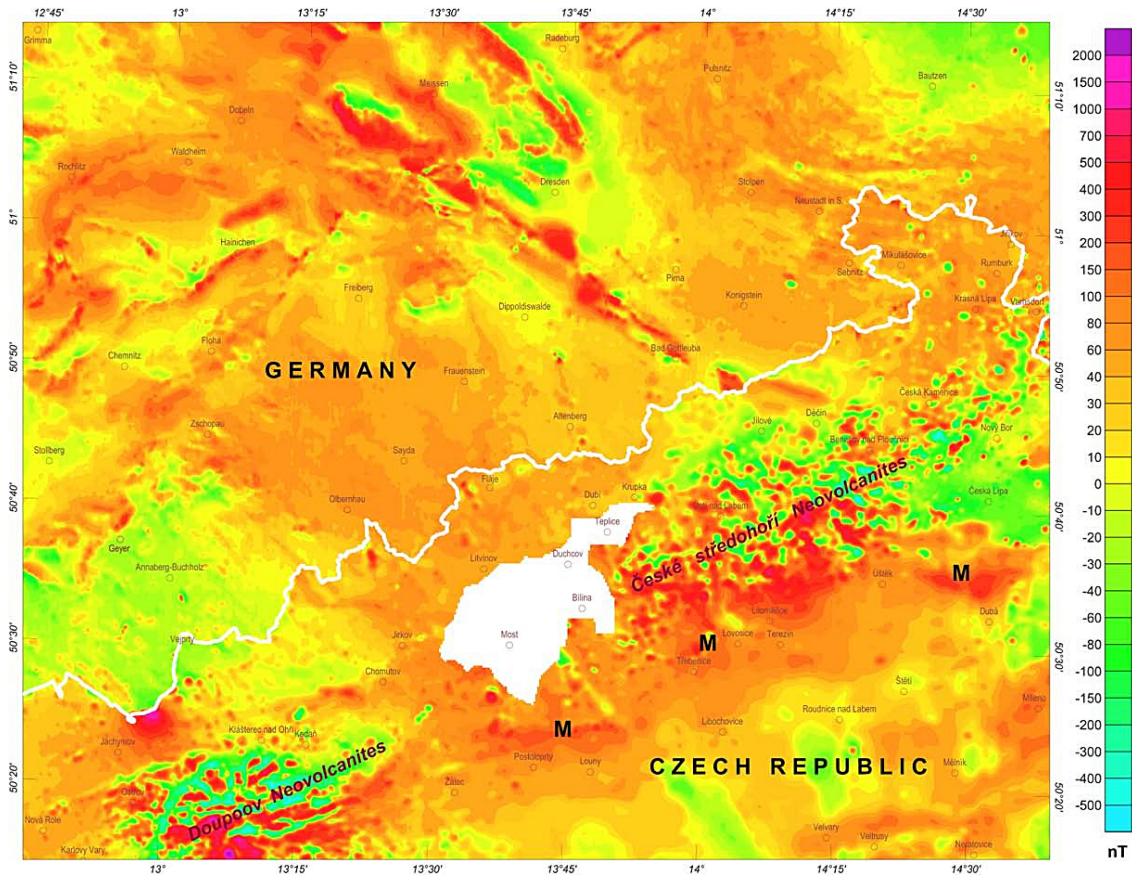
Figure 3.10: *Magnetic map of the NW Bohemia. The short wave anomalies (mosaic-shape fields) are caused by Tertiary volcanites. (Sedlák et al. 2009).*

magnetic maps are often hard to read (Fig. 3.10, compare with the Bouguer anomaly map in Fig. 2.20). The sources of magnetic anomalies could not be very deep since temperatures below $\sim 40\,\mathrm{km}$ should be above the *Curie point*, the temperature at which rocks lost their magnetic properties ($\approx 550\,^{\circ}\mathrm{C}$). Thus local anomalies must be associated with features in the upper crust.

3.3 Magnetism of rocks and minerals

The overall magnetization of the rocks is a vector sum of induced magnetization (the magnetization present only if an external field is applied, ceases, when the external field is removed) and natural remanent magnetization (present even without the external magnetic field). For example, effusive rocks have have the remanent magnetization often much stronger than the induced one.

According to their behaviour when placed into an external magnetic field, the materials could be divided into two main groups – *diamagnetic* and *paramagnetic*
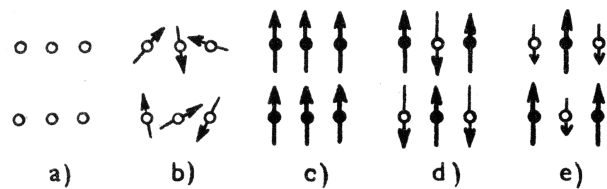

Figure 3.11: *Schematic diagram showing orientation of magnetic moments in the crystal lattice of different materials: a) diamagnetic, b) paramgnetic, c) ferromagnetics, d) antiferromagnetics and e) ferrimagnetic (Mareš and Tvrdý 1984).*

(Fig. 3.11). Diamagnetic material is dominated by atoms with orbital electrons oriented to oppose

the external field – the susceptibility is negative (see Tab.1.1). Diamagnetic materials are graphite, quartz, feldspar, marble, salt, etc.

Atoms of paramagnetic materials have non-zero moments without the presence of external field and magnetic susceptibility of such materials is positive. The direction of magnetization of individual atoms is randomly oriented and their vector sum is non-zero, but weak. In presence of external field, the magnetic atom slightly aligns forming a weak magnetization – an induced magnetization. When the external field is removed, the magnetization ceases. The magnetic effect of diamagnetic and most paramagnetic substances is weak.

Certain paramagnetic materials (iron, nickel, cobalt) could have such strong magnetic interactions that the magnetic moments in large regions – *domains* – align. This effect is called *ferromagnetism* and is about 10^6 times the effect of diamagnetism and ferromagnetism. The ferromagnetism decreases with increasing temperature and ceases when temperature exceeds the Curie point.

Some materials have domains further divided into subdomains with opposite orientation and the overall magnetic moment nearly cancels. These materials are called *antiferromagnetic* and their susceptibility is low. The common example is hematite.

The last group have subdomains also aligned in oppositions, however their net magnetic moment is non-zero. This could be either due to the fact that one orientation of subdomains have weaker moment or that there is less domain with one of orientations. Such substances are called *ferrimagnetic*. Examples of the first type are magnetite, titanomagentite, oxides of iron and of iron and titanium. The second group is represented by pyrrhotite.

The induced magnetization is directly proportional to the susceptibility and concentration of magnetic minerals present in the rocks. The orientation is, naturally, the same as that of the external field (geomagentic field in our case). However, the measured magnetization is not always of this direction. Responsible for this phenomena is the *remanent magnetization*. The remanent magnetization is present even if we remove the external magnetic field. The most common types of remanent magnetization are described below.

Thermoremanent magnetization is created when magnetic material is cooled below the Curie temperature in the presence of external magnetic field (usually the Earth's magnetic field). Its direction depends on the direction of the external field at the time and place where the rock cooled.

Detrital magnetization have fine-grained sediments. When magnetic particles slowly settles they are oriented into a direction of an external field. Various clays exhibit this type of remanence.

Chemical remanent magnetization is created during a grown of crystals or during an alteration of existing minerals. The temperature must be low (below the Curie point). This type might be significant in sedimentary or metamorphic rocks.

Isothermal remanent magnetization is the residual left following the removal of an external field. Its amplitude is low unless it was created within very large magnetic field like during the lightning strike.

Viscous remanent magnetization is produced by a long exposure to an external field. It grows with a logarithm of time. It is common for all rock types, the direction is usually close to the direction of present magnetic field, is quite stable and an amplitude could be up to 80% of the induced magnetization.

Dynamic remanent magnetization is created when a rock is exposed to variate pressures within a magnetic field. The pressures could be of various types ranging from tectonic or seismic pressures up to hammer strikes.

3.4   Field instruments for magnetic measurements

The earliest devices for magnetic prospection were different modifications of mariner's compass to mesaure inclination and declination (see Fig. 3.4). In the course of time different types of

magnetometres were developed. Currently the most often used types are the proton-precession, fluxgate and optically pumped magnetometers.

The proton and fluxgate magnetometers has similar sensitivity (about 1–0.1 nT), the difference is in the components of magnetic field measured. The proton magnetometer measures the *total field* – the overall amplitude of the magnetic field (a vector sum of X, Y, Z directions) whereas the fluxgate magnetometers measure individual components. The fluxgate magnetometres are capable of continuous measurements and hence are used for airborne, ship and satellite measurements. In contrast, the proton magnetometers does not have a drift and are common in ground surveys.

The optically pumped magnetometers (most common is the caesium vapour magnetometer) offers much higher sensitivity (∼0.001 nT) and also high frequency of readings (up to 1000 Hz, usually could log 5 times per second, so that continuous measurements are possible). They are often used for archaeological prospection, but their price is high (more then twice the price of a proton one).

3.4.1   Proton-precession magnetometer

The proton magnetometer is currently the most common type. It is cheaper than the optically pumped magnetometer and has also a lower sensitivity (typically about 0.1 nT). They are based on the precession of protons in the magnetic field. The proton – nucleus of the hydrogen atom – have a magnetic moment which aligns with a direction of an external magnetic field. The nucleus is spinning and when the external magnetic field changes the nucleus aligns with the new direction. Since it is spinning it does not align instantly but it twists around its center, similar to a gyroscope (Fig. 3.12). This effect is called precession. The angular velocity (or frequency) of precession is proportional to the magnetic field.

The proton magnetometer has a container filled with a hydrogen rich liquid (e.g. a water or an alcohol). A coil is wounded around the container. When an electric current is passed into the coil, the magnetic field is generated (about 5 to 10 mT) and the protons are aligned with this field. Then the current is switched off and pro-

Figure 3.12: *Proton precession (Telford et al. 1990).*

tons start to align with the Earth's magnetic field, precessing. In the coil the electric current is induced by the electromagnetic induction. The frequency is measured and strength of the magnetic field computed.

There are two requirements for successful readings. First, the coil has to be roughly aligned so as its field is in a large angle with the direction of the measured field. And second, the field to be measured should be uniform throughout the container. Otherwise protons in different parts of the container would precess with different frequencies and the readings would be wrong. A small, strongly magnetic bodies (e.g. an piece of iron) could cause non-uniformity of the magnetic field in the container.

The measurement of one sample with this type of magnetometer takes several seconds.

3.5   Magnetic surveying

Magnetic surveys are in some respects similar to gravity surveys and the magnetic data well complement the gravity ones. Therefore one often complements the other. Both methods deal with potential field with its inherent non-uniqueness, both are well suited for regional geological surveys, discrimination of different rock types based on the density and susceptibility works reasonably well.

To get an idea how the magnetic anomaly is created imagine a buried magnetized body (Fig. 3.13). To make things simple, lets assume that we can approximate its magnetization with a dipole positioned in its center. The magnetic field produced is indicated by dashed lines. The
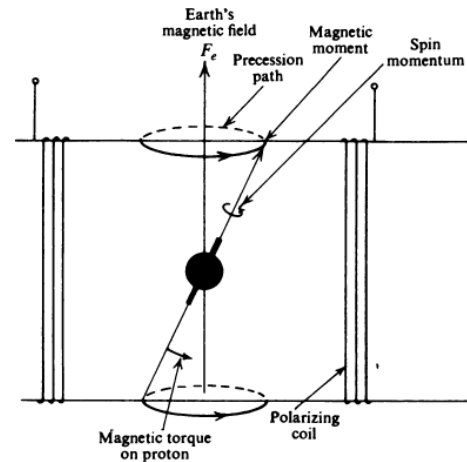
(a) anomaly

(b) addition of fields

(c) field of body

Figure 3.13: *Magnetic field of a burried dipole (Musset and Khan 2000).*

Earth's magnetic field is also present and adds to this field. The overall field is a vector sum of these two components.

At places, where the two fields are opposite, a minimum is created (negative anomaly). The anomaly of a body depends not only on magnetization of the body but also on a direction of Earth's magnetic field which depends on the magnetic latitude – hence the magnetic anomalies are far more complex then the gravity ones. Further is the effect of latitude illustrated in Fig. 3.15.

3.5.1 Magnetic effects of a sphere and a vertical sheet

We have illustrated that the magnetic anomalies are much more complex then the gravity ones. Hence we will not deal with them with such a detail as we did within the gravity chapter. The process of anomaly computation is similar as we have already seen in the gravity chapter and equations needed can be found in textbooks mentioned in references. Nevertheless, we are going to show some simple curves here to give some impression of what one could expect.

The uniformly magnetized sphere has a same magnetic effect as a dipole located in its center. The curves over a magnetic dipole are plotted in Figs. 3.15 and 3.14.

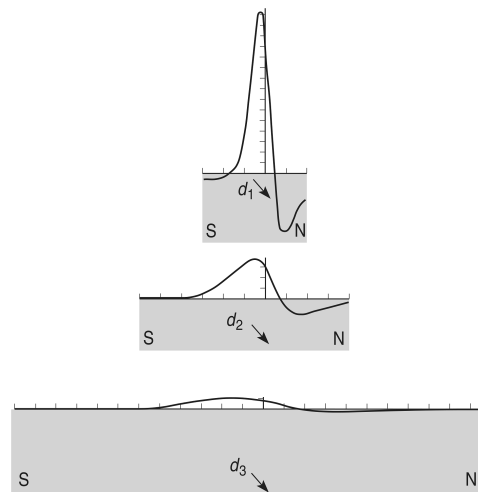The positive and negative poles of magnet are always present together, regardless on how large or small the magnet is. Hence, if we cut a magnet into two, both halves would have its own positive and negative pole. Conversely, if we take two magnets and put them together such that positive pole is next to the negative one, they form a single magnet with poles on its ends.

This is because the magnet is formed from a large number of magnetic atomic dipoles. In the center of the magnet, there is a same number of positive and negative poles and their field cancels. In contrast, at the ends of the magnet one type of poles prevails and hence the magnetic field is produced outside of the magnet here. Therefore, when considering magnetic effect of an extended body we need to consider only the poles that form near the surfaces. On which side of the body the poles appear depends on the direction of the Earth's field (Fig. 3.16) – assuming that the magnetization is in the direction of the Earth's field.

The procedure is further complicated if a remanent magnetization is present. Particularly, the thermoremanent magnetization could be considerably high. The *Königsberger ratio* **Q**, a ratio between the remanent and induced magnetization

$$\mathbf{Q} = \frac{\mathbf{M_r}}{\mathbf{M_i}},$$
(3.4)

could be, especially for the effusive basic rocks, much higher then 1. This means that the measured magnetic

Figure 3.14: *Anomalies of dipoles at different depths (Musset and Khan 2000). Note the changes in amplitude and width of the anomaly.*
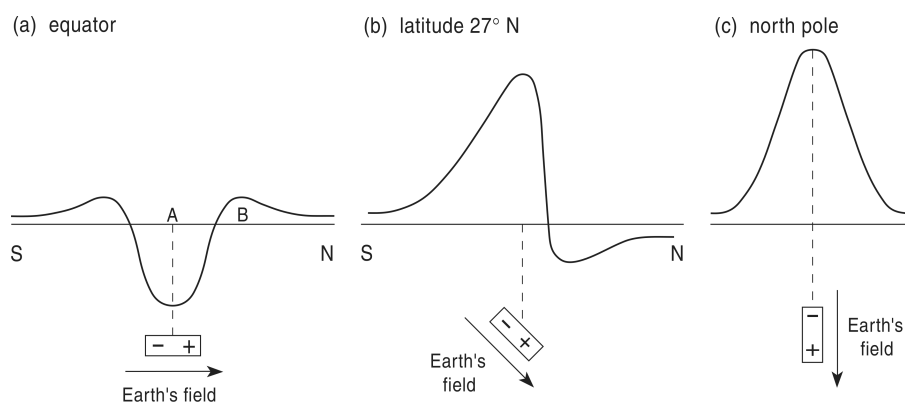
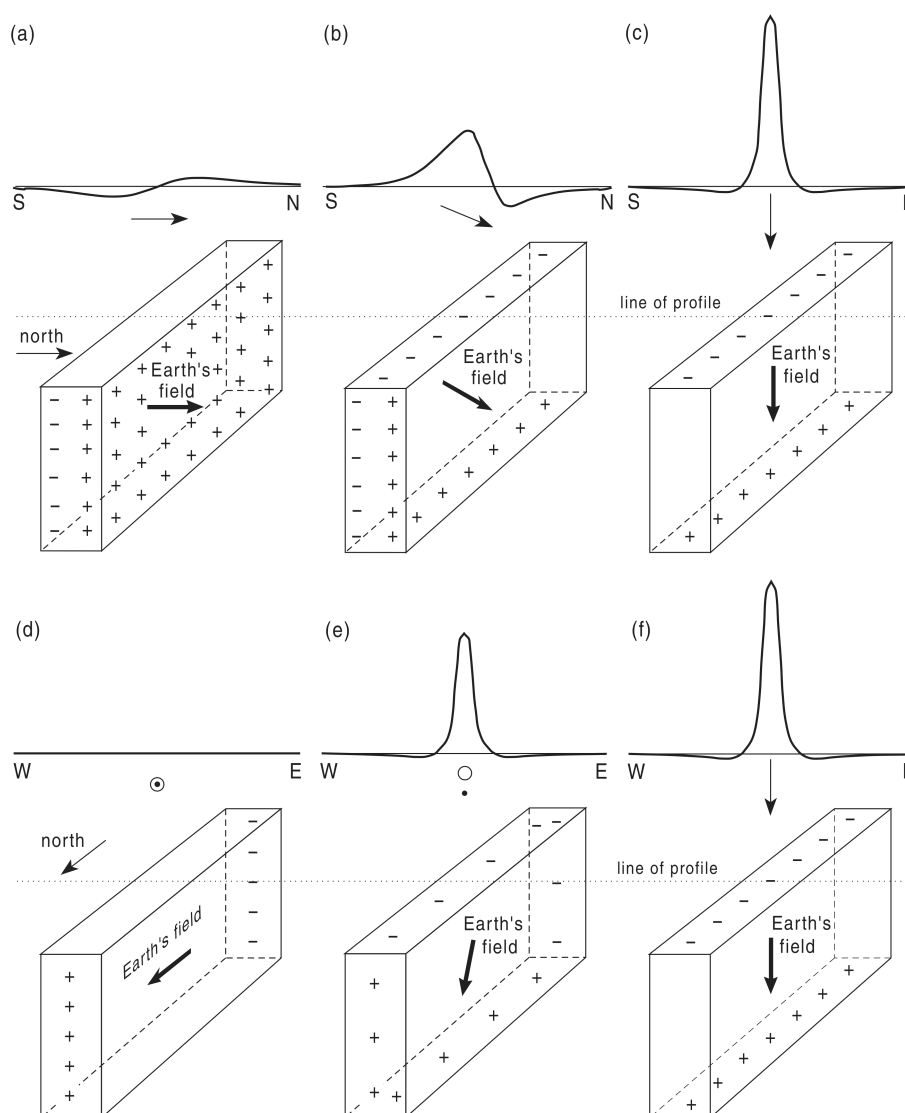**Figure 3.15:** *Anomaly of a dipole at different latitudes (Musset and Khan 2000).*

Figure 3.16: *Poles formed on a thin vertical sheet – anomaly of a dipole at different latitudes (Musset and Khan 2000).*
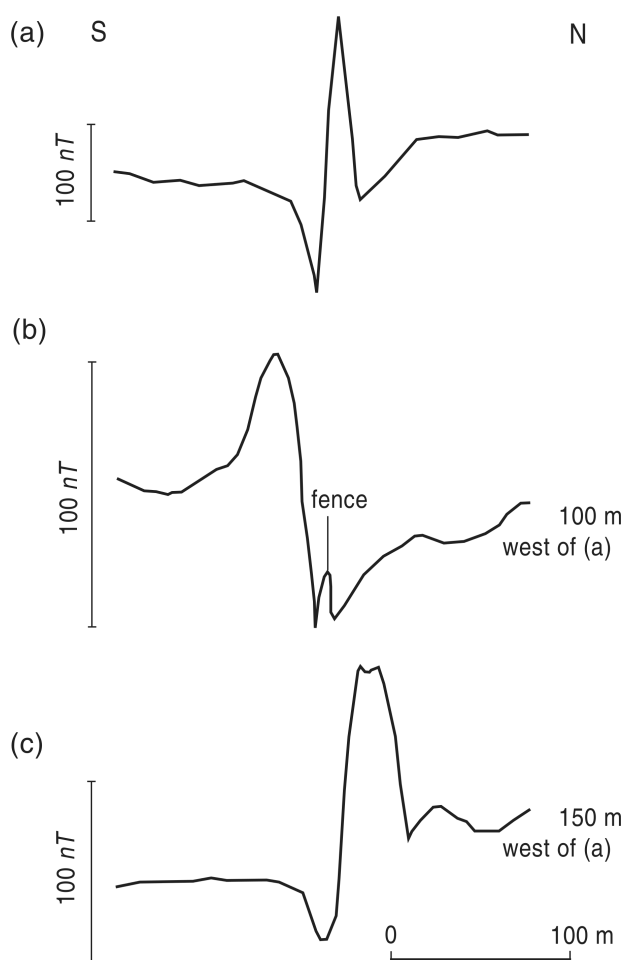
(a)

(b)

(c)

Figure 3.17: *Three profiles across a Tertiary basaltic dyke in NW England (Musset and Khan 2000). The dyke is vertical and strikes roughly E–W. The profile b) is as expected for induced magnetization for such a dyke in northern hemisphere – is asymmetric with peak to the south of a trough. However, profiles a) and c), no more than 100 m away, are reversed – the peak is on the north. Sampling proved that the dyke has reversed remanence. The remanent magnetization exceeds the induce one (Q is larger then 1) at profiles a) and c), but it is less at profile b). Nevertheless, such rapid changes in Q are uncommon.*
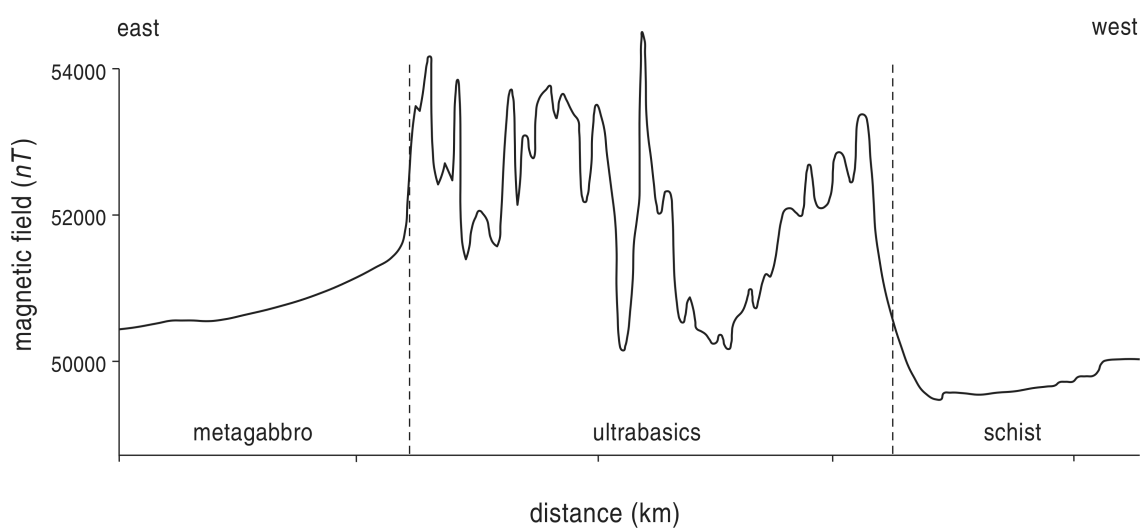

Figure 3.18: *Anomaly across geological contacts, Unst, Shetland Islands (Musset and Khan 2000). The ultrabasics are heavily altered, which causes large variations in their magnetization.*
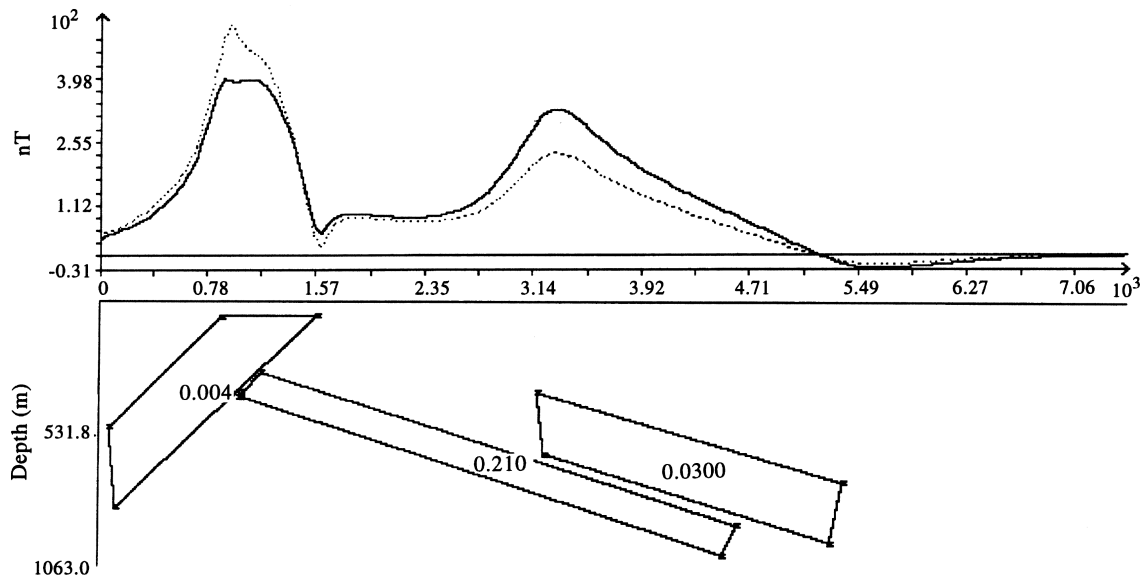
Figure 3.19: *An example of magnetic profile build from the polygonal bodies. Calculated magnetic field anomaly is drawn with solid line and observed data are drawn using dotted line. Susceptibilities (in c.g.s. units) are displayed on bodies. (Cooper 1997).*

anomaly will be mainly driven by the remanent magnetization (and hence reflect the magnetic field from the time of its forming). This ratio could also substantially change even within one body (Fig. 3.17), though this is uncommon.

The shape of anomalies is substantially determined by homogeneity of anomalous bodies (geological units). For example, an alteration could significantly decrease the magnetization, since chemical changes cause also a degradation of magnetic minerals into less magnetic ones – e.g. the susceptibility of hematite or limonite is several orders lower than that of pyrrhotite or magnetite. This is illustrated in Fig. 3.18, where a profile over a contact with ultrabasics is shown. The ultrabasics are inhomogeneous and heavily altered which is reflected in large variations of the anomaly.

3.5.2 Computer modelling

We have already demonstrated, that the magnetic image of geological structures is very complicated. Therefore, more complex anomalies then a simple homogeneous body are almost exclusively modelled using computers. The procedure is close to that one described in the gravity part (section 2.7) – the models are usually build as a set of polygonal bodies with constant physical parameters (Fig. 3.19). The inversion is often carried out using the trial and error technique, similarly to the gravity data.

If the gravity data are measured along with the magnetic ones, both are interpreted together (Figs. 3.20, 3.21 and 3.22). Due to the non-uniqueness of the method, the starting model for the inversion should be as close to the real structure as possible and also strict inversion constraints must be introduced. The starting models (Fig. 3.21) were derived from several 2.5D sections (Fig. 3.20) and the starting model was not allowed to change substantially during the inversion (Fig. 3.22).

However, due to the complexity of magnetic data often only a qualitative analysis is used.

3.5.3 Magnetic gradiometry

As we have seen in the equation (3.1), the strength of the magnetic field decreases with a square of a distance. Therefore, if we would like to decrease or increase the measured values of the magnetic field, we could simply change the height of the magnetometer's sensor. If we move the sensor closer to the ground, we will get higher values and we emphasize effect of the small near surface magnetic
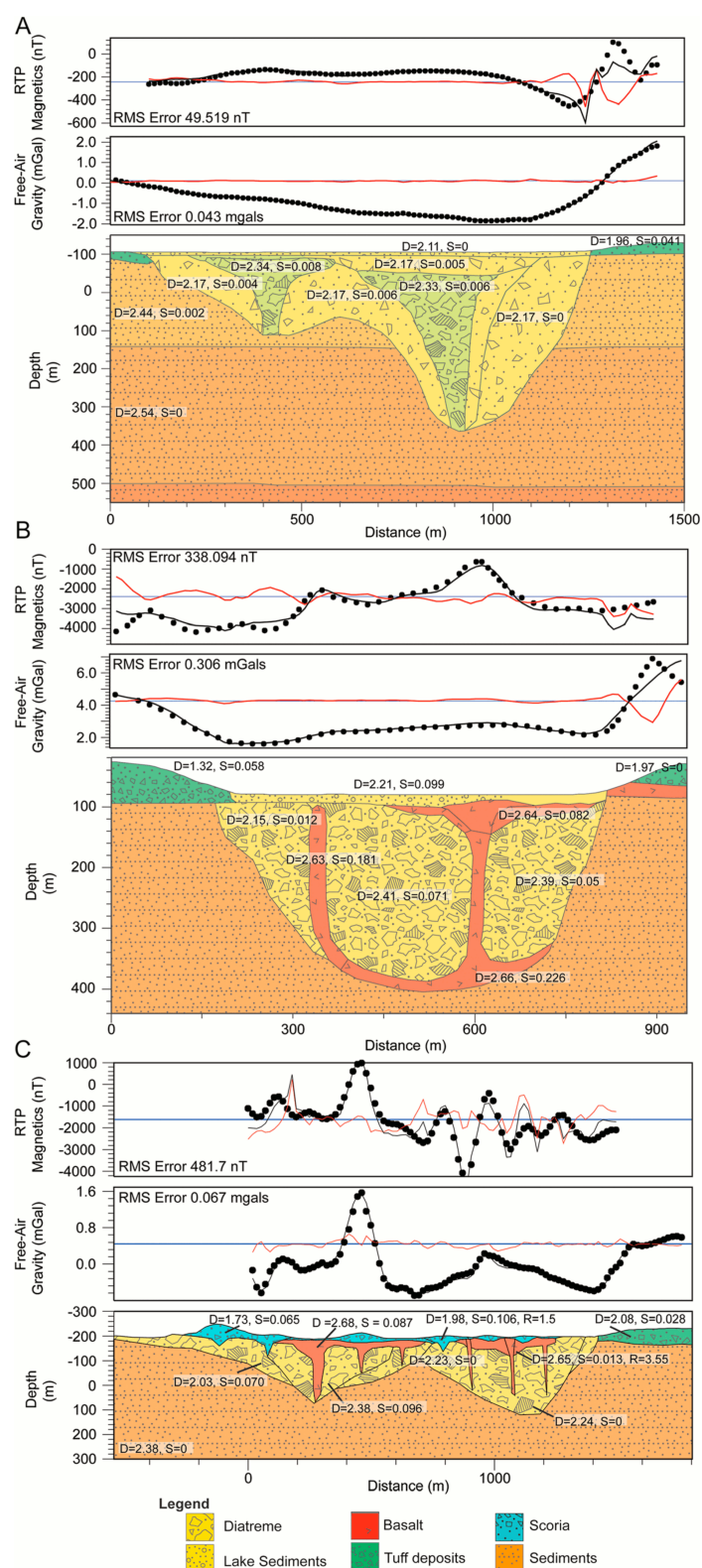
Figure 3.20: *The 2.5D forward models showing the observed and calculated free-air gravity and reduced to the pole magnetic responses and the misfit of the models from (a) Ecklin maar, (b) Lake Werowrap, Red Rock Volcanic Complex, and (c) Mount Leura Volcanic Complex, Australia. (Blaikie et al. 2014).*
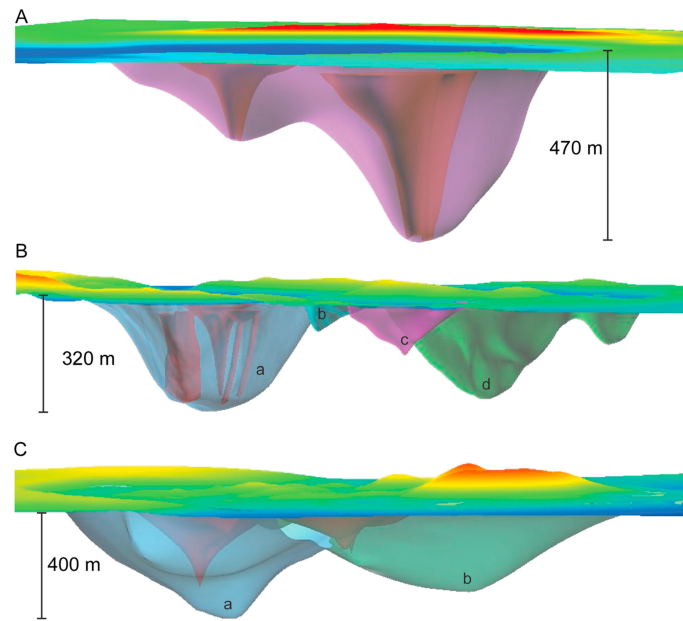
Figure 3.21: *Three-dimensional models of the maar diatremes derived from several 2.5D cross sections (Fig. 3.20). In each image, the colored surfaces represent topography (reds are topographic highs; blues are topographic lows). (a) The Ecklin maar (purple surface is the diatreme; orange surfaces are the vents). (b) The Red Rock Volcanic Complex (Blue, green, and pink surfaces represents the diatremes; red surfaces are the dikes and magma ponds). Small letter a is the Lake Werowrap maar. (c) The Mount Leura Volcanic Complex (blue surface is the maar diatreme, green surface is the diatreme of the tuff ring, and red surfaces are vents and lava flows). (Blaikie et al. 2014).*
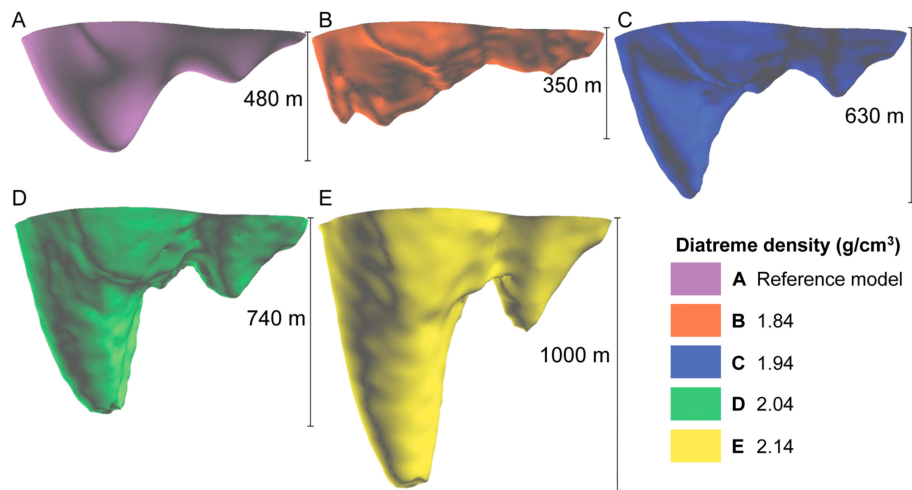

Figure 3.22: *Results of geometric inversions of the Ecklin maar-diatreme model (Figs. 3.20 and 3.21) for variable diatreme densities. Model A shows the original reference models (the one from Fig. fig:mag-maar-3d). Models B–E show the inverted diatreme geometries. The lowest density model (B) results in a broad shallow diatreme. Model C has the same properties as the reference model and is the preferred model. Models D and E are the higher-density models and show deeper diatremes with steeply dipping walls. Blaikie et al. 2014.*
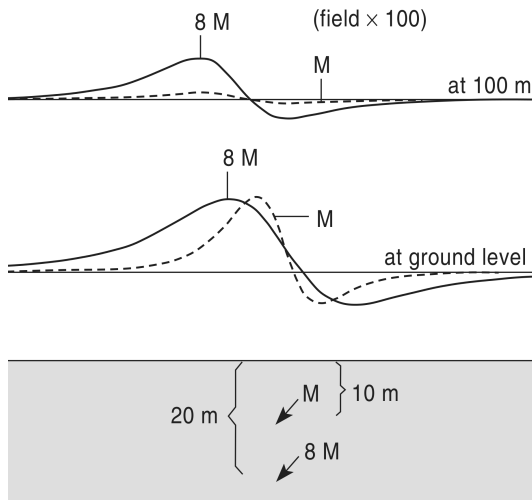
Figure 3.23: *Anomalies at different heights of two dipoles (Musset and Khan 2000). Note the rapid decrease of amplitude of the shallower dipole.*

objects. Conversely, if we increase the height of the sensor we will decrease the response of small near surface bodies (see Fig. 3.23). From the same figure it is also clear that if we subtract these two measurements, we will get high difference for bodies close to the surface, whereas anomalies caused by deep bodies will (almost) cancel. This principle is often used in the field studies. The magnetometer is equipped with two sensors in different heights. The height difference usually varies between 0.5 and 1.5 m. The magnetic field is measured by both sensors simultaneously, hence in this case we do not need to correct data for the diurnal variations (the Earth's magnetic field cancels by subtracting the two readings). The gradiometer surveys can substantially increase a resolution for near surface bodies (Fig. 3.24).

This effect is widely used in tasks dealing with the near surface prospection. Mapping of archaeological objects, search for metallic pipelines or unexploded ordnance and similar applications heavily relies on the gradiometric measurements.

The above described principles could be used also in an ordinary one sensor prospection to determine the height of the sensor. If the target objects are large and deep (e.g. geological structures), one should position the sensor as high as possible to remove an effect of near surface
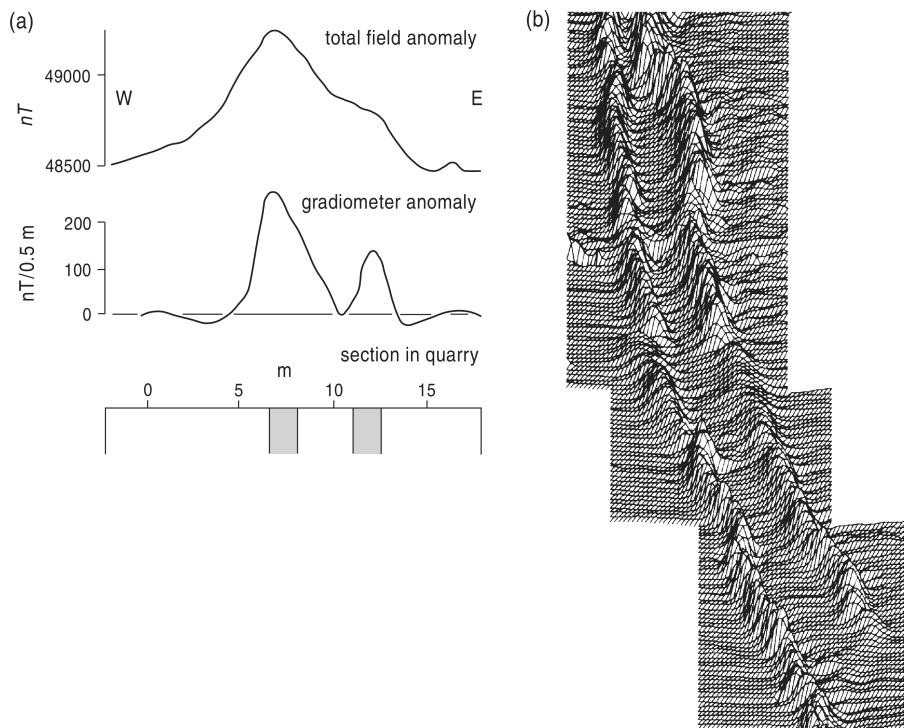

Figure 3.24: *Gradiometer survey of the dolerite Butterton dyke, England (Musset and Khan 2000). The total field (a) does not reveal the fact that the dyke is in fact two thin parallel dykes. Nevertheless , this could be clearly recognised from the vertical gradient data. The set of parallel profiles maps a course of the dyke (b).*
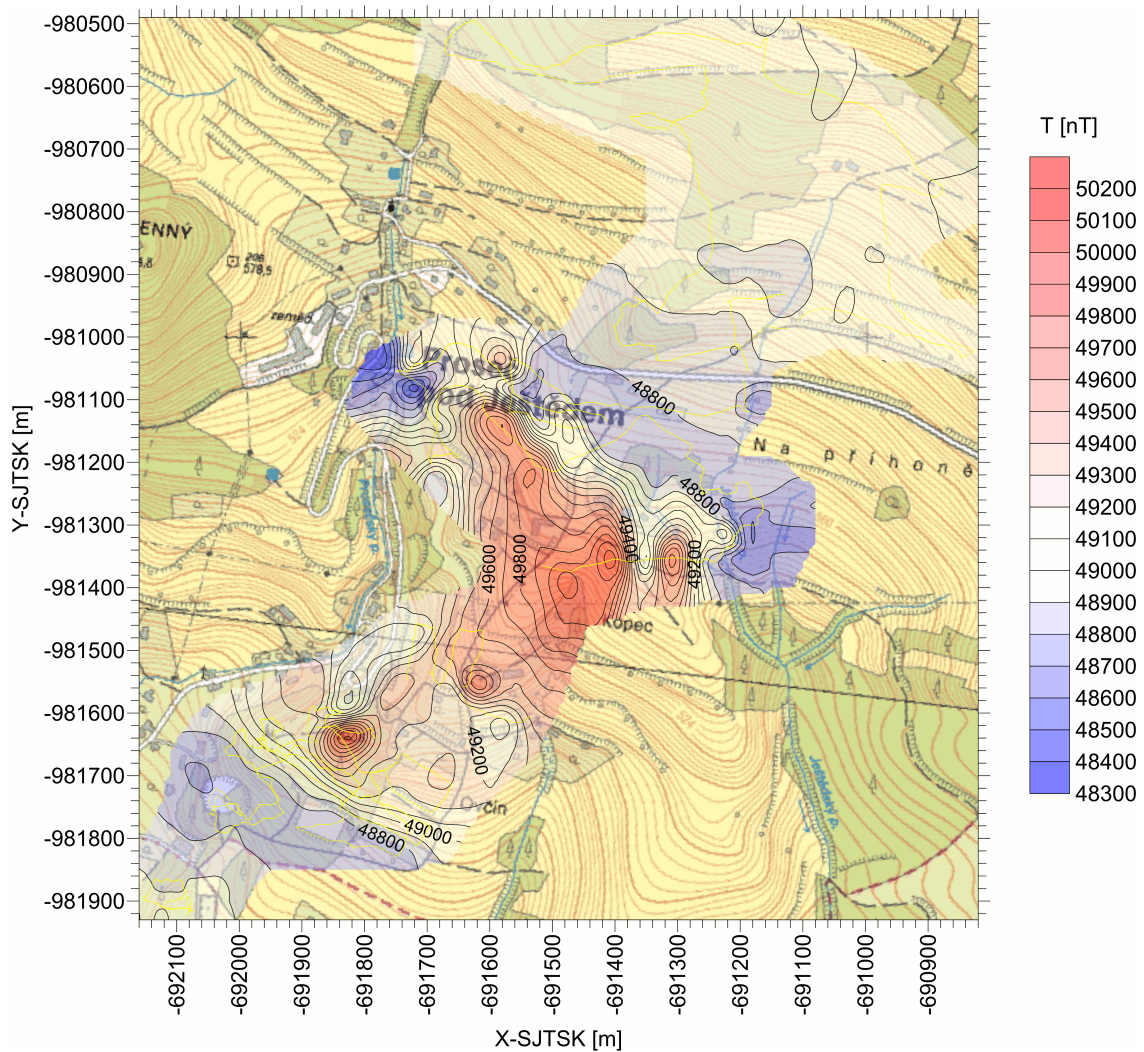
Figure 3.25: *The magnetic image of basic dykes "Devil's walls", northern Czech Republic. A walking-mode caesium magnetometer (gradiometer) was used, the measured path is shown as a yellow line. The data from the top sensor are plotted here, the height of the sensor was 1.5 m. The magnetic highs are caused by the basic dykes, their NE boundary was formed by tectonic movements on the Lusatian Fault.*

objects (considered to be a "noise" in this case). The near surface objects are often highly magnetic anthropogenic objects, pieces of metal (parts of cars, agricultural equipment, cans, etc.). In contrast, in search for small objects, like the archaeological ones, one should position the sensor near the ground (e.g. a height of 0.5 m is often used).

To illustrate the difference in height of sensors, results of a reconnaissance survey for a basic dykes are shown in Figs. 3.25, 3.26 and 3.27.

The survey was carried out to map the Tertiary basic dykes called "the Devil's walls" and their NE boundary caused by movements on the Lusatian fault. The Devil's walls are sets of thin (several meters) vertical dykes several kilometres long, filling pre-existing weakened zones. The reconnaissance survey presented here, was carried out using the Geometrics caesium magnetometer with two sensors, placed in heights of 0.5 and 1.5 m. The walking mode was used for measurements. (A continuous recording with a high sampling frequency – 5 samples per second – and recording of positions with the GPS. This is very effective for general mapping of large areas.) Comparison of data from the bottom and upper sensor (Fig. 3.26) shows all the effects discussed here.
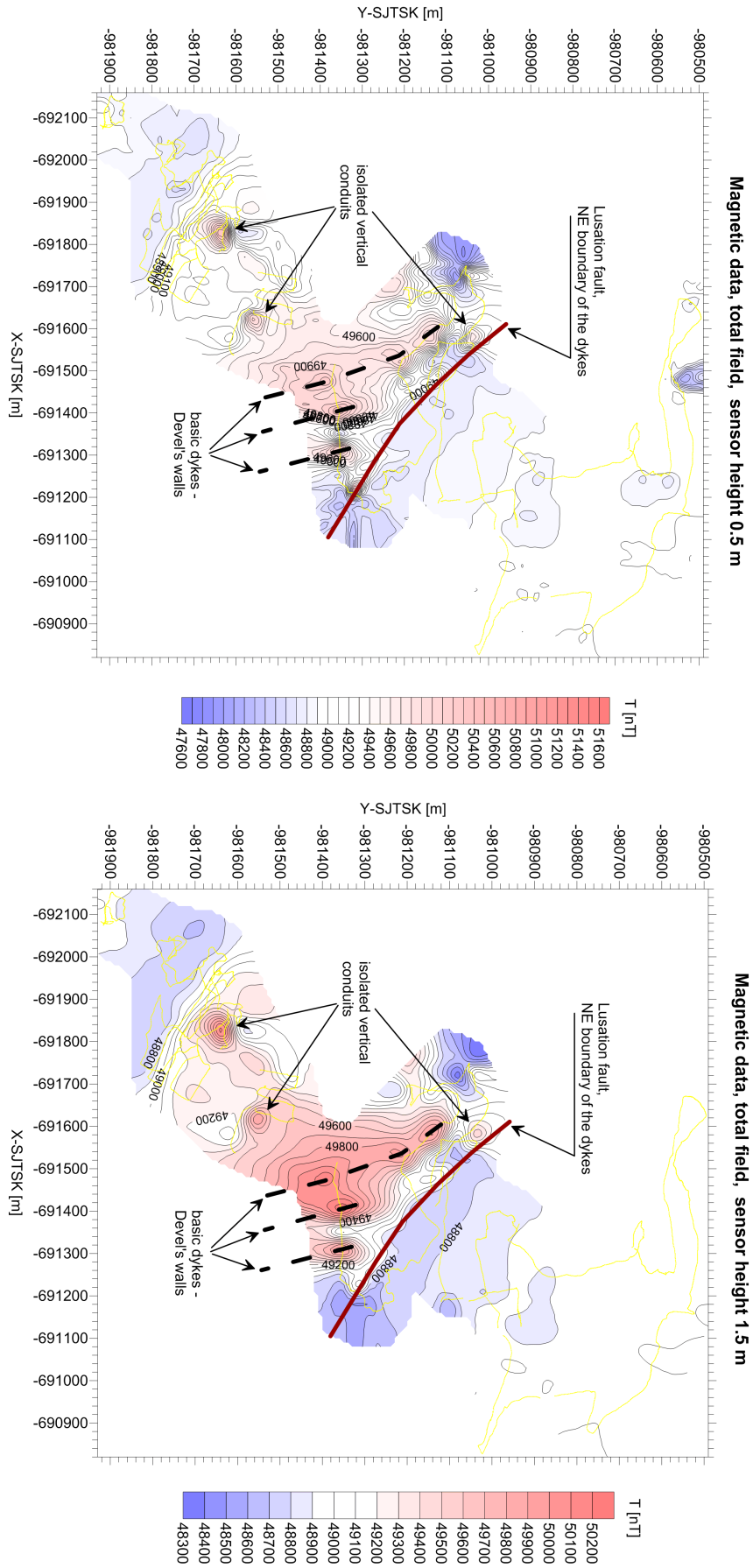
Figure 3.26: *Comparison of different heights of magnetic sensors from the survey in Fig. 3.25. The bottom sensor (left figure) was at the height of 0.5 m, the top sensor (right figure) was at the height of 1.5 m. Note the differences in measured amplitudes – larger amplitudes are for the lower sensor closer to the source. Also note the more erratic course of magnetic field recorded by the lower sensor. This is due to the near surface anomalies (pieces of metal, etc.) and relatively higher changes of the sensor height due to uneven surface. The geological structures are much better imaged with the higher sensor.*

Magnetic data, gradient of the total field

Figure 3.27: *The vertical gradient of magnetic data from Fig. 3.26. Note that the geological anomalies have almost 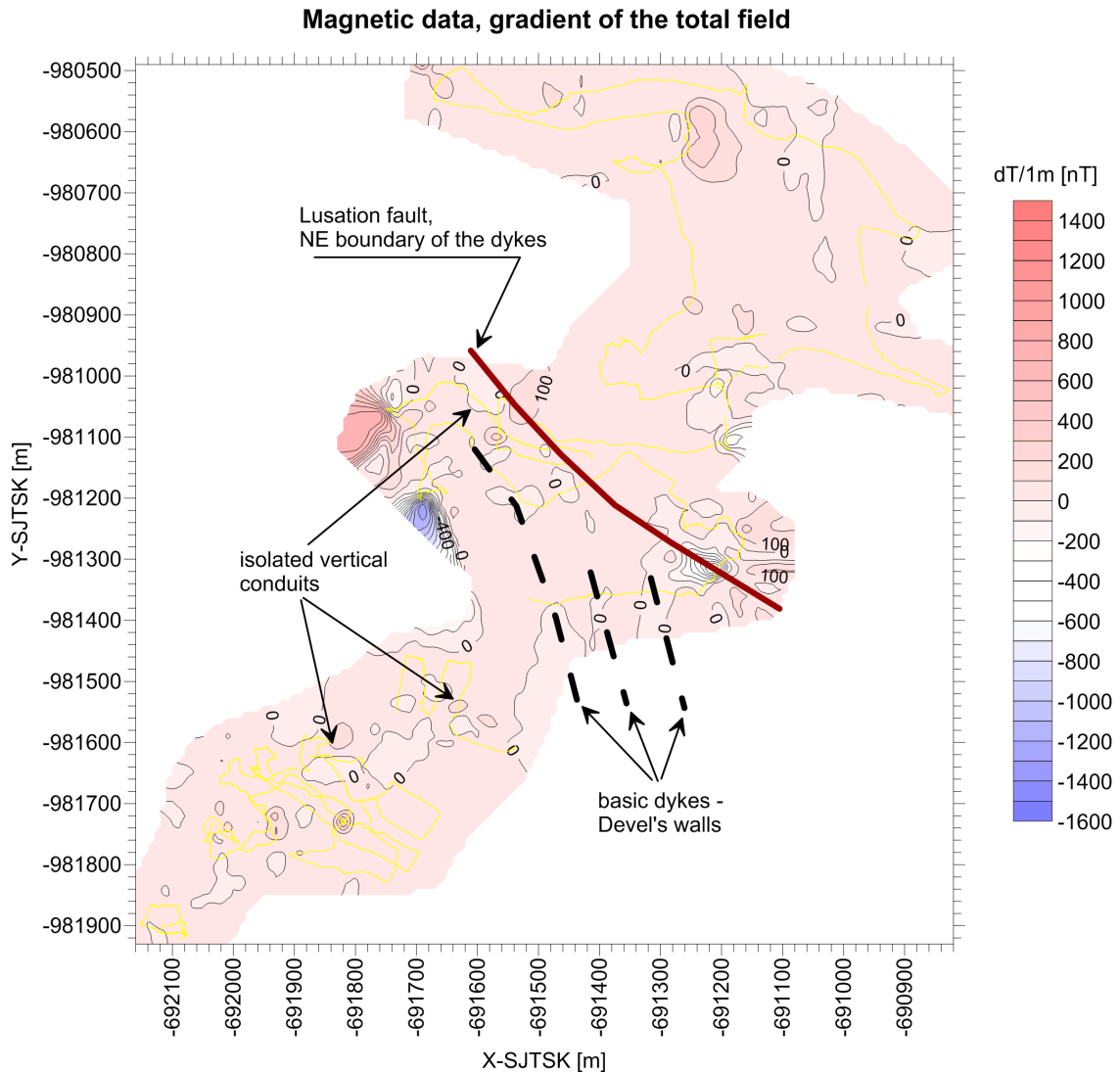zero gradient in contrast to near surface ones. The very low values of vertical gradient also suggests that features interpreted as "isolated vertical conduits" in Fig. 3.26 are of geological (deep) origin and are not caused by some near surface objects.*

The bottom sensor measures larger amplitudes (it is closer to the source of magnetic anomalies) and data from the bottom sensor are more erratic. The reason for this is two-fold. First of all, the near surface inhomogeneities influence the closer sensor more. Second, due to the uneven relief, the relative change of the height is larger for the bottom sensor then for the upper (e.g. a change in the height of 5 cm is 10 % from the height of the bottom sensor whereas the same change is only 3.3 % from the height of the upper sensor).

The vertical gradient data (Fig. 3.27) shows almost zero gradient for the geological structures, whereas the near surface inhomogeneities are identified by large gradient values. It is evident that the vertical gradient can help to distinguish geological features from the near surface objects. The local magnetic highs interpreted as isolated vertical conduits (Figs. 3.26 and 3.27) have large amplitudes of total magnetic fields on both sensors and hence the vertical gradient is close to zero suggesting geological origin of these anomalies. In contrast, the places with a high values of the vertical gradient almost certainly effects of near surface objects (most likely some pipes, power lines or metallic rubbish).
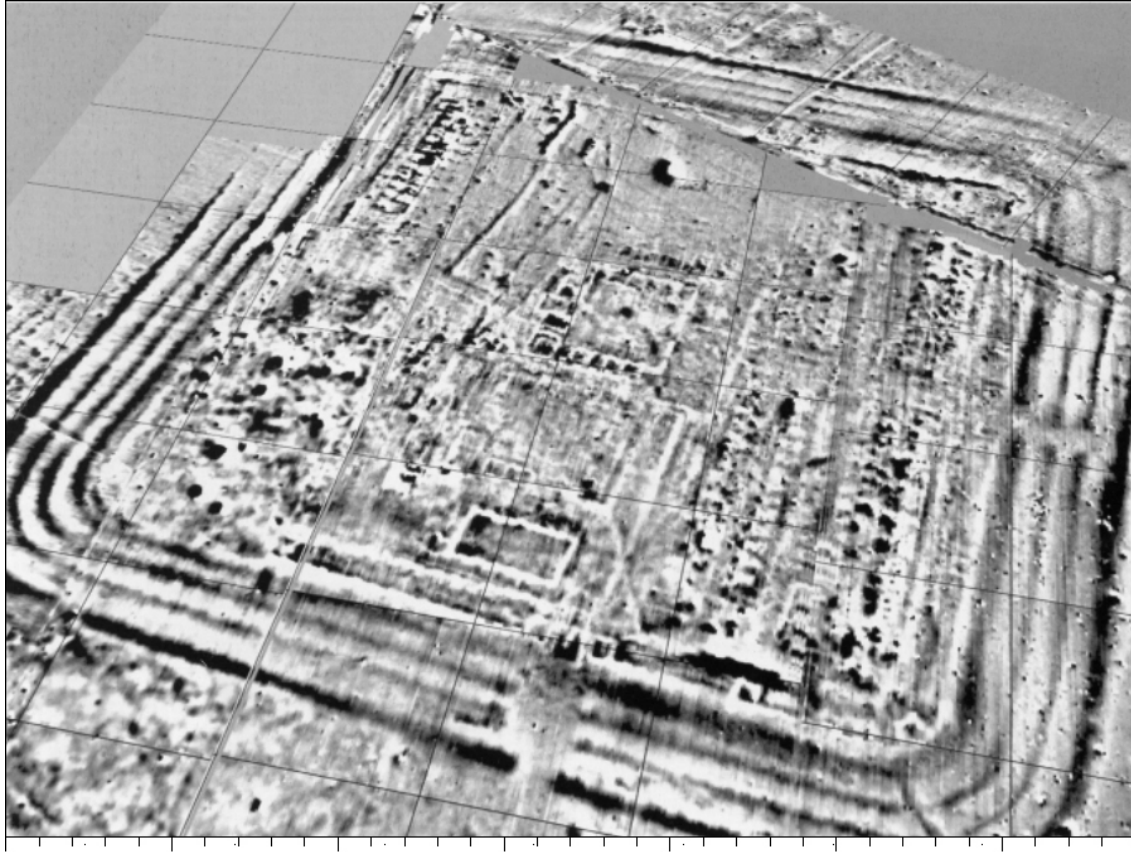
Figure 3.28: *Magnetic image of a Roman castellum at Ruffenhofen, Middle Franconia, Germany (Becker and Fassbinder 2001).*

3.6   Magnetic measurements for an archaeological prospection

The magnetic method started to be used in archaeological prospection with an invention of the proton precession magnetometer which enabled fast and precise measurements with no drift of the instrument. Moreover, further development lead to construction of optically pumped magnetometers, being even more precise and the measurements are fast enough to enable walking-mode measurements. Hence the magnetometry became a standard and most common method in the field of archaeological prospection. Why is the magnetometry so useful in this area and how it can reveal archaeological structures? There are several reasons for this connected to the various types of structures searched for.

The most obvious reason is a search for magnetic iron objects, like remnants of arms or different tools. There are, for example, surveys that found ancient Celtic graves based on magnetic anomalies of swords buried together with fallen warriors.

Another easy to find reason could be search for remnants of walls build from magnetic rocks, like basalt.

However, much subtle and much more common reason for magnetic anomalies connected with archaeological structures is magnetization of a soil. The soil could be magnetized primarily or secondly. The primary magnetization comes from disintegration of bedrock and reflects its mineralogy. The magnetite could originate from volcanic bedrock whereas hematite could come from red sandstones. The secondary minerals are results of chemical and biological processes on soil. These processes could produce a maghemite, goethite, hematite and magnetite.

The secondary processes lead to a fact that the topmost soil could be more magnetized than the bedrock. Hence, if there were, e.g. a ditch dug around a castle and the ditch was slowly filled

by the topmost soil eroded from the neighbourhood by rains and winds, the filled ditch will have a larger magnetization than the surroundings. Therefore, we can easily map it by its magnetization even if it is not visible on the surface any more (Figs 3.28, 3.29). The same applies on all slowly filled holes, like post holes, dug basements of huts and houses, etc.

The magnetic effect of the soil could be further increased by the thermoremanent magnetization. The fire could increase the temperature of earthen structures above the Curie point and during cooling the atomic dipoles would be aligned into the direction the Earth's magnetic field and thus increasing its magnetic effect. This is the case of different bulwarks and mounds of ancient settlements being destroyed by fire, e.g. when being captured by enemy armies. The same process also applies to other places affected by fire, like fireplaces, furnaces, etc.

Figure 3.29: *Magnetogram of the neolithic earthwork, Steinabrunn, Austria (source: Internet-1). Ditches slowly filled with the surrounding topmost soil reveals itself by increased magnetization.*

4

Geoelectrical methods

The geoelectrical methods is a large group of various methods differentiating the subsurface according to its electromagnetical properties. There is a wide range of geoelectrical methods from which we will focus only on some simple DC (direct current) resistivity method. The principal advantage of these methods is twofold. First, they are very versatile in the tasks they can solve. Second, the simple geoelectrical measuring device is cheap and easy to build. (The fine device could be built for 300–400 $. Compare with some 10 000 $ for a basic magnetometer or 75 000 $ for a gravimeter.)

The origin of the resistivity methods is, as is also the case of magnetometry, connected with ore exploration, since most of the ores are conductive.

4.1 Elementary theory

The rocks, as any other material, consists of atoms, which can be viewed as electrically charged particles – a positively charged nucleus surrounded by negatively charged electrons. Usually, the positive and negative particles are in balance and cancels each other. However, certain chemical and physical processes could disrupt this neutrality and the bodies could reveal themselves by an electrical charge. Self potential and induced potential methods are based on this fact. Nevertheless, most of the geoelectrical methods are based on the flow of the current rather than on the potentials.

The electric current is a flow of electrically charged particles – electrons or ions. By convention, current is considered to flow from positive (source) to negative (sink), though in the wire the current is due to electrons moving the other way. The *electrical current I* is measured in amperes (A) and it is the amount that passes any point in the circuit in one second. The current is caused by a *potential difference V* (the amount of imbalance) measured in volts (V). For most materials, including most rocks, the current through a piece of material increases with increasing potential difference (e.g. doubling the difference doubles the current).

The ratio between the potential difference and current is described by *resistance R* of the material. This relation is called the *Ohm's Law*:

$$R = \frac{V}{I},\tag{4.1}$$

and is measured in Ohms (Ω).

Naturally, the overall resistance of a certain media depends on it's electrical properties (the ability to conduct the current) and on the size of the media. For example, if we put a one meter of poorly conductive media into the electrical circuit the overall resistance will be much higher then if we put one millimetre of such material there. The resistance also depends on the diameter of the material – increasing the diameter decrease the resistance ("the thicker the material is, the more electrons could pass through it"). Therefore, to make the life easier, a *resistivity ρ* is defined:
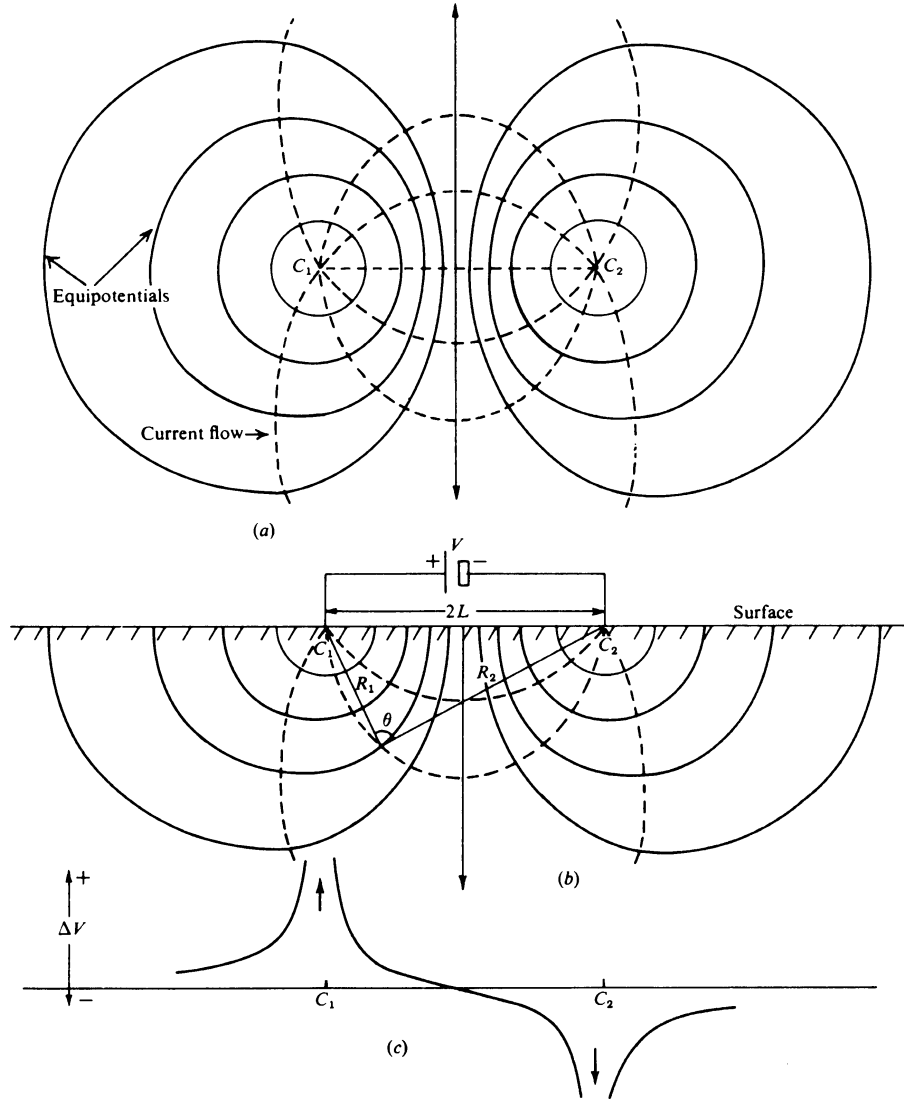
$$\rho = R\frac{S}{l},\tag{4.2}$$

Figure 4.1: *Equipotentials and current flow lines (paths) for two point sources of current on surface of homogeneous ground. (a) Plan view. (b) Vertical section. (c) Potential variation at the surface along a straight line through the point sources.(Telford et al. 1990.)*

where S is the area of cross-section of the material and l is it's length. The units of resistivity are Ohm meters (Ωm). The reciprocal of resistivity is the *conductivity* σ

$$\sigma = \frac{1}{\rho} \tag{4.3}$$

and the units are Siemens per meter (S/m). The conductivity is used in the field of electromagnetical methods.

If there are more layers of material with different resistivities between our measuring probes (electrodes), we will measure some overall value of resistivity. We call this value an *apparent resistivity* ρ_a and it is the value which a homogeneous ground will have for our electrode configuration.

4.2 Resistivities of rocks and minerals

Most minerals forming rocks are insulators, however, the structure of rocks containing pores, cracks and joints filled with water, ore veins, clay minerals, etc. makes the rocks more or less

conductive. Although the pure water is also a good insulator, the water in rocks is almost never pure, but contains dissolved salts coming from weathered rocks. The salts in water dissociate into positively and negatively charged parts – ions. These can move through the water in opposite direction causing an electric current. This is called the *ionic conduction* to distinguish it from the *electronic conduction* in metals, where only electrons are moving. The ionic conduction is the main reason for rocks to be conductive. The concentration of salts in water is usually low and hence also the conductivity is low, however, in some cases the amount of dissolved salts could be increased (e.g. by leaking of sea water, dissolving of salts contained in sediments, etc.) increasing also the conductivity. Hence the range of resistivities for individual rock types is very large (Tab. 1.1) making it hard, or even impossible, to determine the rock type solely from the measured resistivity values. For example, the granite containing $0\,\%$ of water has the resistivity of $1 \times 10^{10}\,\Omega$m, the same sample of granite containing $0.19\,\%$ of water has the resistivity of $1 \times 10^6\,\Omega$m and, finally, with $0.31\,\%$ of water has the resistivity of $4 \times 10^3\,\Omega$m.

Considering the resistivity, clay minerals are specific in this respect. When they are dry, they are non-conductive, however, since it have very fine particles and hence a large surface it can trap water easily and have very low resistivity. Therefore. the resistivity of clays is the lowest from common rock forming minerals starting at magnitude $1 \times 10^0\,\Omega$m and generally being between 10–$100\,\Omega$m. In addition to the clay minerals like kaolin or illite, there are also "physical" clays, which means particles of any minerals sufficiently fine (less than approx $4\,\mu$m) to have similar physical properties to ordinary clays (mainly the large surface area trapping the water).

Another minerals with low resisitivities are some ore minerals and graphite. if they are present in the rock, the overall resistivity of this rock depends not only on their concentration, but also on the fact whether their grains are interconnected or not. If they are not interconnected in a sufficient extent the resistivity of such rock remains high and such ore could not be found by resistivity measurements.

4.3 Resistivity surveying

To get an idea of what is measured with resistivity methods, we have to first look at how the electricity flows through the rocks. The current is injected into ground by a pair of electrodes, metal sticks pushed into the ground. The positive and negative *current electrodes* are often denoted as C_1 and C_2, or A and B. The current flows between the electrodes using the easiest path, which is the path with lowest resistance. As the resistance decreases with increasing diameter of the wire, the current paths spread downwards and sideways (Fig. 4.1). Nevertheless, the highest concentration of the current is near the surface. In uniform ground only about $30\,\%$ of the current penetrates deeper than is the separation of the current electrodes. This also implies that the depth of penetration of the current and a volume of rock sampled depends on the distance between the current electrodes (Fig. 4.2). The further the electrodes are placed, the deeper is the penetration, however, a larger volume of rock is sampled and hence the survey is less detailed.
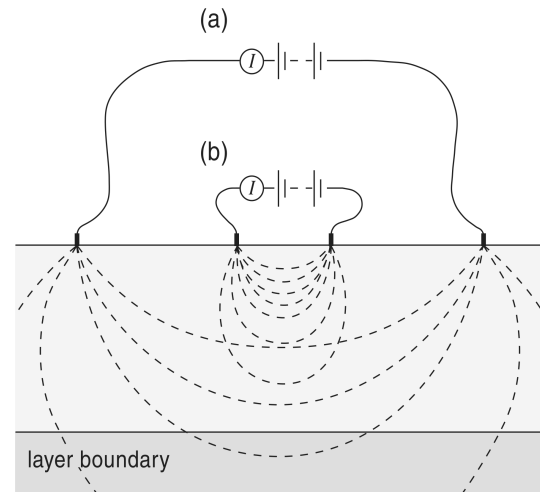

Figure 4.2: *Change of a depth of penetration and of a volume sampled by the electric current for different separations of current elecetrodes (Musset and Khan 2000).*

The potential difference is measured by another pair of electrodes with a voltmeter connected to them (Fig. 4.3). These *potential electrodes* are usually called P_1 and P_2, or M and N. The potential difference measured between the potential electrodes is usually denoted ΔV.
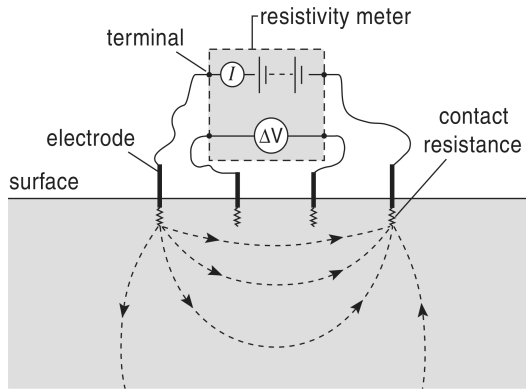
Figure 4.3: *Use of four electrodes – a pair of current and a pair of potential electrodes (Musset and Khan 2000).*

The voltage applied to the current electrodes generally depends on the separation of electrodes and resistivities of the subsurface, but usually is between 100–300 V for the near surface surveys. The current is, however, usually less than one ampere and the potential difference read is in millivolts.

The potential difference readings are heavily affected by ions concentrating on the electrodes creating an additional potential (and often also time-variant). To diminish this effect a less polarizing metal could be used for the electrodes (e.g. a stainless steel or brass), or the current could be reversed few times a second to disperse the ions. If a very precise potential difference readings are needed (the case of measuring spontaneous or induced polarization) the so called *non-polarizing* electrodes are used. They consist of a metal immersed in a saturated solution of its own salt, such as Cu in a $CuSO_4$, contained in a porous permeable ceramic pot. The solution slowly leaks through the pores and ensures a proper grounding.

Up to now, we were examining the current paths in the homogeneous media only. If there would be interfaces of layers with different resistivities, the flow paths would bend or refract similarly to light or seismic raypaths (Figs. 4.4, 4.5 and 4.6). They refract towards the normal when crossing into a rock with higher resistivities and conversely in a rock with lower resistivites. Because the refraction changes the distribution of current when compared with the uniform ground and hence changes also the $\Delta V/I$ ratio, it is possible to measure changes of resistivity.

The resistivity measured over an inhomogeneous media is an overall resistivity combined from resistivities of all layers and bodies affecting the flow paths. This resistivity is called the *apparent resistivity*, ρ_a, and is the resistivity that uniform ground giving the same $\Delta V/I$ with the same electrode separations would have.

There are two basic modes of resistivity surveying – sounding and profiling. The sounding is benefits from the fact that the depth of the penetration increases with a distance of current electrodes. Hence repeated measurements on one place with increasing distance of current electrodes measures different depth levels and a vertical profile of a subsurface could be derived (similar to a borehole). The depth of penetration depends on the resistivity values of rocks encountered, however, as a first rough estimate one fourth of the distance between the current electrodes could be considered as a depth estimate.

The profiling uses the same inter-electrode distances for all measurements, but the whole array moves along the profile. Thus a lateral changes of resistivities could be mapped.
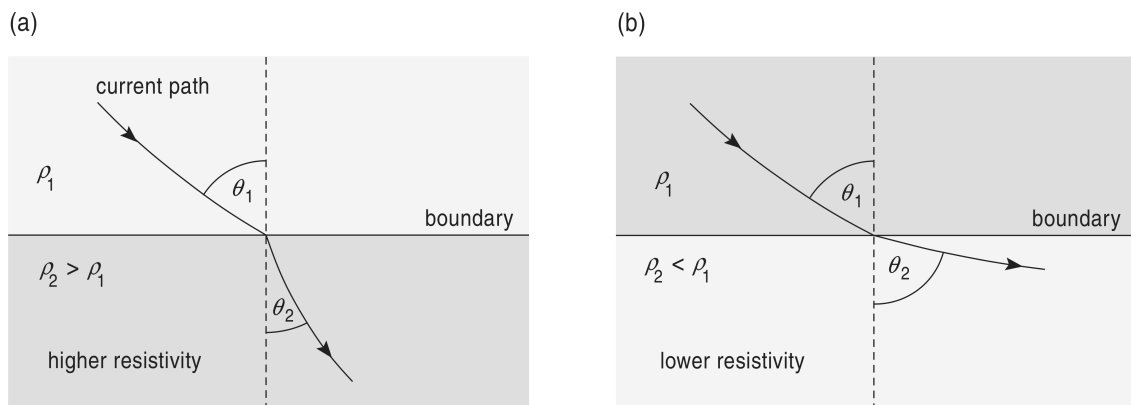

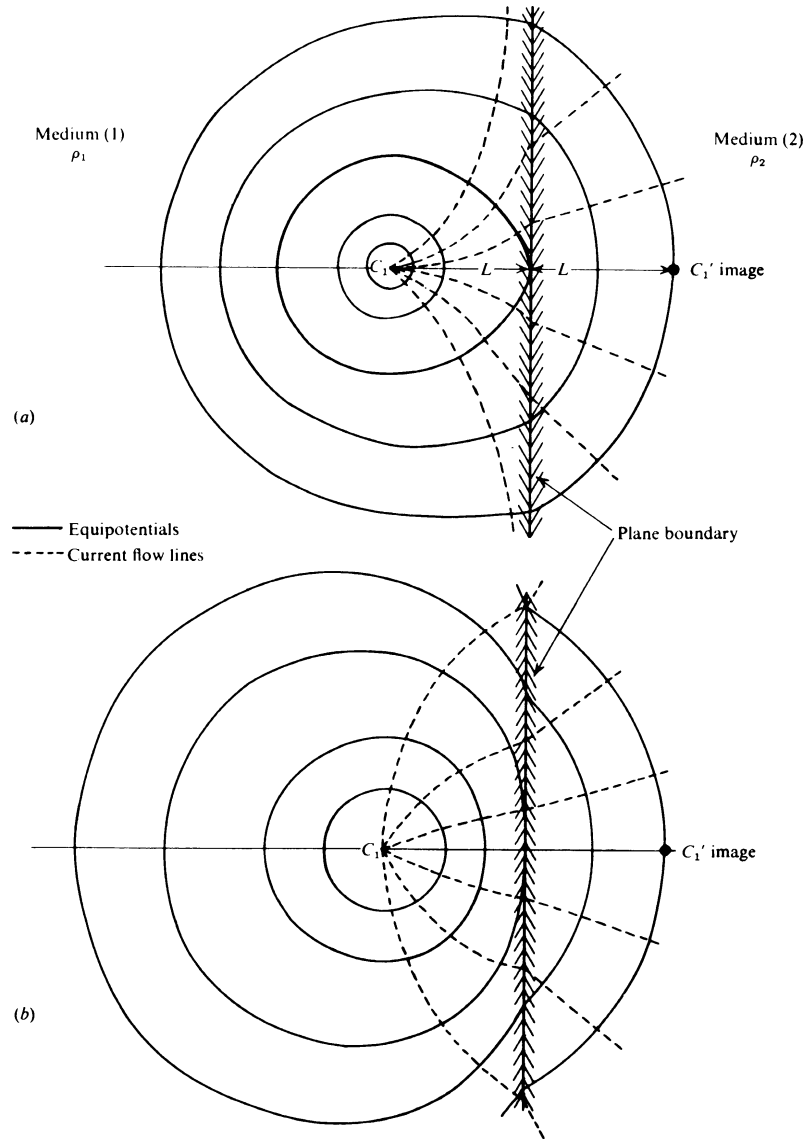*Figure 4.4:* *Refraction of current flow lines (Musset and Khan 2000).*

Figure 4.5: *Distortion of equipotentials and current flow lines at a boundary between two media of different resistivities. (a) $\rho_2/\rho_1 = 3$. (b) $\rho_2/\rho_1 = 1/3$. (Telford et al 1990.)*
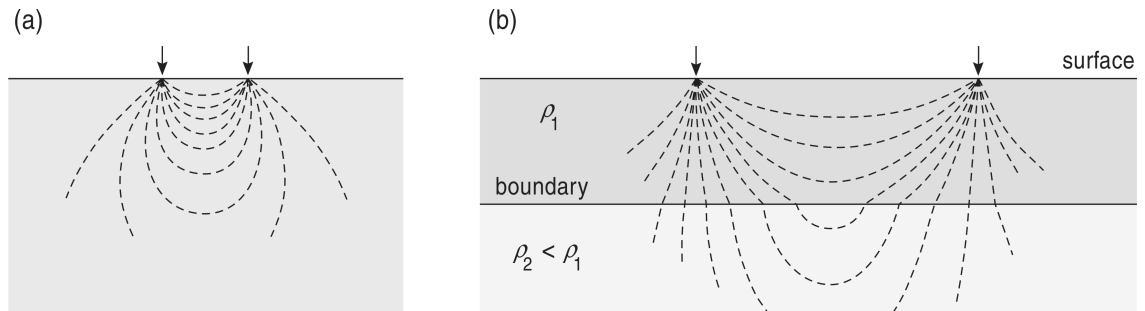

Figure 4.6: *Effect of interface on current flow lines (Musset and Khan 2000).*
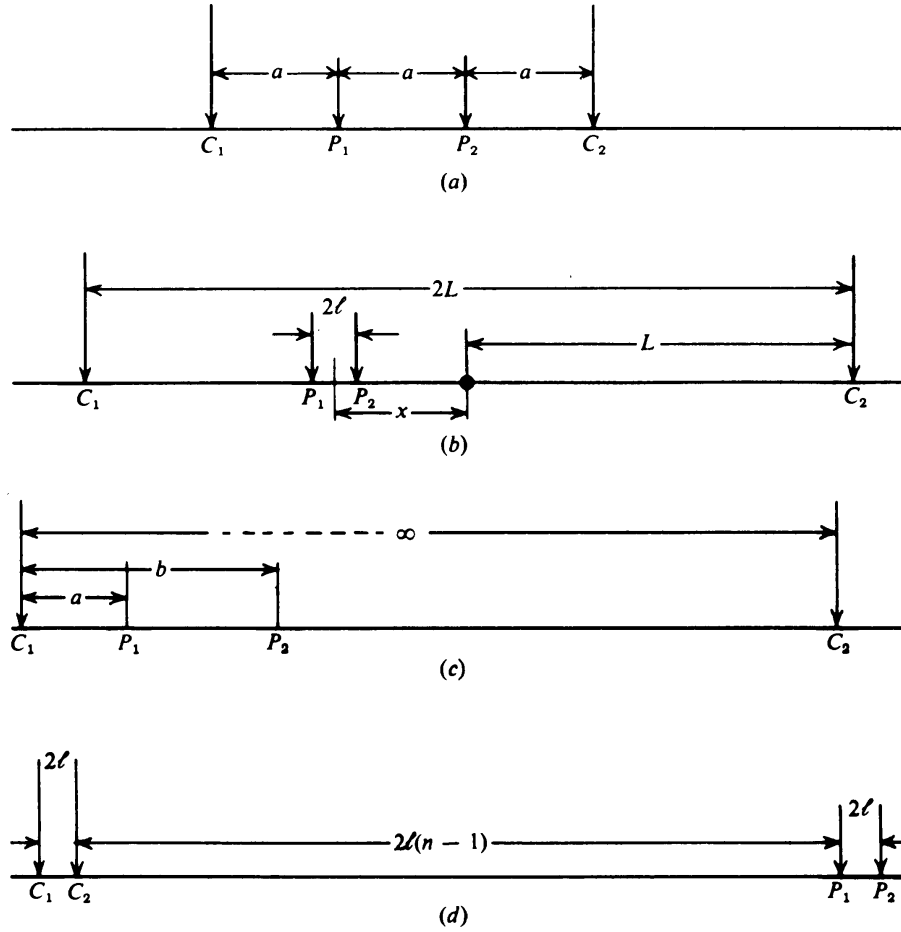
Figure 4.7: *Commonly used electrode arrays (Telford et al. 1990). (a) Wenner (potential) array. All the distances between electrodes are equal. (b) Schlumberger (gradient) array. The distance between the potential electrodes is much smaller than the distance between the potential and current electrodes. The most common configuration is to put the measuring dipole in the center of the array. (c) Pole-dipole array. One of the current electrodes is much further from the measuring dipole than the second one. (d) Dipole-dipole array. The measuring dipole is remote from the current electrodes.*

Finally, a combination of both modes – several measurements on a profile with different inter-electrode distance maps both. the lateral and vertical changes in resistivities producing the 2D resistivity cross-section.

4.3.1　Electrode configurations

From the nature of the method it could be deduced that it is better suited to resolve conductive features than the high resistivity ones. After all, the resistivity method was originally designed for an ore prospection. Nevertheless, the high resistivity anomalies could be detected when an electrode array is carefully selected and the field layout is sufficiently dense.

Up to now, we were not considering any special electrode arrangement. Essentially, four electrodes are necessary, however, their positioning substantially influence the results and could be the factor determining whether the survey is successful or not. The different arrays have different sensitivities for the subsurface inhomogeneities and also a different resistance to a noise. In general, the more sensitive array the more prone to a noise it is.
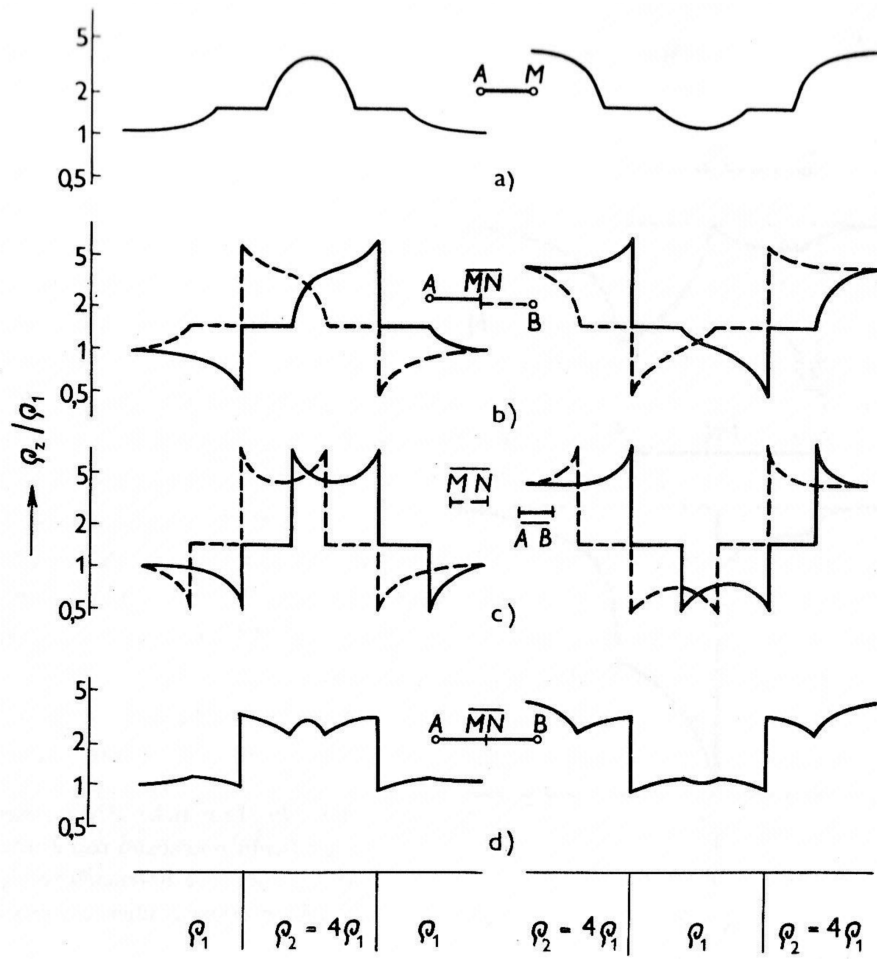
Figure 4.8: *Apparent resistivity (ρ_a) curves over a thick dyka (Mareš and Tvrdý 1984). a) Potential array. b) Pole-dipole and reversed pole-dipole array. c) Dipole-dipole array. d) Schlumberger array. The reference point (the point at which the measured resistivities are plotted) is in the middle of the potential dipole (or at the potential electrode in case of the potential array).*

The electrode configuration inevitably influences the current and potential readings. To be able to compare measurements with different electrode arrays, the measured values must be corrected for the effect of electrode configuration. This is carried out by multiplying readings with a constant of the array, k:

$$\rho = k \frac{\Delta V}{I}. \tag{4.4}$$

The constant of the array depends only on the distances between individual electrodes:

$$k = \frac{2\pi}{\frac{1}{C_1 P_1} - \frac{1}{C_1 P_2} + \frac{1}{C_2 P_2} - \frac{1}{C_2 P_1}}. \tag{4.5}$$

Hence the further the current electrodes are the smaller potential is read. When the potential is too small to be read accurately either better electrode grounding and more powerful electrode source is needed, or increasing the distance between the potential electrodes is necessary. Also, using different electrode array could help, however, changing the array inevitably changes parameters of the whole survey.

The most common electrode arrays are demonstrated in Fig. 4.7. They can be divided into three basic groups: potential, gradient and dipole arrays. The *potential arrays* measure potential between two relatively distant electrodes, the values of voltages read are large (due to the large

distance between potential electrodes) and hence this type of arrays is suitable for surveys with difficulties with grounding of electrodes or where the noise level is high. The *gradient arrays* measures potential difference between two closely spaced electrodes. If this spacing is sufficiently small (zero distance in theory) we can assume that we measure the gradient (the first derivative of potential). Therefore, the measured changes of resistivities will be sharper at boundaries of anomalous bodies. On the other hand, the recorded values of voltages are lower than in the case of potential arrays and the noise level is higher. The *dipole arrays* are the most sensitive, but also the most affected by the noise and also the resistivity curve could be overcomplicated in case of complex geological conditions. The properties of the most common electrode arrays are summarized below:

Wenner array. This potential array has a relatively large distance between the potential electrodes compared with the distance between the potential and current electrodes. Hence the potential readings would be reasonably large and the array is suitable for areas with poor grounding conditions or areas where a high amount of noise is expected.

Schlumberger array. This is a very versatile array. Since it is a gradient array, the measured anomalies are more narrow and better localized than in the case of the Wenner array. This configuration is often used in sounding.

Pole-dipole array. This is a three electrode gradient array. One of the current electrode is placed in a large distance (in an "infinity") from the array and does not move with it. The necessary distance is at least five times the distance between the remaining current electrode and the measuring (potential) dipole. In this case, the effect of the distant electrode is negligible and the electric field of the near electrode resembles that of a point source rather than the field of a dipole. Often used configuration is a combination of two pole-dipole arrays – forward and reversed one. The potential dipole is common for both and the forward dipole has a current electrode on one side of the potential dipole whereas the reversed dipole on the other side. The current electrode in the "infinity" is, again, common for both. Two measurements are taken on each point – forward and reversed, employing both of the current electrodes (an average of these two readings gives the value that would be read if the Schlumberger array would be used). The main benefit is in profiling, where changes in resistivities are clearly mapped (Fig. 4.8). It has a good ratio between the sensitivity and noise.

Dipole-dipole array. This is the most sensitive array of those mentioned, however, also the most prone to the noise. The measured resistivity values clearly delineate subsurface structures, but the image produced is complicated, with side lobes, etc. (Fig. 4.8), which makes things complicated when a complex geology is encountered. The depth estimate with this configuration could be approximately the one fourth the distance the centres of the dipoles. However, the maximal recommended separation between the dipoles is a fifth or six times the distance between electrodes in the dipole. If the distance is larger, too low voltages are read and an error of measurements rapidly increases. If a larger depth of penetration is required, larger separation of electrodes in the dipoles is needed.

Potential array. One of the potential and one of the current electrodes are far way (in "infinity") and only one potential and one current electrode is moving along the profile. The advantage is that only two persons are required for operating the array. The serious disadvantage, however, is that the long wire between potential electrodes induces a lot of noise.

4.3.2   Vertical electrical sounding

A vertical electrical sounding (VES) is a resistivity method enabling detection of changes of resistivities with depth. Resistivities in different depth levels are measured by increasing a distance between current electrodes, while potential ones remains at one place (cf. Fig. 4.2). The result are changes of resistivites below the measuring point. This is similar to, say, a borehole with the difference that one VES measurement is much quicker and cheaper. On the other hand, the geophysical measurement suffers from non-uniqueness and also the geophysical parameters not necessarily corresponds to the geological ones. Hence the best way is to carry out the geophysical
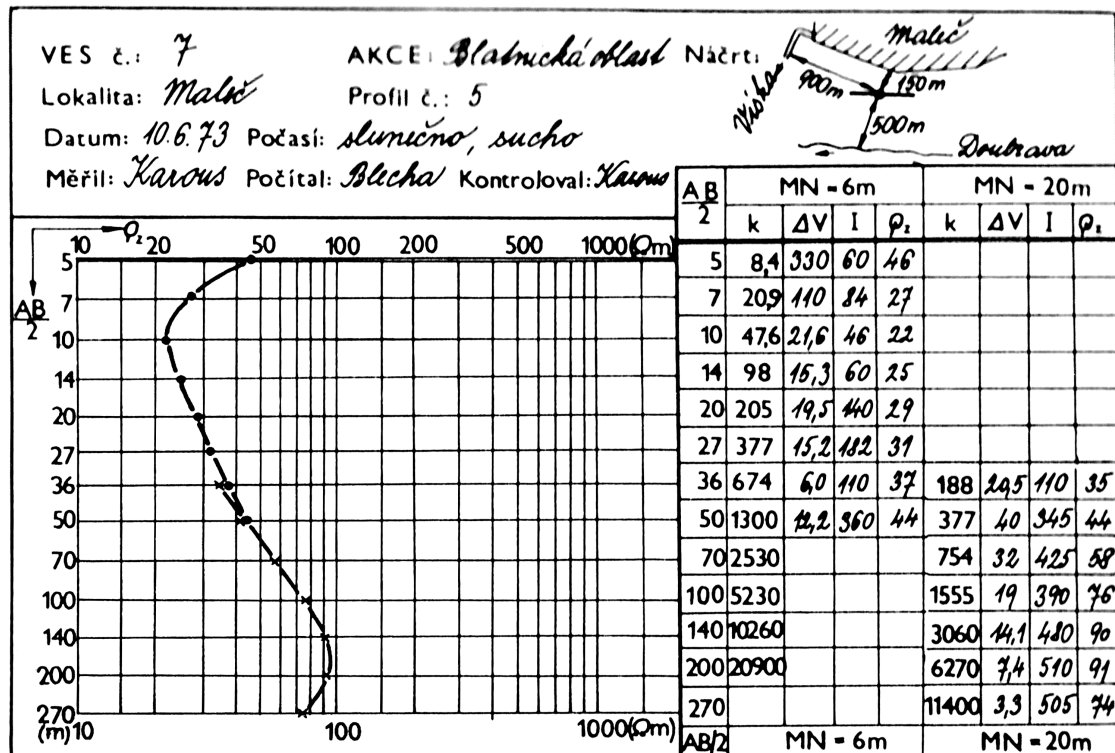
VES č.: 7 AKCE: Blatnická oblast Náčrt: Malič
Lokalita: Malič Profil č.: 5
Datum: 10.6.73 Počasí: slunečno, sucho
Měřil: Karous Počítal: Blecha Kontroloval: Karous

AB/2	MN = 6m				MN = 20m			
	k	ΔV	I	ρ_s	k	ΔV	I	ρ_s
5	8,4	330	60	46				
7	20,9	110	84	27				
10	47,6	21,6	46	22				
14	98	15,3	60	25				
20	205	19,5	140	29				
27	377	15,2	182	31				
36	674	6,0	110	37	188	29,5	110	35
50	1300	12,2	360	44	377	40	345	44
70	2530				754	32	425	58
100	5230				1555	19	390	76
140	10260				3060	14,1	480	90
200	20900				6270	7,4	510	91
270					11400	3,3	505	74
AB/2	MN = 6m				MN = 20m			

Figure 4.9: *An example of the VES terrain chart (Mareš and Tvrdý 1984). For surveys mapping the near surface in more detail the first AB/2 (half of the current electrode separation) is usually 1 m and the starting MN (potential electrodes) distance is also 1 m. Note that the AB/2 distances are equidistantly sampled in a log scale. This is due to the exponential decrease of resolution with depth.*

research and subsequently verify the results with several boreholes on selected places. The VES measurements are most often used for assessing interfaces within the sedimentary basins – geological mapping, hydrogeological applications (mapping of potential aquifers), find depth to bedrock for the constructions industry, etc.

As was stated earlier, the most common electrode array for the VES measurements is the Schlumberger array. the main reason is that for changing the depth reach only the current electrodes needed to be moved (in contrast to Wenner or dipole-dipole array). Hence, to measure the VES point, the electrodes are positioned at the desired point and the current and voltage values for the first current electrode separation (depth level) are measured. The resistivity is computed and plotted into the log-log graph (Fig. 4.9). Then the current electrodes are moved to the next position, values measured, plotted, etc. When the measured potential becomes too low, it is necessary to increase the distance between the potential electrodes. In this case it is necessary to measure several points with both potential dipole separations to be able to connect both sets of measurements (Fig. 4.10). Finally, when all the desired points are measured the resistivity curve is checked for a smoothness. Any outliers are most likely errors and should be measured once more.
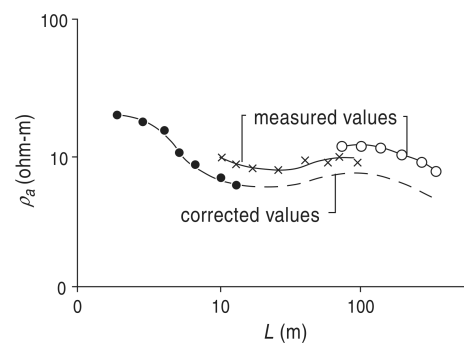
Figure 4.10: *The individual branches of the resistivity curves could have offset if different potential electrode separations are used. Measuring several points with both offsets gives the redundancy necessary for correction. (Musset and Khan 2000.)*
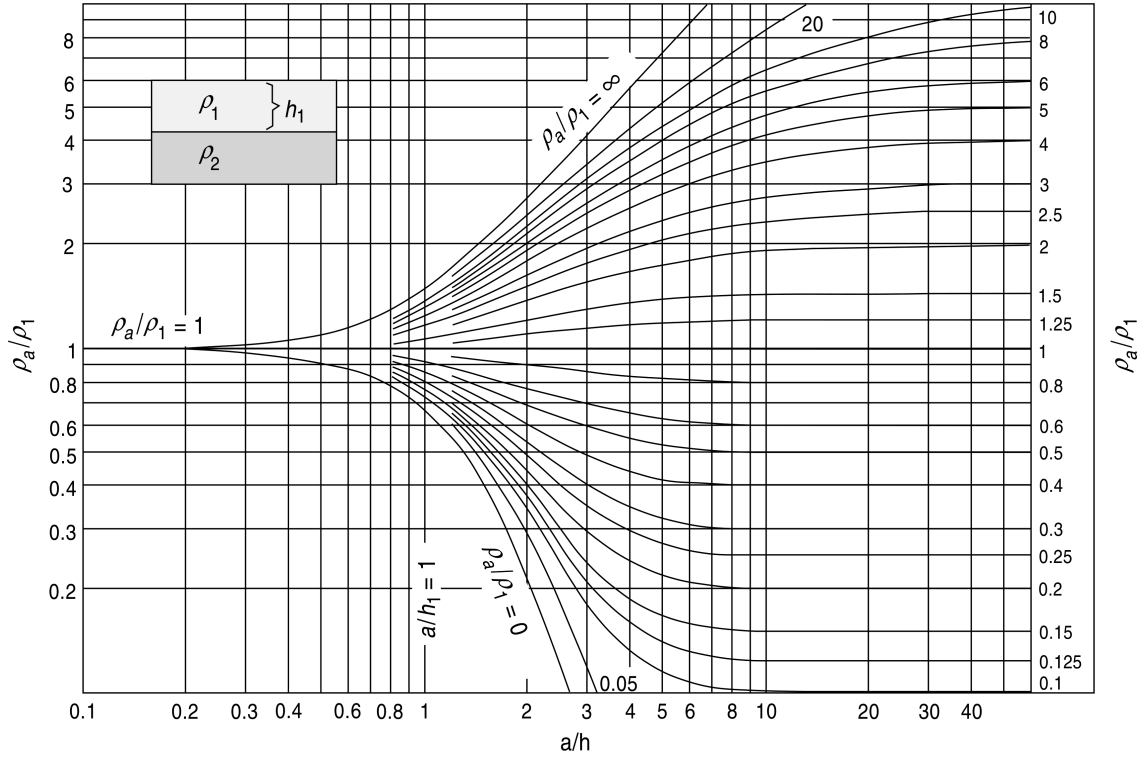
Figure 4.11: *Wenner array master curves for two layers (Musset and Khan 2000).*

To convert measured apparent resistivities to resistivities and current electrode separations into depth of interfaces nowadays an inversion process is carried out on the computer. In past, a set of master curves (Fig. 4.11) was used for this task. Anyway, even a computer modelling requires certain experience with assessing layers to field data. However, first of all the principle of equivalence have to be mentioned.

The principle of equivalence limits the uniqueness of the interpretation for thin layers. If there is a thin layer with resistivity much higher then the surrounding layers (Fig. 4.12) then replacing the layer with another one with the same product of $t\rho$ has a negligible effect on readings (t being a thickness of the layer). Conversely, if the thin layer has the resistivity lower then layers having the same ratio of t/ρ will appear the same.

To asses the starting model for further inversion, first of all, one have to decide, how many layers are present. Every change of the direction of the measured resistivity curve indicates a layer that could be detected. For the two layer case the curves looks as those on the master curve diagram (Fig. 4.11). They start at the resistivity of the upper layer and slowly changes to the value of resistivity of the bottom layer (asymptotically – it will reach that value at infinity). In case three layers are present, the resulting model consists of two two-layer cases (Fig. 4.13). The curves start at the resistivity value of the uppermost layer, then slowly changes to the resistivity values of the second layer, but will not reach it, and, finally, turns to the resistivity value of the third layer. The more complex models could be constructed in a similar way.
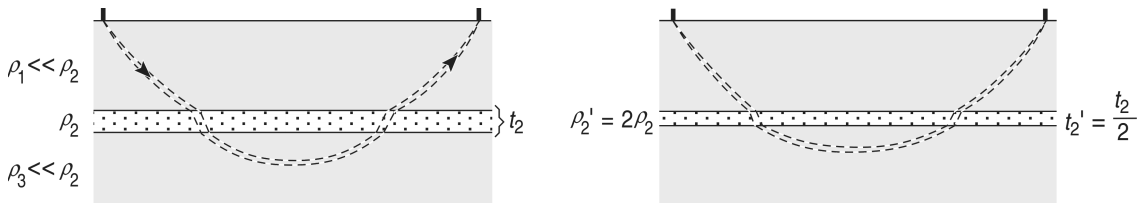

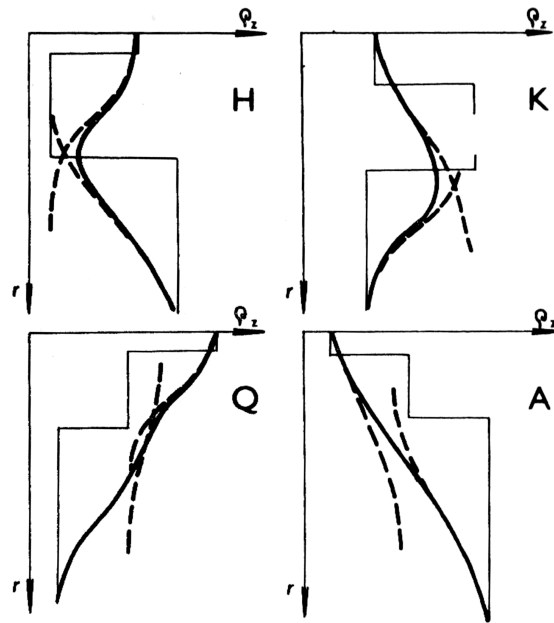**Figure 4.12:** *Principle of equivalence (Musset and Khan 2000).*

Figure 4.13: *The four types of three layer curves and corresponding two layer cases (Mareš and Tvrdý 1984).*
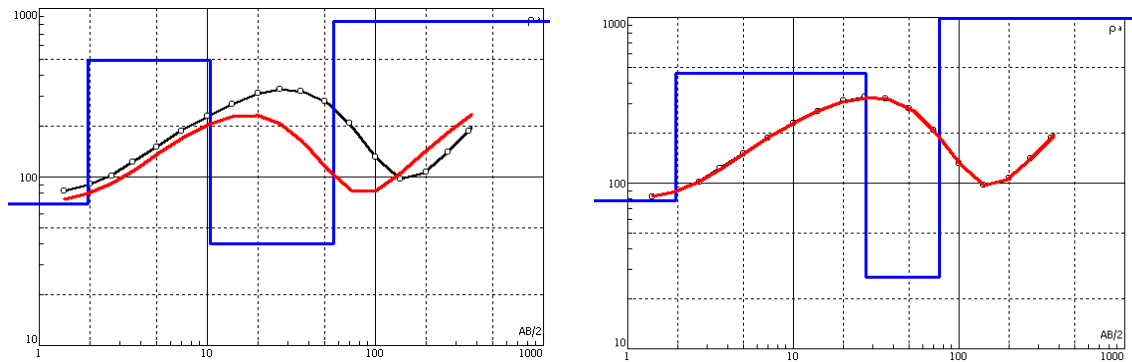

Figure 4.14: *Example of a VES curve inversion. The approximate starting model (left) is adjusted to a perfectly fitting model (right).*
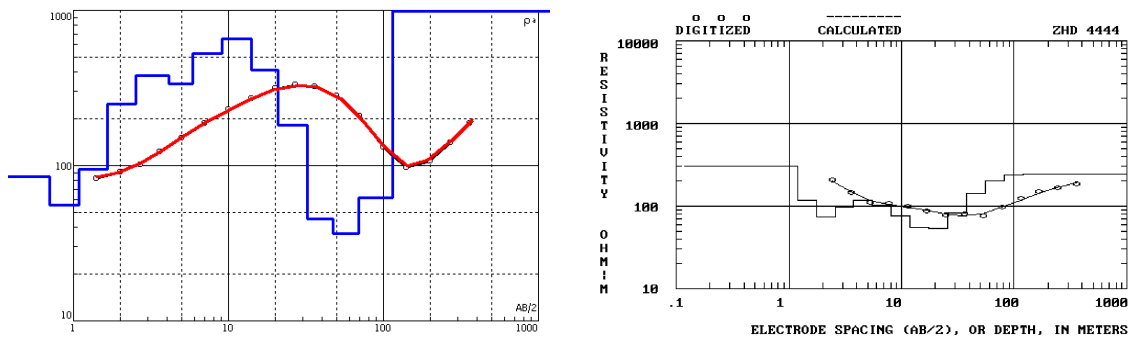

Figure 4.15: *The VES curve from Fig. 4.14 interpreted using a gradient model (left) and a field example of the gradient environment (right) – a VES curve over a weathered granite. Each measured resistivity point represents one layer.*
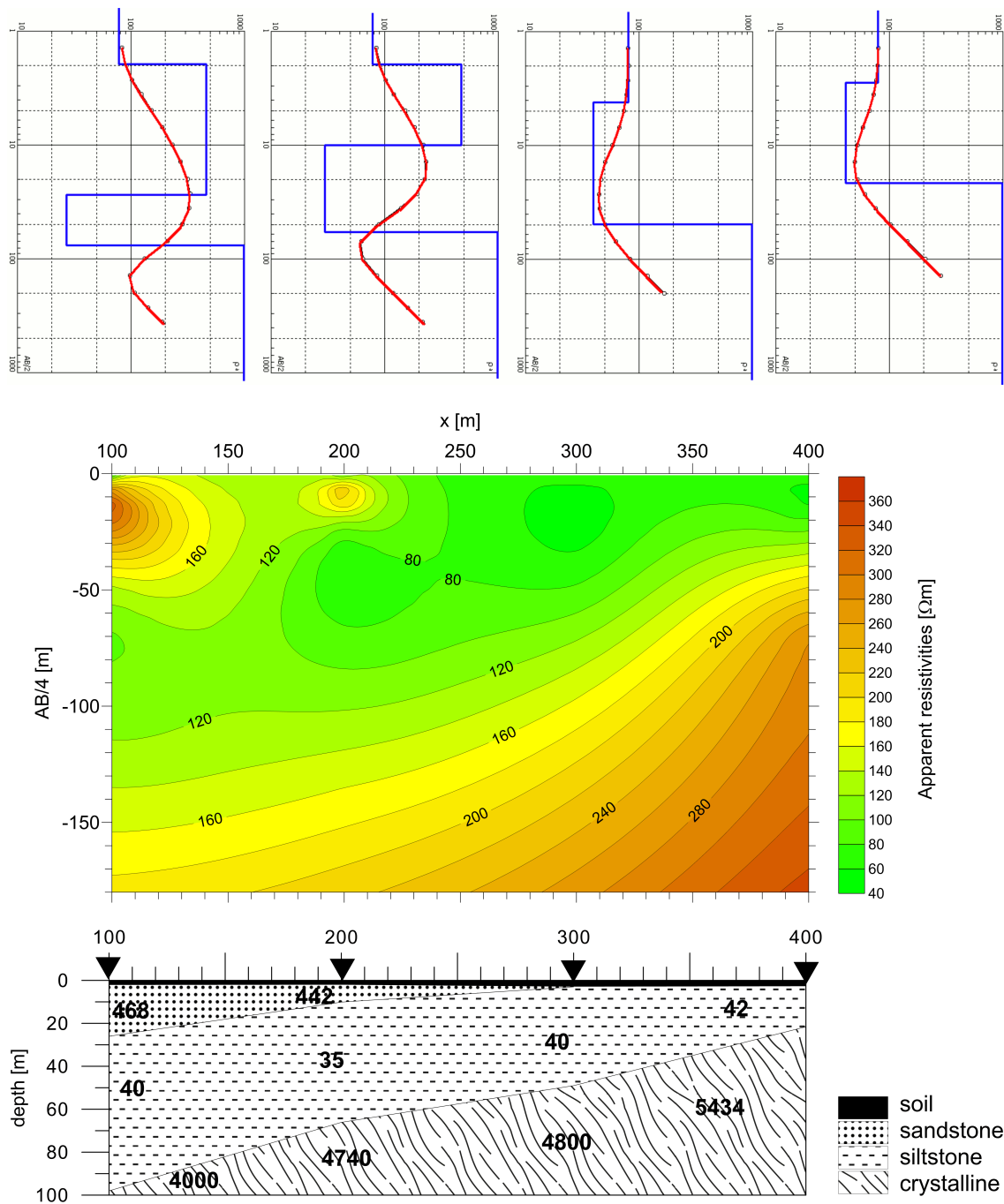
Figure 4.16: *Four VES curves measured on a profile with a hundered meter distance (top). A resistivity pseudosection (middle) and an interpreted geological section (bottom) created from four VES curves on profile. The distance between individual VES points was 100 m. Interpreted resistivity values are added to the geological section.*
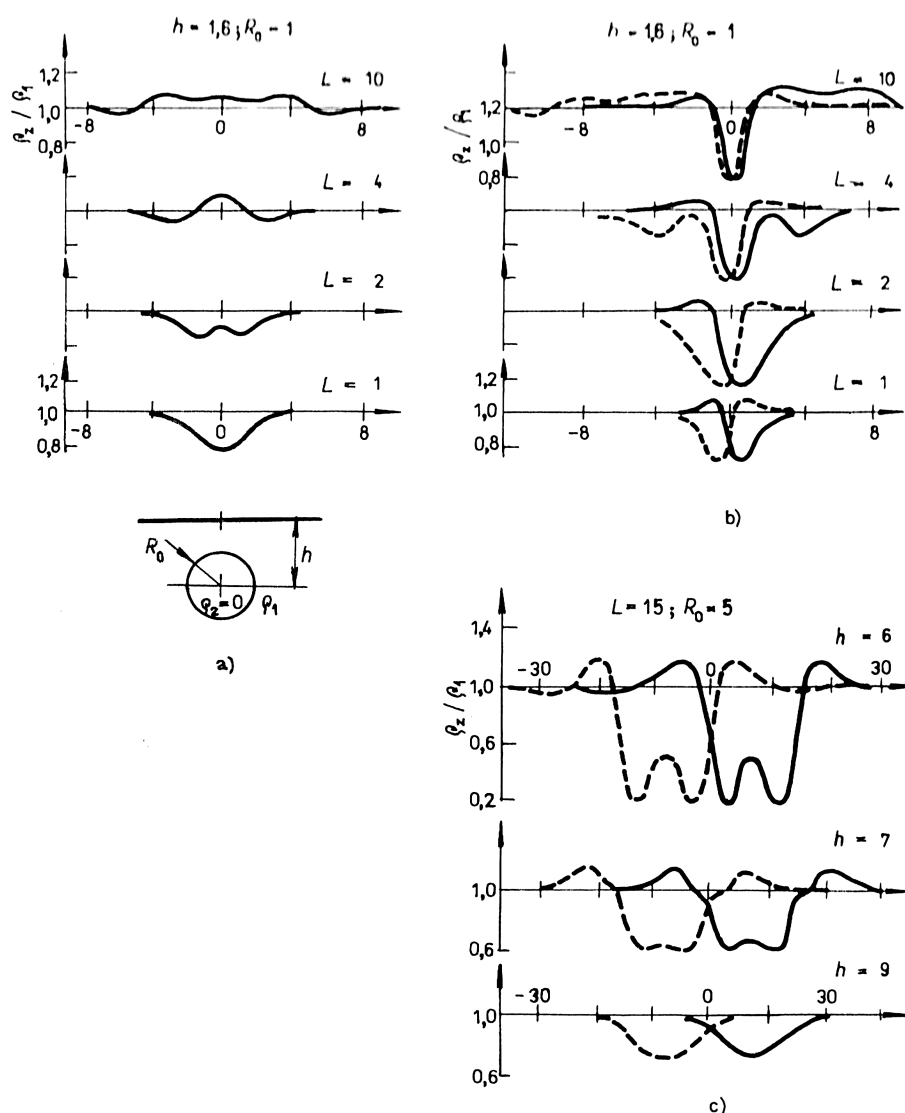
Figure 4.17: *Resistivity curves over a conductive sphere (Mareš and Tvrdý, 1984). a) Potential array. b) Pole-dipole and reversed pole-dipole. Station is a midpoint of potential electrodes. c) Dipole-dipole array. Station is a midpoint of potential electrodes. R_0 is a diameter of the sphere and h is the depth of its center.*

When the starting model is completed, the computer is used to fine-tune the model to fit the data (Fig. 4.14).

The presented layer model is useful, when the survey is carried out in the area with layered geology (e.g. sedimentary basins). In case, there is a gradual change of rocks (e.g. a weathered crystalline complex – the weathered clayey rocks near the surface are becoming less weathered with increasing depth up to the sound rock at large depths), the layer model might not be sufficient. In such case, the model could consists of a large number of layers – each measured point would represent one layer (Fig. 4.15). The large number of thin layers simulates the desired smooth change.

If there are several VES measurements on the profile, the measured apparent resistivity values can be plotted against certain depth estimate (e.g. AB/4 – one fourth of the current electrode distance) to form a *resistivity pseudosection* (Fig. 4.16). Next, individual sounding curves are interpreted and a geological section could be constructed in a similar way as if the sounding curves were boreholes.

4.3.3 Resistivity profiling

In contrast to the sounding examining a resistivity-depth distribution, the resistivity profiling maps lateral distribution of resistivities. The method is very versatile and hence used for various tasks, scales and depths. The depth of investigation is selected by the distance of current electrodes and character of measured anomalies (complexity, precision of anomaly indicators, etc.) depends on the electrode configuration. The small inter-electrode distances could provide a very detailed image of near-surface inhomogeneities for archaeological prospection. In contrast, large inter-electrode distances easily maps depths of tens of meters.
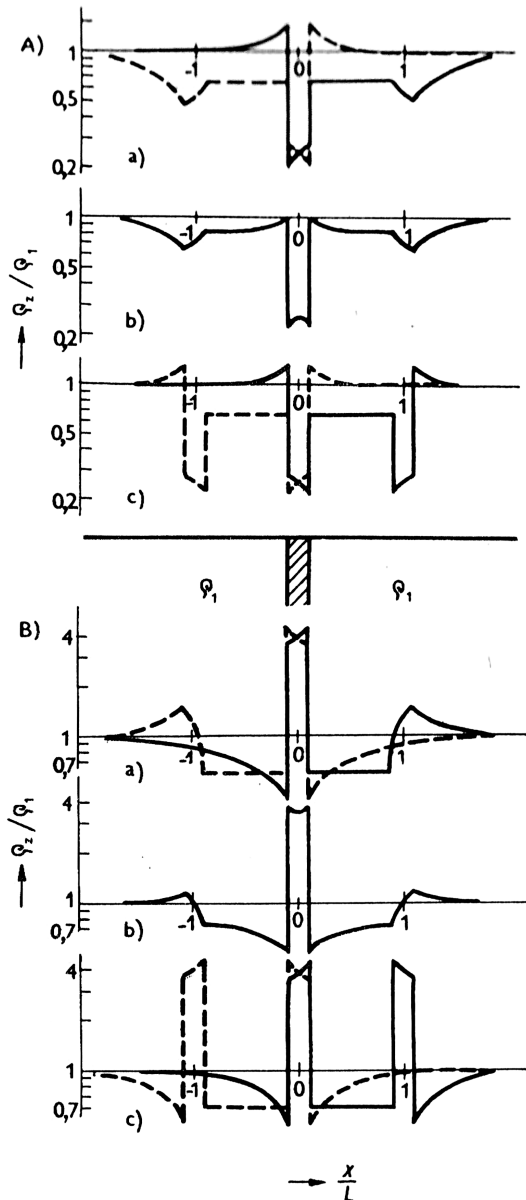

Figure 4.18: The resistivity curves over a thin dyke (Mareš and Tvrdý, 1984). a) Pole-dipole and reversed pole-dipole array. b) Schlumberger array. c) Dipole-dipole array. A) The case of a low resistivity dyke. B) The case of a high resistivity dyke. L is the length of the array.

The selection of the electrode array is determined by target structures and desired outputs. If a thin structure (e.g. a fault or a vein) is to be found by several profiles, the best is to use some of the high-resolution arrays, like pole-dipole or dipole-dipole (Figs. 4.8, 4.17 and 4.18). On the other hand, if a distribution of resistivities is to be mapped for, e.g. a lateral distribution of fluvial sediments or an archaeological prospection (Fig. 4.21), it is better to choose an array with a simple and clear image – a Wenner or a Schlumberger array (Fig. 4.8).

For the precise location of (relatively) thin objects there is a graphical "trick" for the pole-dipole and dipole-dipole configurations. The reference point is the middle of the potential dipole for both configurations. During the pole-dipole survey, the values for the pole-dipole and reversed pole-dipole are measured and plotted into one graph. Both of the curves have slightly different character when crossing the boundaries of bodies and the curves intersect just in the middle of the vertical dykes, sphere or cylinders (Figs. 4.8, 4.17, 4.18 and 4.19). For the dipole-dipole arrays the "trick" is similar. The reference point is in the middle of the potential dipole and the resistivity curve is plotted. Now, due to the reciprocity of the electrodes (the resistivity curves are the same if we swap current and potential electrodes), we can assign the reference point to the middle of the current dipole and plot the curve for this point. Hence we get two resistivity curves shifted for the length of the array. Both resistivity curves intersect in the middle of the bodies again (Figs. 4.8, 4.17, 4.18 and 4.20).

The best suited targets for the resistivity methods are conductive anomalies (ore veins, fault zones, etc.), however, the high resistivity bodies could be mapped as well.

It was mentioned that fault zones could be mapped as low resistivity anomalies. The rocks within the fault zone are usually fragmented, which increases a degree of weathering and amount of clay in the affected volume. The increased content of clay decreases the resistivity significantly and hence the low resistivity anomaly is measured. The faults are detected either as a conductive zone (due to the presence of clay par-
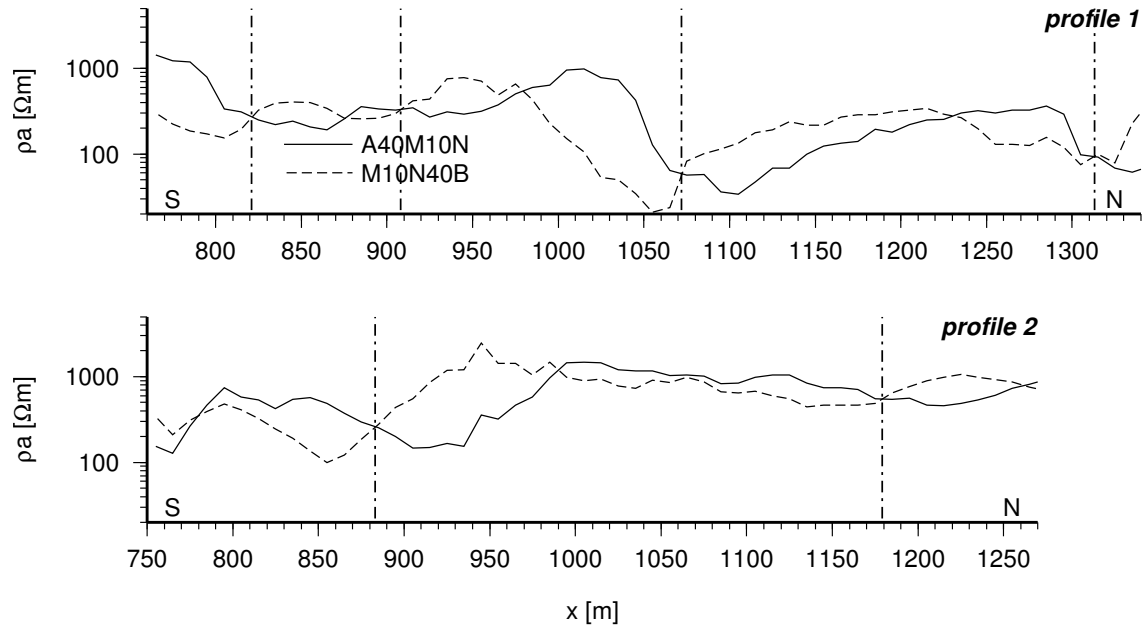
Figure 4.19: *Pole-dipole survey over the Pošumavský Fault (the Onen Svět site), Czech Republic. The geological media is formed by a different types of gneiss. A reference point is in the middle of the potential dipole (MN). Full line AMN (pole-dipole) resistivity plot, dashed line MNB (reversed pole-dipole) resistivity plot. Dot-and-dashed vertical lines indicate the conductors – fault zones. The legend shows inter-electrode distances in metres (hence also specifying the electrode array). Note the logarithmic scale for apparent resistivities.*
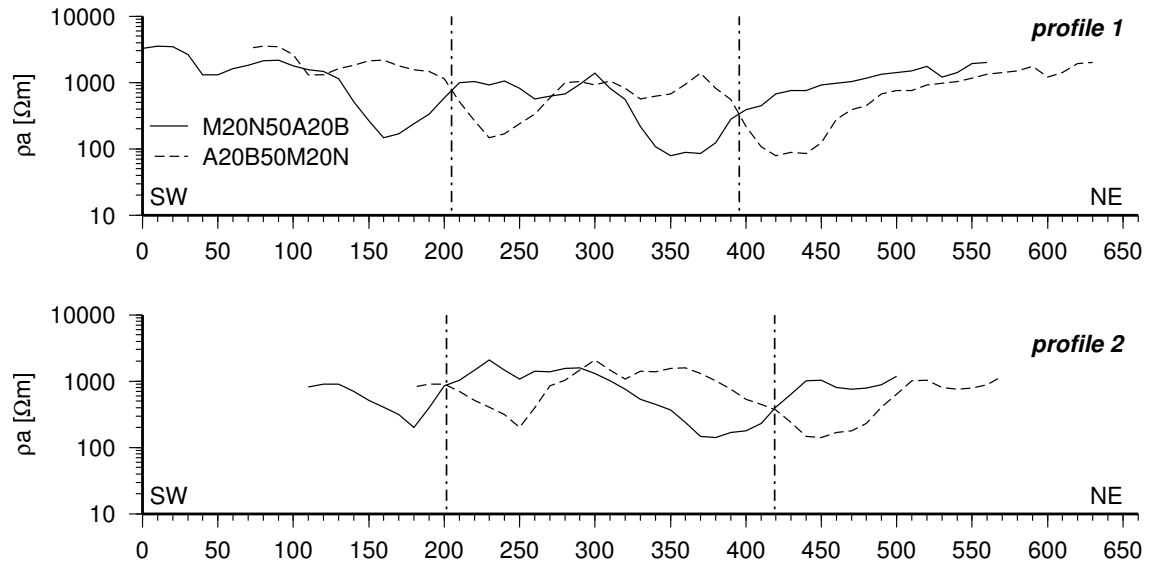

Figure 4.20: *Dipole-dipole survey over the Pošumavský Fault (the Pstružný site), Czech Republic. The geological media is formed by a gneiss. Two resistivity curves are plotted for the measured configuration (a reference point is in the middle of potential dipole MN) and reciprocal configuration (swapped current and potential dipoles, the reference point is now in the middle of current dipole AB). Hence the two resistivity curves are shifted for the length of the array. Dot-and-dashed vertical lines indicate the conductors – fault zones. The legend shows inter-electrode distances in metres (hence also specifying the electrode array). Note the logarithmic scale for apparent resistivities.*
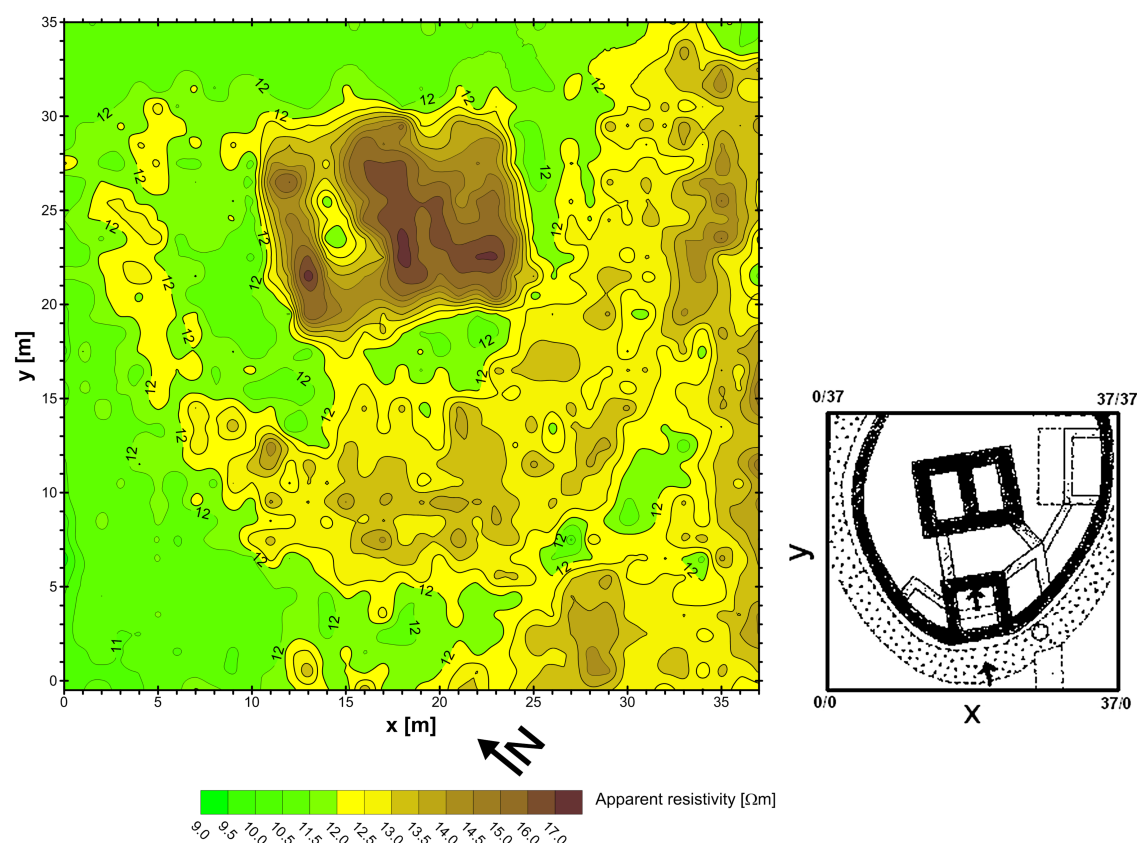
Figure 4.21: *Resistivity survey over the former medieval fortress, Czech Republic. Wenner array with a 1 m inter-electrode distances was used, the resistivities were mapped in the 1×1 m grid. The map of apparent resistivities (left) indicates the remnants of masonry as zones with increased resistivities. The interpreted ground-plan (right) shows the central tower, entrance with a gate, fortifications with adjacent smaller buildings and a ditch (dotted).*

ticles) or as a resistivity contrast (due to the different lithology on both sides of the fault). The most common arrays for the fault mapping are the pole-dipole and dipole-dipole arrays. The latter is suitable for a simple geological conditions, whereas the former could be recommended on most of the cases.

The potential and gradient arrays are often used in a prospection when a complex distribution of resistivities is expected – an archaeological prospection (Fig. 4.21), leaking of contaminants from waste dumps, etc.

5

Final word

We have seen that the geophysical methods could be very effective in solving various geological, hydrogeological and other tasks. However, the principal problem is that they do not show the structures directly, but are just proxies, mapping the distribution of selected physical parameter. The selection of this parameter and subsequent interpretation of measured data is the key point of every geophysical survey. Another serious drawback of the geophysics is the non-uniqueness of the interpretation. To, at least partially, overcome the problems it is always advisable to measure several physical parameters with as wide spectra of methods as possible. Then, the joint interpretation of obtained results usually leads to correct and useful results.

References

Becker H. and Fassbinder J.W.E. (eds.), 2001. Magnetic Prospecting in Archaeological Sites. ICOMOS Monuments and Sites, VI, 104 p.

Blaikie T.N., Ailleres L., Betts P.G. and Cas R.A.F., 2014. Interpreting subsurface volcanic structures using geologically constrained 3-D gravity inversions: Examples of maar-diatremes, Newer Volcanics Province, southeastern Australia, Journal of Geophysical Research Solid Earth, 119, doi:10.1002/2013JB010751.

Blecha V., Štemprok M. and Fischer T., 2009. Geological Interpretation of Gravity Profiles through the Karlovy Vary Granite Massif. Studia Geophysica et Geodetica, 53, 295–314.

Cooper G.R.J., 1997. Forward modelling of magnetic data. Computers & Geosciences, 23, 10, 1125–1129.

Cooper G.R.J., 2012. Grav2dc – gravity modelling and inversion, Version 2.10. Johannesburg, University of the Witwatersrand. http://www.wits.ac.za/academic/science/geosciences/research/geophysics/gordoncooper/6511/software.html, visited April 4th 2012.

Hammer S., 1939. Terrain corrections for gravimeter stations. Geophysics, 4 (3), 184–194.

Internet-1. Ludwig-Maxmilians Universität München, Department of Earth and Environmental Sciences. http://www.geophysik.uni-muenchen.de/research/archaeologicalprospection/magnetometry

Krijgsman W. and Langereis C.G., 2008. Dating, magnetostratigraphy. In: V. Gornitz (ed.), Encyclopedia of Paleoclimatology and Ancient Environments, Springer, Dordrecht, 252-255.

Longman I. M., 1959: Formulas for Computing the Tidal Accelerations Due to the Moon and the Sun. Journal of Geophysical Research, 64, 2351–2355.

Mareš S. and Tvrdý M., 1984. Introduction to applied geophysics. Kluwer, Dordrecht.

Milsom J. and Eriksen A., 2011. Field Geophysics. John Wiley & Sons, Chichester, UK.

Musset A. E. and Khan M. A., 2000. Looking into the Earth. Cambridge University Press, New York, USA.

Nettleton L. L., 1939. Determination of density for reduction of gravimeter observations, Geophysics, 4 (3), 176–183.

Sedlák J., Gnojek I., Scheibe R. and Zabadal Z., 2009. Gravity response of igneous rocks in the northwestern part of the Bohemian Massif. Journal of Geosciences, 54, 325–342.

Snopek K. and Casten U., 2006. 3GRAINS: 3D Gravity Interpretation Software and its application to density modeling of the hellenic subduction zone. Computers and Geosciences, 32, 592–603.

Talwani M., Worzel J.L. and Landisman M., 1959. Rapid gravity computations for two-dimensional bodies with application to the Mendocino submarine fracture zone, Journal of Geophysical Research, 64(1), 49–59.

Telford W. M., Geldart L. P. and Sheriff R. E., 1990. Applied geophysics. Cambridge University Press, Cambridge, UK.

Ziegler A.T. and Geissman J.W., 2011. Magnetostratigraphy of the Upper Triassic Chinle Group of New Mexico: Implications for regional and global correlations among Upper Triassic sequences. Geosphere, 7, 802–829.